Experimental Techniques for the Fabrication and Characterization of Organic Thin Films for Field-Effect Transistors

Yugeng Wen, Yunqi Liu,* Yunlong Guo, Gui Yu, and Wenping Hu

Beijing National Laboratory for Molecular Sciences, Key Laboratory of Organic Solids, Institute of Chemistry, Chinese Academy of Sciences, Beijing 100190, P. R. China

CONTENTS

1. INTRODUCTION

As a result of the continuous drive to fabricate electronic devices on lightweight, large-area plastic substrates by low-cost processing techniques, organic electronics is currently running in the fast lane. Following this trend, organic thin-film transistors (OTFTs) have developed rapidly over the past decade due to their promise as components in cheap and flexible electronic circuits. Many potential applications have been demonstrated, ranging from flexible displays[1−5] and sensor systems[6−10] to radio frequency identification (RF-ID) tags,[11−13] and some of these systems are now getting excitingly close to the commercial world.[14] There have been two motivations for the surge in OTFT research and development in the past 5−10 years. The first is the need to manufacture products at very low cost. The manufacture of commercial liquid crystal displays (LCDs) has moved through a series of technology generations, defined by the

increasing size of the substrate, which gives rise to considerable challenges. On the one hand, conventional integrated circuits for large-area LCDs are currently patterned by photolithographic processes, and the manufacturing costs associated with this technique increase rapidly with this increase in size. On the other hand, amorphous silicon (a-Si) thin-film transistors (TFTs) are now capturing a large fraction of the market as backplane circuits for active matrix liquid crystal displays. Fabrication of films of this material becomes both very challenging technically and also costly for such large size displays. The unique properties of organic materials have opened the door to a suite of fabrication techniques that can simplify the equipment and reduce the processing complexity required to meet the demands of large-scale LCDs.

Another motivation is flexible or stretchable electronics. Organic electronic devices or circuits fabricated on lightweight, bendable plastic substrates have great potential for applications in electronic displays, electronic smart cards, or biomedical systems that are not easily achieved by conventional inorganic electronics.[15] Organic TFTs and electronic circuits deposited by printing-like techniques can be expected to meet the new needs of the next generation of large area flexible backplanes.

Progress in OTFTs has been driven by advances in experimental techniques, material synthesis, and theoretical calculations, and new improved experimental techniques are playing an increasingly important role in this expansion. We believe that the next rapid advance will come if low-cost, large-area printing-like manufacturing techniques become sufficiently mature for successful commercial-scale production. Many innovative techniques have been developed for fabrication of OTFTs, but no one technique has been found to be clearly superior in a manufacturing environment. In fact, every technique has its advantages and disadvantages, and therefore it is necessary to have a comprehensive understanding of these experimental techniques in order to be able to exploit the various strengths of the different techniques. This review begins by describing the use of characterization techniques in OTFTs, including high-resolution microscopy techniques, various spectroscopic techniques, and other characterization methods. Next, we describe fabrication or processing techniques—ranging from patterning and printing techniques to deposition techniques—that have been successfully employed in the fabrication of the key components of organic devices. Finally, we conclude with some discussion of likely future trends and advances in such sophisticated experimental techniques for the fabrication and characterization of OTFTs.

2. TECHNIQUES FOR CHARACTERIZATION OF OTFTS

Before products based on active organic thin-film transistors can reach the market, a great deal of work first needs to be done in the laboratory to keep the manufacturing costs in the future as low as possible. Many processing techniques have been developed in research demonstrations of discrete transistors in an effort to meet the requirements of low-cost applications. However, before the goals of flexibility, long lifetimes, and inexpensive processing can be achieved commercially, a variety of challenges must be overcome; these involve choice of materials, device design, optimization of key components of transistors, and innovation in fabrication techniques.[16−18] All the challenges relating to organic transistors are actually on the micro- or nanoscale level, and, in order to meet these challenges, there is

a clear need for characterization techniques to correlate our macroscopic manipulation with important properties of organic electronic devices on the micro- or nanoscale. Therefore, before discussing fabrication techniques, we first introduce the tools available for the characterization of the micro- or nanoscale properties of OTFTs.

2.1. Electrical Scanning Probe Microscopy

Electrical scanning probe microscopy (SPM) techniques are some of the most common tools to characterize the surface properties of organic semiconductors and study fundamental questions of charge injection, trapping, and transport in organic electronic devices. The different SPM techniques have made a number of important contributions in many research fields,[19,20] and here we only highlight those techniques directly used in the study of OTFTs, including tapping mode atomic force microscopy (TM-AFM), conducting atomic force microscopy (C-AFM), electric force microscopy (EFM), and scanning Kelvin probe microscopy (SKPM). Since these techniques have been described in detail elsewhere,[21−23] we will only summarize them below.

2.1.1. Tapping Mode Atomic Force Microscopy. AFM is a technique that can measure surface textures of various materials and quantitatively examine shapes/profiles of technologically important surface structures. In a typical AFM experiment, the sample surface is scanned by a sharp tip mounted beneath a cantilever, and the vertical separation between probe and sample can be precisely controlled by a piezoelectric actuator to keep the force between tip and sample at a given set-point level. Two modes of AFM are employed in studies of surface topography. One is the contact mode, where the tip stays in permanent contact with a sample during scanning. The other is the tapping mode, where the tip interacts with the sample surface while the cantilever oscillates with a constant resonant frequency, resulting in a change in the dynamic parameters of the cantilever; the cantilever motion is magnified by means of a laser beam, which is deflected in a regular pattern over a photodiode detector.

Tapping mode AFM is the most common technique for topographic imaging of organic semiconductors in OTFTs for two reasons. One is that the intermittent tip−sample contact leads to gentler imaging without the shearing associated with the contact mode; another is that many organic semiconductors such as self-assembled organic molecules and polymers have heterogeneous surfaces, which require the minimization of tip−sample interactions to avoid damage to these soft material surfaces. It is recognized that the performance of OTFTs is strongly influenced by the first few organic monolayers close to the dielectric layer[24] and that the nucleation and film-growth mechanisms are significantly affected by the surface properties of a dielectric substrate, resulting in different morphologies of thin films.[25] Therefore, TM-AFM is a powerful tool to characterize crystalline morphologies and the intrinsic heterogeneities of organic thin films on dielectric substrates.

The importance of the TM-AFM technique for topographic imaging of organic semiconductors in OTFTs can be illustrated by one typical example from the literature. In order to investigate the effects of the phase state (ordered or disordered) of self-assembled monolayers (SAMs) on the growth mode of pentacene films and the performance of OTFTs, Lee and co-workers deposited pentacene molecules on ordered or disordered octadecyltrichlorosilane (ODTS) monolayers at various substrate temperatures (30, 60, and 90 °C).[26] They found significant
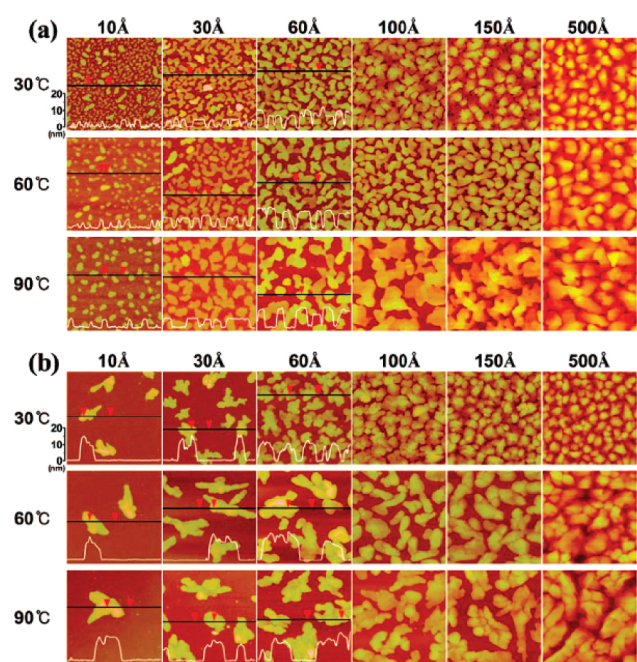
Figure 1. AFM images and height profiles taken at various thicknesses during the formation of pentacene films on ordered (a) and disordered (b) ODTS monolayers at substrate temperatures of 30, 60, and 90 °C. All images are 2 μm × 2 μm in size. Reprinted with permission from ref 26. Copyright 2008 American Chemical Society.

Figure 2. (a) Schematic diagram of the C-AFM experiment. (b) C-AFM topographs of 5 nm thick pentacene films on the poly(α-methylstyrene)/Al$_2$O$_3$ dielectrics II (based on etched Al foil) and III (based on sputtered Al). (c) C-AFM current images of the areas in the white boxes in b, as collected at V_{bias} = 2 V. (d) Cross-sectional height and current profiles. Reprinted with permission from ref 33. Copyright 2010 American Chemical Society.

differences between the growth mechanisms on ordered and disordered monolayers (as shown in Figure 1). At each temperature, numerous two-dimensional (2-D) islands were formed on the ordered ODTS monolayers, whereas conglomerated island-type structures were formed on the disordered ODTS monolayers. It was also found that the pentacene films grown on the ordered ODTS monolayers had a better interconnectivity between the pentacene domains—which directly serves to enhance the field-effect mobility—than those grown on the disordered ODTS monolayers.

In addition, a great deal of other information can be provided by the TM-AFM technique independently or in combination with other characterization techniques, about the nucleation density, the grain size, grain boundaries, molecular orientation, and crystalline phases.[27−30] TM-AFM can be employed in various environments (vacuum, gas, liquid) and at controlled temperatures and therefore is certain to be further developed as an advanced scanning probe technique with broad applications in OTFT research.

2.1.2. Conducting Atomic Force Microscopy. Conducting AFM (also called conducting probe AFM) is mainly used to study electrical transport in nanotubes, nanoparticle assemblies, nanoscale semiconductor devices, and individual molecules on local length scales. In the C-AFM experiment, the surface topography is measured using a metal-coated AFM tip, which is directly in contact with the sample controlled by feedback electronics capable of maintaining a set-point load with a precision of several nanonewtons. The current flowing through the biased tip−sample junction is recorded in order to measure the current−voltage (I−V) relationship for the sample. Since C-AFM can characterize samples surrounded by insulating regions due to its feedback mechanisms being independent of the sample conductivity, C-AFM is one of the most attractive techniques for electrical transport measurements in OTFTs.
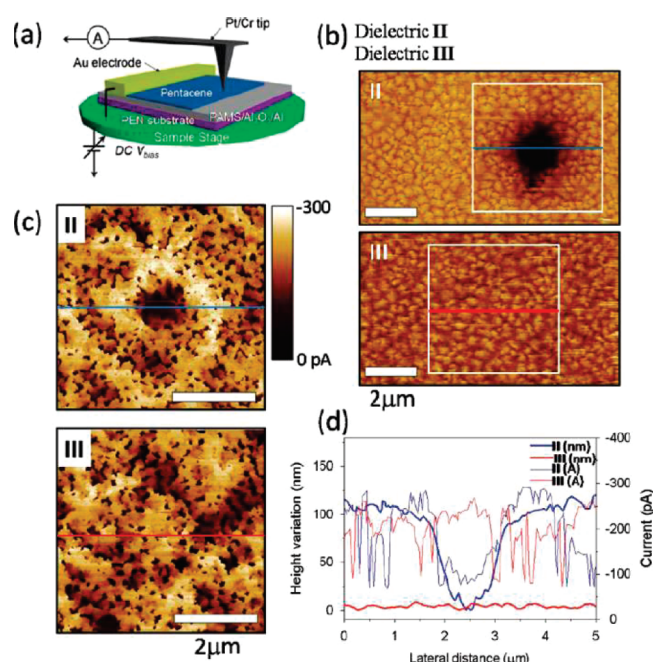
C-AFM has been used to map the lateral transport properties in a number of polycrystalline grains.[29,31,32] For example, Yang and co-workers used C-AFM to measure lateral current variations for 5 nm thick pentacene films deposited on different dielectric layers.[33] They found that the current variation across the edges of dimples on a dielectric surface was only slightly different from that across the grain boundaries of a flat dielectric surface (Figure 2). It was therefore concluded that the presence of microscale curvature on the local dielectric surface does not affect the growth of pentacene in terms of the contact length scale of the seeding molecules.

In addition to obtaining qualitative maps of variations in electric current, C-AFM has also been used to characterize contact resistance in molecular junctions. The metal−molecule interface can be probed by C-AFM in order to examine how the metal−molecule contact affects the I−V characteristics of the junction.[34,35] Furthermore, C-AFM has also been used to measure the carrier transport in organic semiconductor sexithiophene crystals in order to understand the key role played by grain boundaries in the transport properties of OTFTs.[36,37] C-AFM has become a useful tool to measure variations in local charge transport as a result of local heterogeneity and to analyze the effects of microstructure and contacts on the performance of OTFTs.

2.1.3. Electric Force Microscopy. Electric force microscopy (EFM) can be used to map the electric-field gradient at a film surface. The basic principle of EFM is that tapping mode AFM imaging is used to determine surface topography on a first pass. On a second pass, the AFM tip retraces the topography while oscillating at a constant distance over the sample, and simultaneously the tip is biased at a voltage with respect to the substrate.
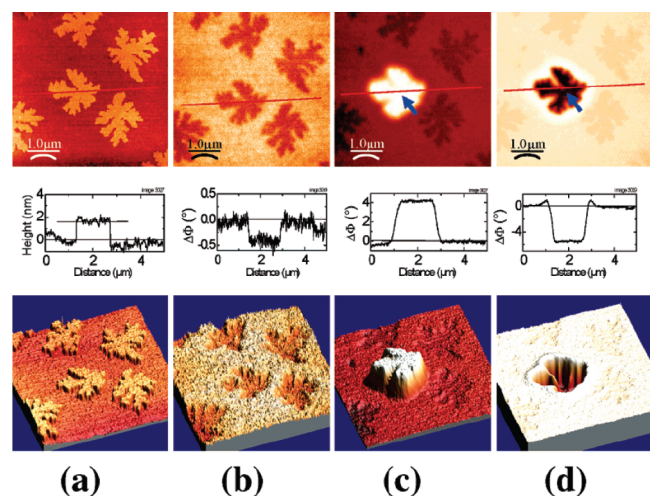
Figure 3. From top to bottom: 2-D images, section profiles along the red line and 3-D images of pentacene islands on an n-type silicon wafer covered by ~4 nm thick thermal oxide. (a) TM-AFM images of the islands. (b) EFM images (phase shift, $V_{EFM} = 4\,V$, $z = 80\,nm$) of the same islands before charge injection. (c) EFM images (phase shift, $V_{EFM} = 4\,V$, $z = 80\,nm$) of the same islands after a local injection ($V_{INJ} = +2\,V$ for 4 min) on the central island (injection point marked by the arrow). (d) EFM images (phase shift, $V_{EFM} = 4\,V$, $z = 80\,nm$) after a subsequent local injection at $V_{INJ} = -2\,V$ for 4 min. All images are $5\,\mu m \times 5\,\mu m$ in size. Reprinted with permission from ref 41. Copyright 2004 American Chemical Society.

Finally, the shift in the cantilever resonant frequency is recorded as a function of the tip voltage allowing the measurement of potential profiles with the high resolution of scanning probe microscopy. Comprehensive details of the principles of EFM can be viewed in ref 38, and we will limit our attention to applications of the EFM technique in characterizing OTFTs.

The EFM technique specializes in exploring the charge properties or electrostatic behavior of semiconducting materials,[39,40] and EFM has also been used to examine charge trapping and injection effects in OTFTs. Heim and co-workers have used EFM to measure the 2-D distribution and concentration of locally injected electrons and holes in a single pentacene monolayer island, and reported how the injected carriers either remain localized or are able to delocalize over the island depending on the molecular conformation (ordered vs disordered) of this island.[41] Figure 3 shows the TM-AFM image of pentacene monolayer islands on a substrate with low roughness and the EFM images before and after the charge injection. The dark features in the EFM image before the charge injection are due to the capacitance coupling effect and/or to a small residual charge in the islands. The large bright feature seen in the EFM image after the charge injection (Figure 3c) indicates that a net positive charge is now stored in the islands as a result of the delocalization of the injected charges along the entire pentacene island, and the strong dark feature seen in Figure 3d indicates that a net negative charge is now stored in the island, demonstrating that the excess negative charges are now totally delocalized over the entire domain. Such a charge delocalization is consistent with good molecular packing in the island, and it demonstrates that a good $\pi-\pi$ overlap exists in the pentacene monolayer.

Marohn and co-workers have resolved charge traps using EFM measurements on pentacene-based OTFTs. They found that trapping was not associated with visible grain boundaries in the films, and the traps were distributed inhomogeneously in space.[42]

By monitoring the EFM signal as a function of time in a fixed location, the same group showed that the trap density in these devices is on the order of ~1 trapped charge per 640 pentacene molecules in regions of maximum trap density,[43] and that the trapping rate is dependent on the free hole density.

To summarize, the EFM technique is a useful tool to study charge trapping and injection effects in OTFTs. It can also be used to study the electronic properties of isolated conducting materials and various semiconductor films on dielectric substrates at an early stage of growth. The injection/EFM detection technique is also playing a key role in characterizing other monolayers and molecules of interest for molecular-scale electronics.[44,45]

2.1.4. Scanning Kelvin Probe Microscopy. Scanning Kelvin probe microscopy (SKPM) is a well-established technique for measuring lateral potential profiles between a conductive tip and a sample. In its basic operation, it is similar to EFM; however, in contrast to EFM, SKPM uses a nulling feedback technique to keep the tip–surface potential difference at 0 V, and in the second pass, the mechanical oscillation of the cantilever is replaced with an alternating current (AC) voltage waveform and a direct current (DC) voltage offset to the tip. A lock-in amplifier is used to measure the resulting mechanical oscillation, and a feedback loop to the bias voltage nulls the oscillation.

To date, the most important application of SKPM in the study of OTFTs is in examining the influence of contact resistance on device performance. For example, Nichols and co-workers reported large potential drops at the source with magnitude dependent on contact metallurgy in bottom-contact pentacene transistors, indicating that device performance can be contact-limited under operating conditions.[46] Puntambekar and co-workers have also studied the potential drop between source and drain in top- and bottom-contact pentacene transistors using SKPM.[47] Their results showed that the bottom-contact transistors were contact-limited at large gate voltages, while top-contact devices were not contact-limited but bulk-limited. These results, along with other experiments,[48,49] demonstrate that SKPM is a powerful tool to characterize contact resistance, thus allowing a more detailed understanding of transport in OTFTs.

Additionally, SKPM has also been employed for the surface potential imaging of working OTFT devices.[50–52] Teague and co-workers have described SKPM studies of the potential distribution in solution-processed, bottom-contact OTFTs with the aim of determining the role of film microstructure in device performance.[50] By analyzing the variations in potential drop, they found that different factors determine the mobility of working devices with different channel lengths. For a $5\,\mu m$ channel OTFT device, the grain size of material has the same order of magnitude as the channel length (Figure 4A), and when the device is operating in the linear region, the primary voltage drop occurs at the source electrode–semiconductor contact, with only a gradual voltage drop across the organic semiconductor itself (Figure 4B). Such a potential profile indicates that the main barrier to charge transport in this device is charge injection into the organic semiconductor from the source electrode. As the channel length increases, grain boundaries and regions of poorly nucleated material play a more important role in determining the mobility of the system due to the potential drop variations, as was clearly demonstrated by the SKPM studies.[50]

Recently, SKPM has also found other applications, such as indirectly monitoring trap evolution through variations in threshold voltages and potential profiles in OTFTs,[53] and assessing the
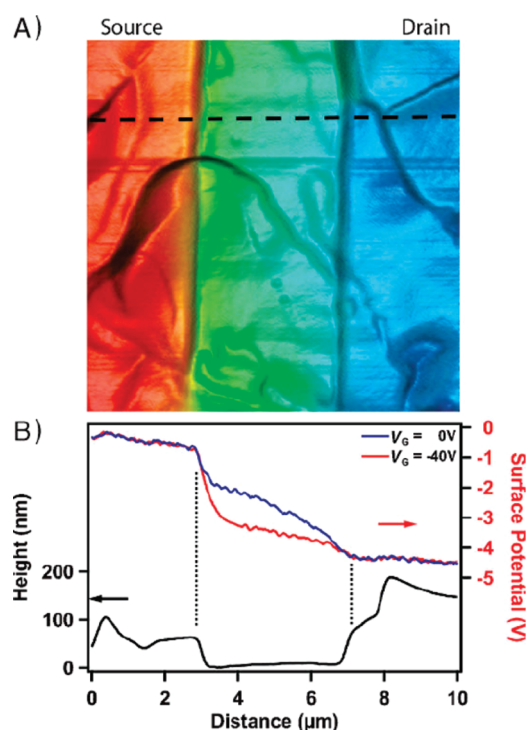
Figure 4. (A) SKPM data for a $5\,\mu$m OTFT device structure ($V_{ds} = -5$ V, $V_{gs} = -40$ V): the SKPM potential map (color) is overlaid on top of the corresponding 3-D topographic AFM image. The topographic and potential data were acquired simultaneously. The horizontal dashed line in (A) corresponds to the location of the topographic and potential line profiles shown in (B), and the vertical dotted line in (B) indicates the location of the Au contact edges. Reprinted with permission from ref 50. Copyright 2008 Wiley-VCH Verlag.

recombination profile in ambipolar OTFTs.[54] Its broad applications make SKPM one of the most useful techniques for characterization of OTFTs, and SKPM is certain to be further developed in order to study the intricate details of device behavior.

2.2. Spectroscopic Characterization Techniques

Spectroscopic characterization techniques, mainly electronic and vibrational spectroscopic techniques, are powerful methods for characterizing organic semiconductors and organic interfaces. Such techniques include near-edge X-ray absorption fine structure (NEXAFS) spectroscopy, photoelectron spectroscopy, Fourier-transform infrared spectroscopy (FTIR), IR + visible sum-frequency generation (SFG) vibrational spectroscopy, micro-Raman spectroscopy, and optical spectroscopy. They can provide complementary information about many aspects of OTFTs, such as the interface-related properties of organic semiconductors, the chemical composition in the surface region of organic semiconductor films, the changes in the vibrational characteristics of organic semiconductors during operation of OTFTs, and the molecular orientation and the structure evolution in organic nanoscale films. In this section, we review how these spectroscopic techniques can be used in the characterization of OTFTs and compare the results obtained using the different methods in order to highlight their complementary capabilities.

2.2.1. Near-Edge X-ray Absorption Fine Structure Spectroscopy. NEXAFS spectroscopy can be used to quantify

chemical composition, molecular orientation, and defects in a variety of organic semiconductor films in OTFTs. NEXAFS is a nondestructive, synchrotron-based spectroscopic technique in which soft X-rays are absorbed, causing resonant excitations of core K- or L-shell electrons to unoccupied molecular orbitals, which may have either π- or σ-symmetry. The absorption probability for linearly polarized X-rays depends on the relative orientations of the vector of the resonance orbital and the electric field vector of the incident X-ray,[55] and therefore the dependence of the intensity of a particular absorption resonance on the polarization direction of the electric field of the incident X-ray reveals any preferential orientation of the molecular groups. From this simple relationship, one can derive the order parameters, which describe quantitatively the average molecular orientation. In addition, due to its controlled sampling volume and elemental sensitivity, NEXAFS spectroscopy can detect defects in semiconductor films by chemical recognition of the underlying substrate such as an oxide dielectric.

In order to provide a basis for understanding the practical implementation of this technique, we present several examples of NEXAFS analysis of commonly used semiconductors in OTFTs. DeLongchamp and co-workers have used NEXAFS spectroscopy to quantify the molecular orientation of solution-processable oligothiophene semiconductors by evaluating the angular dependence of carbon K-edge spectra.[56] The carbon—carbon π^*- and σ^*-resonant intensities (Figure 5a) exhibit a strong angular dependence that corresponds to a dipole defined by the spatial orientation of the final state orbital. As shown in Figure 5b, the π^* resonance is a vector normal to the conjugated plane, while the σ^* resonance vector lies along the long axis. The formula defined in Figure 5b indicates that the resonance intensity is proportional to the square of the cosine of the angle between the incident electric field vector and the resonance vector. Therefore, if the π^* intensity is largest at normal incidence (90°), this indicates that the conjugated plane of the oligothiophene tilts away from the substrate in an "edge-on" orientation, and if the σ^* intensity is greatest at glancing incidence (20°), this means that the long axis of the oligothiophene is normal to the substrate in a "standing-up" orientation.

Yuan and co-workers used NEXAFS spectroscopy to provide the average tilt angle over all molecules of the molecular conjugated plane with respect to surface normal.[57] In the NEXAFS spectroscopy studies, they measured Auger electron yield (AEY) and total electron yield (TEY) simultaneously. Because of different degrees of surface sensitivity of the two yield signals, the comparison of peak intensities in these two spectra can identify the molecular orientation near surface. NEXAFS spectroscopy has many capabilities but is most powerful when it is combined with crystallographic techniques such as grazing incidence X-ray diffraction (GIXD) or scanning probe techniques such as AFM.[58−61] By means of such combinations, one can obtain details of the molecular packing in thin organic semiconductor films and more detailed microstructure information that can be correlated to fundamental electronic properties or device performance. NEXAFS spectroscopy is only beginning to be used effectively in the field of organic electronics such as OTFTs, and the combination of NEXAFS with the wealth of other characterization techniques available, together with the knowledge already gained in this field, will drive its further implementation.

2.2.2. Photoelectron Spectroscopy. Photoelectron spectroscopy, which has been one of the major surface science
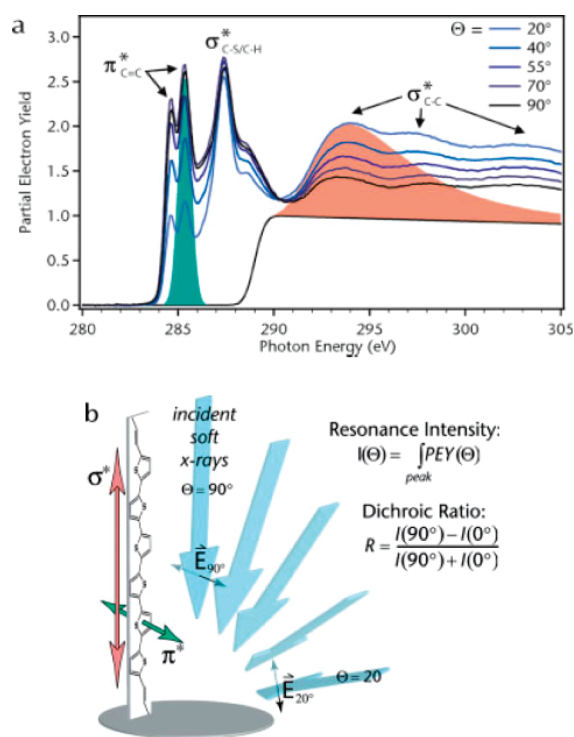
Figure 5. (a) NEXAFS carbon K-edge spectra collected at different incident angles from a film of the symmetric sexithiophene obtained by thermal treatment at 200 °C. Spectra are normalized to the net carbon signal. The green area indicates the oligothiophene π^* resonance used to determine the planar orientation, while the pink area indicates the σ^* resonance used to determine the long-axis orientation. (b) Image depicting the orientation of symmetric sexithiophene and spatial orientations of its primary K-edge carbon resonances. Blue arrows indicate incident polarized soft X-rays with electric field vectors extending normal to the plane of photon polarization. An off-axis component to the σ^* resonance of symmetric sexithiophene exists that has been omitted for simplicity. Reprinted with permission from ref 56. Copyright 2005 Wiley-VCH Verlag.

techniques in the field of inorganic semiconductor research for decades, has also been successfully applied more recently to study organic semiconductors and their interfaces. The interface between the electrodes and the semiconductor has always been recognized as key topic in OTFT research considering its role in OTFT geometries. However, this device interface cannot be regarded as a simple contact between the metal and the organic layer. In fact, it is very complicated, and energy level alignments at the metal−semiconductor junction, partial interfacial contamination, and structure disorder near the contact, as well as other factors, must all be taken into account. Therefore, techniques to study the electronic structure of metal−organic semiconductor interfaces are required. Ultraviolet photoelectron spectroscopy (UPS) together with X-ray photoelectron spectroscopy (XPS) are the commonly used techniques for probing the electronic structure of various metal−organic semiconductor interfaces in OTFTs.

In UPS, a sample in a vacuum is irradiated with high energy monochromatic radiation, and the induced photoelectrons that escape into the vacuum are collected, energy resolved, slightly retarded, and counted; this results in a spectrum of electron intensity as a function of the measured kinetic energy. The kinetic energy values are then converted into binding energy values

which are more readily applied and understood.[62] XPS is used to study the energy levels of atomic core electrons for chemical analysis, since it is based on the principle that the core levels have small chemical shifts depending on the chemical environment of the atom which is ionized, allowing chemical structures to be determined. It can be used to obtain chemical information about an interface region of around 2 nm in depth in OTFTs.

UPS is a powerful technique for studying the electronic structure of organic materials and has been extensively applied in studying a wide variety of solids and interfaces.[63−65] However, since XPS is particularly useful in probing possible band bending of an organic layer by virtue of its element-specific nature and XPS can be rather easily incorporated with UPS, combined studies by UPS and XPS are more powerful than UPS alone. For example, Duhm and co-workers carried out both UPS and XPS measurements on α,ω-dihexyl-sexithiophene (DH6T) on Ag(111), and they found that the ionization potential of the molecule varied by up to 0.6 eV depending on whether the molecule is lying flat on the substrate or standing upright.[66] DH6T is commonly used in OTFTs,[67] and the molecules in a monolayer adsorb lying (L) flat on metal surfaces, whereas molecules in a multilayer are "standing" (S) with their long axis close to the surface normal.[68] Figure 6a shows experimental UPS spectra of DH6T on Ag(111) in the monolayer and multilayer regime: all the three low-binding-energy peaks, which are derived from the highest occupied molecular orbital (HOMO), the HOMO-1 and the HOMO-2, are at lower binding energies (by 0.6 eV) for the S-regime compared with the L-regime. To understand the physical origin of this binding-energy shift, the XPS technique was used to investigate whether the core levels are affected in the same way as the valence levels. The XPS spectra of the sulfur 2p core levels showed that whereas only one doublet ($2p_{3/2}$ at 164.40 eV and $2p_{1/2}$ at 165.65 eV) is observed in the L-regime, a second doublet appears in the S-regime which is shifted by 0.6 eV toward lower binding energy (Figure 6c). This demonstrates that such combined UPS and XPS studies can be used to study interfacial electronic structures and provide in-depth understanding of experimental phenomena.

UPS, independently or in combination with inverse photoemission spectroscopy (IPES), can be used to measure the valence band and conduction band (HOMO and LUMO) positions with respect to the metal Fermi level and the presence of any interfacial dipoles, which are normally used to calculate carrier injection barriers in OTFTs in actual operation.[69−71] UPS can also be employed to measure the change of the work function of a metal at a metal−organic interface[72] or the electronic structure of an organic semiconductor−dielectric interface.[73] Although work in this field is still ongoing, photoelectron spectroscopy will receive more attention in the future by virtue of its role in studying interfacial electronic structures.

2.2.3. Fourier Transform Infrared Spectroscopy. Fourier transform infrared spectroscopy (FTIR) is widely used to collect infrared spectra. Instead of recording the amount of energy absorbed when the frequency of the infrared radiation is varied (by a monochromator), the IR radiation is guided through an interferometer. After passing through the sample, the measured signal is the interferogram. Performing a Fourier transform of this signal data results in a spectrum identical to that from conventional infrared spectroscopy.[74] One of the most outstanding characteristics of FTIR is that the information at all frequencies is collected simultaneously, and this allows multiple spectra to be collected and averaged, resulting in an improvement in
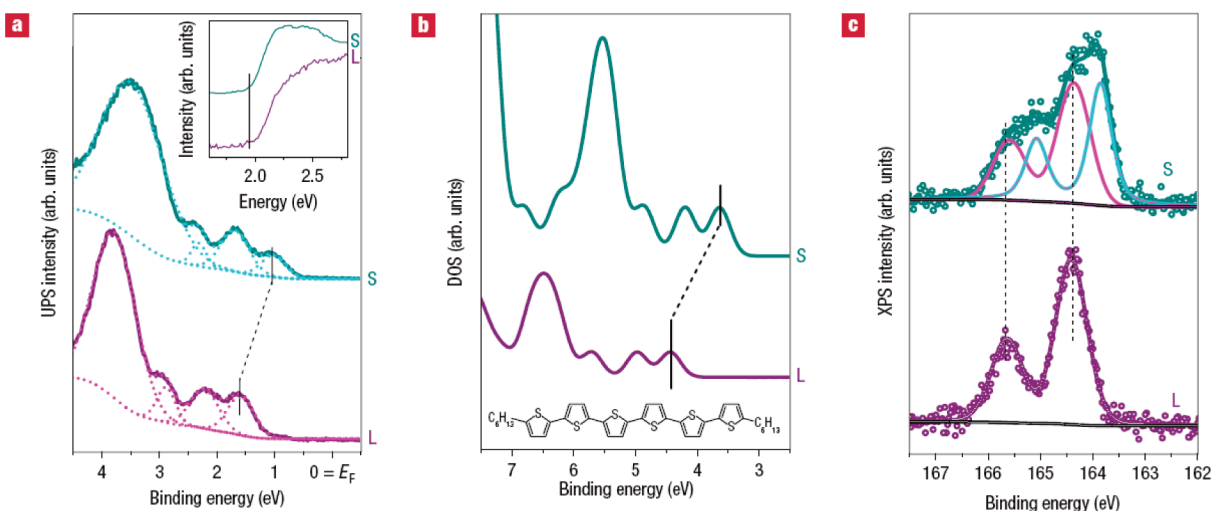
Figure 6. Experimental and theoretical photoelectron spectra of DH6T. (a) Experimental UPS spectra showing the valence region of 4 Å of DH6T (purple), and 40 Å layers of DH6T (cyan) on Ag(111), corresponding to a flat-lying monolayer (L) and a second standing layer (S), respectively. The dotted lines indicate the least-squares fit to determine the peak positions. The inset shows the secondary-electron cutoffs used to determine the work function of the respective samples. (b) DFT-calculated density of states (DOS) of a single flat-lying (purple) and standing (cyan) DH6T molecule; the origin of the energy scale is the respective vacuum level. The inset shows the chemical structure of DH6T. (c) Experimental XPS spectra in the sulfur 2*p* region for 4 Å (purple) and 40 Å (cyan) layers of DH6T on Ag(111), corresponding to a flat-lying monolayer (L) and a second standing layer (S), respectively. Reprinted with permission from *Nature* (http://www.nature.com), ref 66. Copyright 2008 Nature Publishing Group.

sensitivity. Applications of the FTIR technique in the study of OTFTs focus on revealing details about the molecular structure of the semiconductor material based on analysis of its absorption characteristics.[75,76]

Recently, Zhuo and co-workers used FTIR to reveal photo-induced doping that involves both oxygen and water dissolved in a polymer matrix when exposed to light.[75] For example, they investigated the effect of water and light on regioregular-poly(3-hexylthiophene) (rr-P3HT) by analyzing the spectroscopic changes after exposure to different environments (Figure 7). Upon exposure to the ambient atmosphere even in the dark, broad absorption bands that are characteristic of molecular H_2O, molecular CO_2, or even hydrogen-bonded H_2O dimers and trimers were found (Figure 7b), indicating that H_2O and CO_2 are easily sorbed into the P3HT matrix. These features persist throughout the experiment (Figure 7c) and confirm that equilibrium was attained. The FTIR technique therefore conclusively shows that the thiophene backbone of rr-P3HT is readily perturbed by sorption of H_2O, O_2, and/or CO_2.

In addition, Lee and co-workers used FTIR to investigate the molecular structure of aminopropylsiloxane films as a function of the curing temperature.[77] It was possible that Si−N bonds could be formed at 250 °C from the aminopropylsilsesquioxane structure; this is very interesting, since it introduces new chemistry into the cross-linking of silsesquioxane structures which can be used in fabricating dielectric thin films. Furukawa and co-workers employed the FTIR technique to investigate carriers induced by field effects in polymer TFTs.[78] The bands observed in the FTIR difference-spectra were attributed to the carriers injected into the polymer layers under the application of a negative gate bias. The wavenumber of the band around 1300 cm^{-1} depends on the gate voltage, indicating that the structure of the carrier depends on the carrier concentration. Grazing angle attenuated total reflectance FTIR (GATR-FTIR) spectroscopy was performed by Ito and co-workers[79] in order to investigate monolayer density and ordering. They found that

spin-cast films showed similar GATR-FTIR spectra to the most compressed and highly ordered Langmuir−Blodgett (LB) films, which indicate that the spin-cast and LB films have a similar monolayer density and high degree of order. The broad applications of FTIR technique in the study of OTFTs demonstrate that this technique is very useful and that infrared absorption measurements can provide valuable structural information.

2.2.4. IR + Visible Sum-Frequency Generation (SFG) Vibrational Spectroscopy. IR + visible sum-frequency generation (SFG) vibrational spectroscopy is a surface-sensitive technique for the study of surface properties. This technique makes use of a wave mixing process that mixes two input waves at frequencies $\omega_{visible}$ and ω_{IR} and generates an output at $\omega_{sum} = \omega_{visible} + \omega_{IR}$. As a second-order nonlinear optical process, SFG is electric dipole forbidden in a centrosymmetric medium but necessarily allowed at an interface where the inversion symmetry is broken. Consequently, it is intrinsically surface specific. Surface vibrational spectra can be obtained through resonant enhancement when ω_{IR} scans over surface vibrational resonances, providing information about the composition.[80,81] SFG surface vibrational spectroscopy has been applied to surface and interface studies in many fields[82] and has been used to investigate interfaces in OTFTs.

Ye and co-workers probed interfaces in organic field-effect transistors (OFETs) in situ during operation using SFG,[83] and they observed strong correlations between the structure and the electronic properties of organic semiconductors at the dielectric−semiconductor interface. SFG spectra were taken while V_G was tuned from −80 V to +80 V, all at $V_{SD} = 0$ V (Figure 8). An increase in the ratio of the CH_2 symmetric stretch (CH_2-ss) peak (2845 cm^{-1}) to that of the CH_3 symmetric stretch (CH_3-ss) peak (2880 cm^{-1}) was observed when increasing negative V_G, while no discernible change in the peak intensity ratio was observed at positive V_G. Additionally, in the SFG spectra of a thicker semiconductor film, they observed that the increase in the peak intensity ratio of CH_2-ss/CH_3-ss with increasing negative
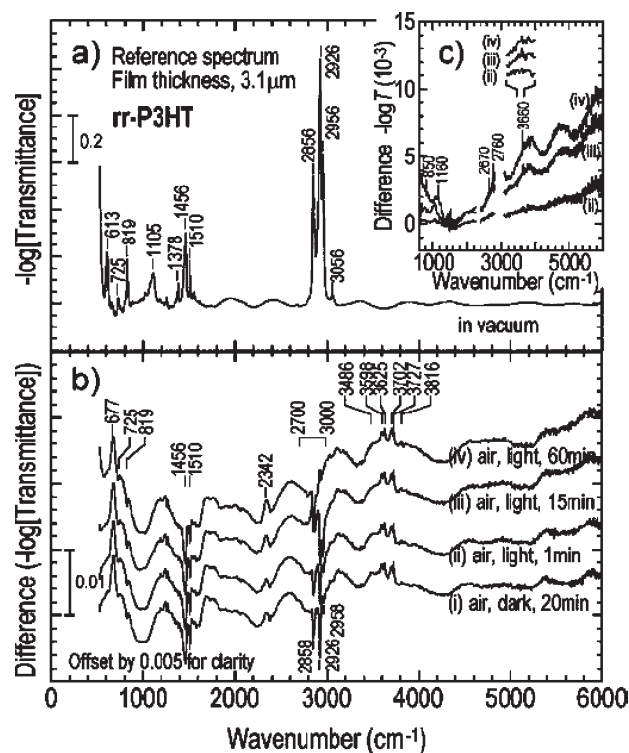
Figure 7. FTIR spectra of a rr-P3HT film acquired sequentially after different in situ exposures to cleanroom air. (a) Reference spectrum of the film in a vacuum. (b) Difference spectra obtained by subtracting the spectrum of the film in a vacuum, offset for clarity. Spectra of gas-phase H_2O and CO_2 have also been removed for clarity. (c) Difference spectra obtained by subtracting the spectrum of the film in air and in the dark: spectra labels are the same as in (b). "Air" is cleanroom air (22 °C, relative humidity (RH) 60%), and "light" corresponds to an absorbed photon flux intensity of 2.0×10^{15} ph s^{-1} cm^{-2}. Reprinted with permission from ref 75. Copyright 2009 Wiley-VCH Verlag.

V_G was approximately halved, therefore confirming that the changes in the signal observed are from the dielectric−semiconductor interface. These results suggest that field effects on electronic conduction in OTFTs are correlated to interfacial nonlinear optical characteristics.

Especially when combined with other surface-sensitive techniques such as AFM and contact angle goniometry, SFG vibrational spectroscopy is a very powerful technique for surface studies. For example, Zhang and co-workers used a combination of these surface-sensitive techniques to study the surface properties of polymer blends.[81] They found that the surface structure of a polymer blend is very different from the bulk, and a more complete picture of the surface of a polymer blend was obtained by using these techniques. Polymer blends are receiving more attention in OTFT research, and studies using SFG and other surface-sensitive techniques can lead to a better fundamental understanding of the interfacial phenomena in such polymer blends.

2.2.5. Micro-Raman Spectroscopy. Micro-Raman spectroscopy is a spectroscopic technique used to study vibrational, rotational, and other low-frequency modes in a system by means of a microscope lens. It relies on inelastic scattering, or Raman scattering, in which the difference in energy between the absorbed and re-emitted photons corresponds to the energy required to excite a molecule to a higher vibrational mode. When
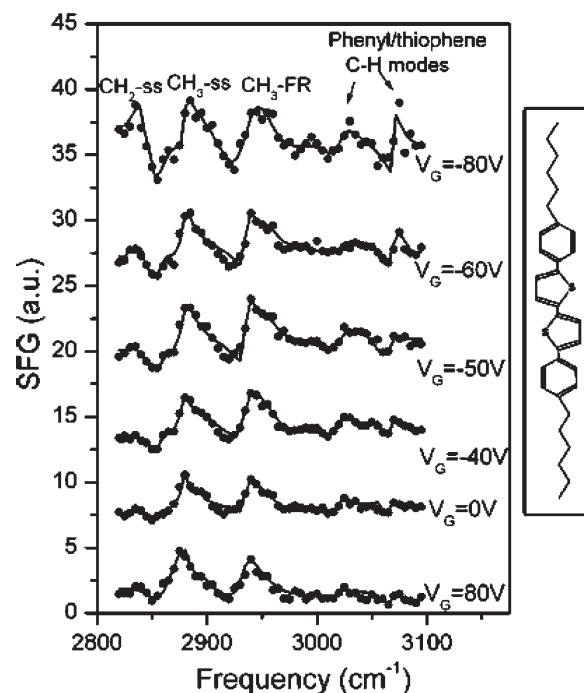

Figure 8. SFG spectra in ssp polarization (s-polarized sum-frequency (SF) out, s-polarized visible input, and p-polarized infrared input) of the 5,5′-bis(4-hexylphenyl)-2,2′-bithiophene (6pttp6; molecular structure shown in the right-hand panel) OFET recorded at different V_G. The black dots represent raw data points, while the solid line is a fit of the data to the expected SF signal intensity equation[80] consisting of nonresonant and resonant terms. Reprinted with permission from ref 83. Copyright 2006 American Chemical Society.

high intensity laser radiation with wavelengths in either the visible or near-infrared regions of the spectrum is passed through the sample, photons from the laser beam are absorbed by the molecules, exciting them to a virtual energy state. If the final vibrational state of the molecule is more energetic than the initial state, then the emitted photon will be shifted to a lower frequency in order for the total energy of the system to remain balanced. This shift in frequency is designated as a Stokes shift. If the final vibrational state is less energetic than the initial state, then the emitted photon will be shifted to a higher frequency, and this is designated as an anti-Stokes shift. Raman scattering is therefore an example of inelastic scattering because of the energy transfer between the photons and the molecules during their interaction. A change in the molecular polarization potential with respect to the vibrational coordinate is required for a molecule to exhibit a Raman effect. The magnitude of the polarizability change will determine the Raman scattering intensity. The pattern of shifted frequencies is determined by the rotational and vibrational states of the sample.

The most advanced type of micro-Raman spectroscopy which has been used to study OTFTs is resonance Raman (RR) spectroscopy, which provides information about the vibrations of organic molecules. In resonance Raman spectroscopy, when the frequency of the laser beam is tuned to be near an electronic transition (resonance), the vibrational modes associated with that particular transition exhibit a greatly increased Raman scattering intensity. This usually overwhelms Raman signals from all of the other transitions. For instance, resonance with a $\pi-\pi^*$ transition enhances stretching modes of the π-bonds
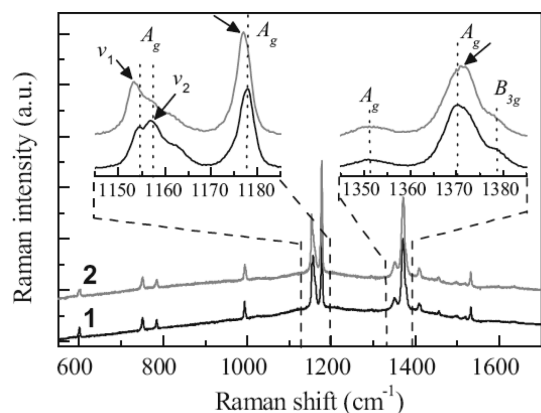
Figure 9. Raman spectra (λ_{exc} = 633 nm) of pentacene within the channel of an OFET device: (1) before operation, (2) after continuous operation for 20 h, after which the specimen was kept in dry air conditions for 20 h. The dashed lines serve as guidelines to the eye. Reprinted with permission from ref 84. Copyright 2008 Wiley-VCH Verlag.

involved in the transition, while the other modes remain unaffected. The main advantage of RR spectroscopy over conventional Raman spectroscopy is that the resonant enhancement of Raman intensities gives the level of sensitivity required to study intermolecular coupling effects in the organic films used in OTFTs.

Cheng and co-workers used RR spectroscopy to analyze the microstructural modifications of pentacene in the small active channel of an OTFT during device operation.[84] In their experiment, spectra were excited using a red excitation line (λ_{exc} = 633 nm) with energy located at the absorption peak of pentacene molecules within the crystals.[85] Significant differences were detected in the C—H in-plane bending and C—C aromatic stretching vibrations in the energy ranges 1140—1190 cm^{-1} and 1340—1390 cm^{-1} before and after long-term operation (Figure 9). The former modes are assigned to the motion of atoms located at the end and both sides of the pentacene molecule, and are expected to be dominant compared with the latter modes as a result of an "edge-to-face" stacking of pentacene molecules in a herringbone motif. Therefore, it can be concluded that the intermolecular vibrational coupling energy of the C—H bending modes between pentacene molecules increases after long-term operation, indicating an increased intermolecular force between pentacene molecules after long-term operation.

Additionally, the same group performed micro-Raman techniques which provided accurate information about the molecular structure of pentacene within the active channel during OTFT operation,[86] and also demonstrated that the measured field-effect mobility of pentacene-based OTFTs is strongly related to the C—H bending mode and its splitting.[87] Parylene structures used as a gate dielectric in OTFTs were also characterized by micro-Raman spectroscopy in a study reported by Jakabovic and co-workers,[88] which confirmed the perfect homogeneity and structural properties of the parylene layers. Hosoi and co-workers studied molecular orientation in pentacene films in OTFTs using micro-Raman spectroscopy.[89] They found that the relative intensity of the 1596 cm^{-1} band (B_{3g}) is sensitive to the molecular orientation and therefore demonstrates the different molecular orientations in pentacene films on SiO$_2$ dielectric layers and Au electrodes in these devices. The broad applications

of micro-Raman spectroscopy indicate that it is a powerful technique that can be used to study the changes in the vibrational characteristics of organic semiconductors in OTFTs, which may offer useful information about variations in device properties.

2.2.6. Optical Spectroscopy. Optical absorption spectroscopy is the most commonly used optical spectroscopic techniques in OTFTs, which can provide just as important insight into molecular packing and electronic structure of organic semiconductors in FETs. Absorption spectroscopy refers to spectroscopic techniques that measure the absorption of radiation, as a function of frequency or wavelength, due to its interaction with a sample. The sample absorbs energy, that is, photons, from the radiating field. The intensity of the absorption varies as a function of frequency, and this variation is the absorption spectrum. Infrared and ultraviolet—visible spectroscopy are particularly common in analytical applications.

A material's absorption spectrum is the fraction of incident radiation absorbed by the material over a range of frequencies. The absorption spectrum is primarily determined by the atomic and molecular composition of the material. Radiation is more likely to be absorbed at frequencies that match the energy difference between two quantum mechanical states of the molecules. The absorption that occurs due to a transition between two states is referred to as an absorption line and a spectrum is typically composed of many lines. The frequencies where absorption lines occur, as well as their relative intensities, primarily depend on the electronic and molecular structure of the molecule. The frequencies will also, though, depend on the interactions between molecules in the sample, the crystal structure (in solids), and several environmental factors (e.g., temperature, electromagnetic field).

Another type of spectroscopy, that is, luminescence spectroscopy, is usually coupled with absorption spectroscopy to provide more information about optical properties of organic semiconductors in FETs. Luminescence is the generation of light without heat. Various types of luminescence are often distinguished according to the source of the energy which excites the emission. When the light energy emitted results from ultraviolet, visible, or infrared radiation, the emission is called photoluminescence, and electroluminescence if the energy comes from the application of an electric field. Emission has a reciprocal relationship with absorption. Emission is a process by which a substance releases energy in the form of electromagnetic radiation. Emission can occur at any frequency at which absorption can occur, and this allows the absorption lines to be determined from an emission spectrum.

The optical properties of the small molecules or polymers can be investigated by UV—visible and photoluminescence (PL) spectroscopies both in solutions and as thin films. For example, the substituent effect for a series of organic semiconductors is more pronounced if the whole absorption and emission spectra will be compared, which reflects the interplay of molecular structure, substitution, core length, and solid-state packing.[90—92] Recently, the Sirringhaus'group demonstrated the integration of a rib waveguide distributed feedback structure into a light-emitting polymer field-effect transistor (LEFET).[93] In electroluminescence (EL) spectrum studies, they found the position of the recombination zone has an impact on the EL spectrum of the surface emission that is induced by the second-order distributed feedback grating. The incoupling into the resonant mode is optimized when the recombination zone is positioned above the waveguide ridge, and the resonance wavelength, indicated by a

characteristic Bragg dip, can be shifted by varying the grating period and duty cycle, as well as the ridge height.

Charge modulation spectroscopy (CMS) is a powerful technique to image charged-induced absorptions in an operational transistor device. In CMS an electric field is used to induce charges in the semiconductor, by applying a gate bias in a transistor. CMS is applied to an all-polymer transistor using poly[(9,9′-dioctylfluorene)-*co*-bithiophene] (F8T2) as the semiconducting polymer.[94] With CMS, the optical absorptions due to the presence of the charges, which are responsible for the transistor current, can be measured in an operational device. An alternating voltage is applied to the gate, modulating the charge density in the device, and the change in transmission as a function of this modulation is recorded for a range of wavelengths. This allows direct observation of the charge carriers in the operational device via their spectroscopic signature; the technique is by design very sensitive to the properties of the semiconductor—dielectric interface.

2.3. Other Characterization Techniques

The basic rules of design and control of the organic semiconductor and device characteristics should be clearly understood in order to facilitate the development of OTFTs. In addition to the above-mentioned characterization techniques, many other experimental techniques are commonly used to study the complicated chemical and physical phenomena in OTFTs. These are reviewed in this section, and include X-ray scattering techniques, electron spin resonance (ESR), neutron reflectivity (NR), dynamic secondary ion mass spectrometry (DSIMS), optical second harmonic generation (SHG), polarized optical microscopy (POM), and transmission electron microscopy (TEM). In addition, electrical characterization techniques are selectively mentioned in this section.

2.3.1. X-ray Scattering. X-ray scattering techniques are a family of nondestructive characterization techniques which reveal information about the crystallographic structure, chemical composition, and physical properties of materials and thin films. These techniques are based on observing the scattered intensity of an X-ray beam hitting a sample as a function of incident and scattered angle, polarization, and wavelength or energy. A series of X-ray scattering techniques have been successfully employed to study OTFTs, including powder diffraction (XRD), grazing incidence X-ray diffraction (GIXD), X-ray reflectivity, and wide-angle X-ray scattering (WAXS). The most popular X-ray scattering technique used to study OTFTs is XRD, which is commonly used to characterize the crystallographic structure, crystallite size (grain size), and preferred orientation in polycrystalline or powdered solid samples (If there is a bias of orientations of one or more particular crystallographic plane, then this is known a preferred orientation. Preferred orientation is likely the most common cause of intensity variations in XRD powder experiments). The other three techniques have begun to receive more attention for the study of OTFTs, and as a result they will be reviewed in detail here.

Grazing incidence X-ray diffraction (GIXD) is actually based on the X-ray total reflection phenomenon whereby X-rays are known to be totally reflected at the surface of flat substances and strongly attenuated at small incident angles less than a critical angle relative to the surface plane. According to the geometrical setup of the instrument, the diffracted radiation can be collected by a one-dimensional (1-D) position-sensitive detector or a two-dimensional (area) detector. The 1-D GIXD techniques have

been commonly used to analyze in-plane crystal structures of thin surface layers, whereas 2-D GIXD can simultaneously probe both in-plane and out-of-plane crystal structures. In principle, in 1-D GIXD, the 1-D detector must be scanned over a range along the horizontal scattering vector q_{xy} and integration over the whole q_z window of the 1-D detector yields the Bragg peaks. Simultaneously, the scattered intensity recorded in channels along the 1-D detector, but integrated over the scattering vector q_{xy} in the horizontal plane across a Bragg peak, produces q_z-resolved scans called Bragg rods, which can also yield useful structural information.

X-ray reflectivity is an analytical technique for determining thickness, roughness, and electron density of monolayer and multilayer thin films. The basis of the technique is the reflection of a beam of X-rays from a flat surface and measurement of the intensity of X-rays reflected in the specular direction (i.e., when the reflected angle is equal to the incident angle). If the interface is not perfectly sharp and smooth then the reflected intensity will deviate from that predicted by the Fresnel reflectivity equation. The deviations can then be analyzed to obtain the density profile of the interface normal to the surface. This technique has been particularly applied to probe the electron density profile in organic monolayer or multilayer thin films in OTFTs.[95−97]

A combination of GIXD and X-ray reflectivity often gives more information about in-plane and out-of-plane order in organic thin films. Recently, Smits and co-workers have used GIXD and X-ray reflectivity to establish the extent of order in a SAM.[97] The longer-wavelength oscillations with maxima at about 0.14 and 0.30 Å^{-1} seen in Figure 10a originate in the SAM layer. The SAM is characterized by comparing the measured data with a calculated reflectivity curve, and the good data fit is consistent with a perfect out-of-plane order with the molecules standing almost perpendicular to the substrate (as shown in the inset in Figure 10a). The characteristic SAM (11 L), (02 L), and (12 L) in-plane Bragg rods are seen in the GIXD spectra shown in Figure 10b. The inset in Figure 10b shows the presence of Bragg rods at in-plane scattering vectors of 1.407, 1.635, and 1.997 Å^{-1}, indicative of two-dimensional crystalline in-plane order in the SAM.

For semiconducting thin films, GIXD profiles displayed by both the horizontal and vertical scattering summation of the crystals distributed in the films can provide considerable insight into the variation with thickness of the crystal packing and orientation in the films ranging from the monolayer in direct contact with the substrate through the subsequent multilayer. Therefore, it is very suited for characterization of the in-plane π-stacking of organic thin films in OTFTs, such as pentacene,[98] P3HT,[99,100] and other polymer thin films.[101−104] These examples of results obtained using GIXD indicate that GIXD is a valuable method for characterizing the molecular packing and orientation in semiconductor thin films.

Similarly, wide-angle X-ray scattering (WAXS) can also be used to determine the crystalline structure of polymers. In contrast to GIXD, WAXS specifically refers to the analysis of Bragg peaks scattered at wide angles (scattering angles 2θ larger than 5°). WAXS is normally employed to investigate the organization of polymer films in OTFTs as it can easily determine the chain-to-chain spacings, π-stacking distances, and structural in-plane anisotropy in such materials.[105,106] WAXS is a diffraction technique where only crystallites which are parallel to the substrate surface diffract, so perpendicular and parallel WAXS measurements are often performed to confirm the
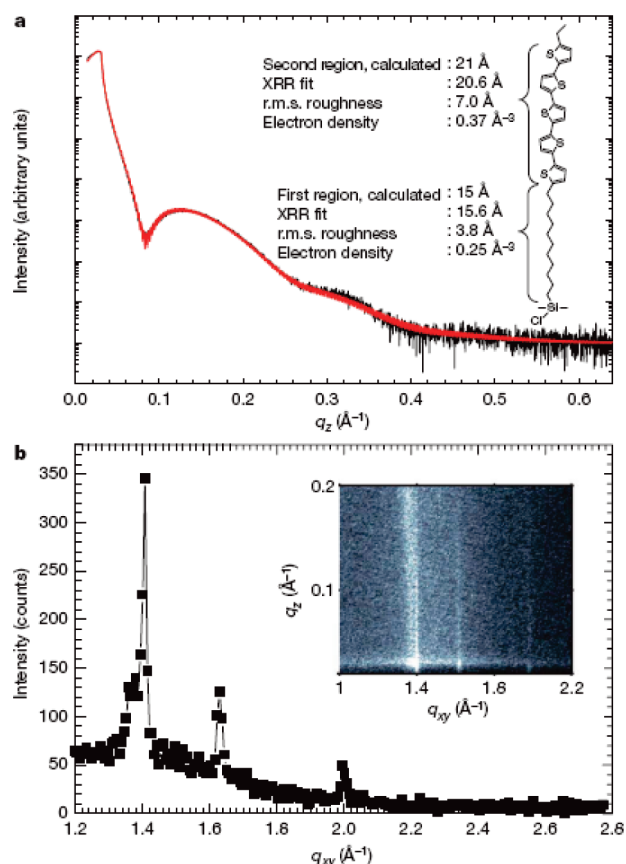
3367

dx.doi.org/10.1021/cr1001904 |*Chem. Rev.* 2011, 111, 3358–3406

Figure 10. SAM microstructure. (a) X-ray reflectivity (XRR) of an SAM on silicon dioxide. The solid red line is the fit to the experimental data. The inset shows the chemical structure of the molecule used in the SAM and the thicknesses, root-mean-square (r.m.s.) roughness values and electron densities obtained from the fit. The measurements reveal a layer thickness equivalent to one monolayer. (b) Synchrotron grazing-incidence diffraction measurements showing the diffracted intensity as a function of in-plane scattering vector, q_{xy}. The inset shows the presence of Bragg rods at in-plane scattering vectors of 1.407, 1.635, and 1.997 Å^{-1}, indicative of two-dimensional crystalline in-plane order in the SAM. Reprinted with permission from *Nature* (http://www.nature.com) ref 97. Copyright 2008 Nature Publishing Group.

molecular orientation and order (Figure 11);[106] these have a significant influence on the charge carrier mobilities in polymer transistors.

In conclusion, X-ray scattering techniques have been successfully employed as powerful characterization tools to measure in-plane and out-of-plane crystal structures in OTFTs, determine thickness and electron density of thin films of samples, and investigate the state of the crystal packing and orientation in such films. These techniques are likely to become more important in the characterization of OTFTs, especially when combined with other experimental and computational techniques.

2.3.2. Electron Spin Resonance. The electron spin resonance (ESR) technique is a powerful and sensitive method for the characterization of the electronic structures of materials with unpaired electrons. ESR is a magnetic resonance technique, based on the interaction of unpaired electron spins with an external magnetic field, and it is widely used to study organic or inorganic systems that have one or more unpaired electrons, such as organic and inorganic free radicals or organic charge transfer complexes. The
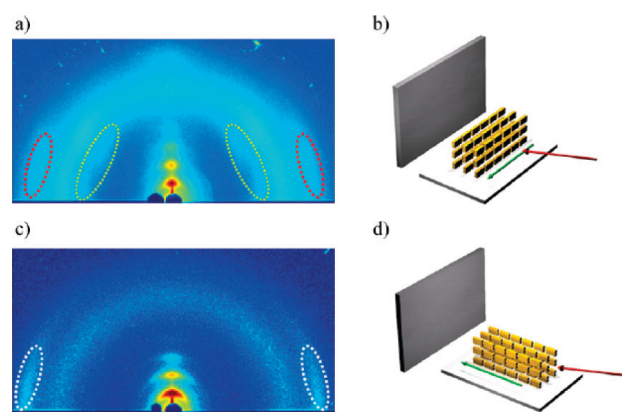

Figure 11. Grazing incidence WAXS of dip-coated (molecular-weight, $M_n = 50$ kg mol^{-1}) cyclopentadithiophene−benzothiadiazole copolymer (CDT-BTZ) films after annealing. The patterns were recorded (a, b) perpendicular to (red and yellow dashed lines suggest the scattering related to the repeat units along the polymer backbone) and (c, d) parallel to the dipping direction (white dashed lines point toward the scattering from the in-plane π-stacking). The green arrow in the schematic drawings indicates the dipping and alignment direction, while the red arrow corresponds to the incident X-ray beam. Reprinted with permission from ref 106. Copyright 2009 Wiley-VCH Verlag.

Figure 12. First-derivative field-induced ESR signals obtained for regioregular P3HT with various V_{gs} values without applying V_{ds}. The external magnetic field is perpendicular to the substrate. The inset shows the V_{gs} dependence of the induced spin concentration per thiophene monomer unit. The solid line shows a linear guide to the eye. Reprinted with permission from ref 108. Copyright 2009 American Institute of Physics.

detailed principles of ESR can be seen elsewhere,[107] and we here focus on its applications in the study of OTFTs.

The ESR technique has been shown by Tanaka and co-workers[108] to be a viable method of accurately obtaining the concentration of the charge carriers in operating FETs. The g-value ($g = 2.003$) of field-induced ESR signals defined in Figure 12 indicates that the injected carriers are positive polarons of regioregular P3HT associated with unpaired π-electrons. The inset shows that the spin concentration starts to linearly increase as $|V_{gs}|$ increases and the spin density tends to saturate above about 0.2% for higher $|V_{gs}|$ values ($V_{gs} < -40$ V), indicating the formation of spinless charged states such as bipolarons. This phenomenon has not been observed in the case of pentacene,[109,110] showing that the formation of spinless charged states is an intrinsic property of the P3HT polymer chain.

Figure 13. Neutron reflectivity profiles and fitted concentration profiles (in the insets) of deuterium-labeled d-TIPS-pentacene in the ratio 1:1 (by mass) blended films of d-TIPS-pentacene and PαMS for (a) the blend with PαMS of $M_{r,n} \approx 1.3$ kg·mol^{-1} and (b) the blend with PαMS of $M_{r,n} \approx 575$ kg·mol^{-1} in the as-cast and the annealed (20 min at 100 °C) films. The fitted reflectivity curve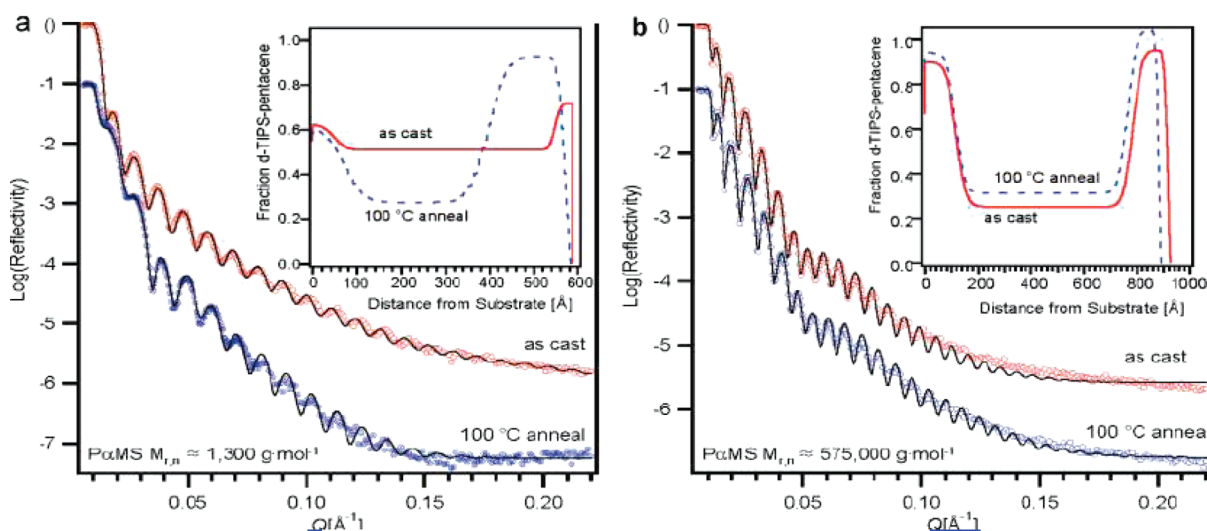s from the modeled density profiles are shown by black solid lines. Reprinted with permission from ref 116. Copyright 2008 American Chemical Society.

In principle, OTFTs based on organic radicals should be also capable of characterization by ESR, although cases are rare in practice because of the instability of organic radicals. Wang and co-workers used the ESR technique to characterize an OTFT utilizing 1-imino nitroxide pyrene radicals as the semiconductor layer.[111] The ESR curves consist of a broad single line, without hyperfine splitting, and the g value in the powder form is 2.00748, consistent with that in film form. Sugiyama and co-workers analyzed the angular variation of the line position (g value) of ESR spectra of P3HT and revealed that the thiophene ring of P3HT is oriented along the substrate normal axis.[112] The ESR line width varied as a function of angular rotation, indicative of 1-D spin−chain interactions in the P3HT thin films with a linear network of spin−chains. The ESR technique can also be used to characterize charge transfer systems in which unpaired electrons can be detected.[113,114] In particular, ESR provides definitive evidence of the presence of organic systems with one or more unpaired electrons in organic electronic or magnetic devices.

2.3.3. Neutron Reflectivity. Neutron reflectivity (NR) is a relatively new experimental technique for measuring the structure of thin films. Neutron reflectivity is a specular reflection technique, where the angle of the incident beam is equal to the angle of the reflected beam. The reflection is usually described in terms of a momentum transfer vector, denoted q_z, which describes the change in momentum of a neutron after being reflected from the material. Conventionally, the z-direction is defined to be the film normal direction, and for specular reflection, the scattering vector has a z-component only. A typical neutron reflectivity plot displays the reflected intensity (relative to the incident beam) as a function of the scattering vector, and then the Abeles matrix formalism or the Parratt recursion can be used to describe the specular signal arising from the interface.[115] This technique has been recently employed to provide structural information about molecule−polymer thin film blends in OTFTs, since it allows the molecule−polymer blend depth profiles to be investigated with nanometer-scale resolution.

Recently, Kang and co-workers used the NR technique to investigate the segregation characteristics of molecule−polymer

blend systems.[116] The reflectivity data in Figure 13a indicated that film blends of bis(triisopropyl-silylethynyl) pentacene (TIPS-pentacene) with a low molecular weight insulating polymer poly(α-methylstyrene) (PαMS) exhibit distinctly different features for as-cast films and films annealed at 100 °C, as indicated by the appearance in the spectra of the annealed films of a longer wavelength envelope superimposed on the short wavelength features observed for the as-cast films. Upon annealing the film blend at 100 °C, a nearly pure TIPS-pentacene layer of thickness ca. 177 Å at the air surface and a PαMS-rich middle layer of thickness ca. 326 Å were formed; these facilitate high field-effect mobilities of this blend when used in a top-gated OTFT structure. In contrast, the phase-segregated structure obtained with high molecular weight PαMS was different, with a nearly pure TIPS-pentacene layer (with thickness ca. 134 Å) formed not only at the air surface but also at the silicon substrate interface (with thickness ca. 117 Å) (Figure 13b). This feature is critically important for fabricating bottom-gate/bottom-contact OTFT structures, provided that the TIPS-pentacene molecules in the segregated thin films form a highly crystalline structure with the π−π stacked molecular layers oriented parallel to the film surface.

There is an increasing trend to fabricate organic transistors by using low-cost, large-area printing-like manufacturing techniques. Methods that employ solution-processed blended films of a semiconducting molecule and an insulating polymer as the active layer not only lead to high performance of the resulting OTFT devices but also allow the simple fabrication of transistors by printing manufacturing techniques. The NR technique is a powerful tool to study the segregation characteristics of such molecule−polymer blend systems and allows the most critical structural information underlying the observed electrical properties of the thin blend active layer to be obtained.

2.3.4. Dynamic Secondary Ion Mass Spectrometry. Secondary ion mass spectrometry (SIMS) is a technique used in materials science and surface science to analyze the composition of solid surfaces and thin films by sputtering the surface of a specimen with a focused primary ion beam and collecting and
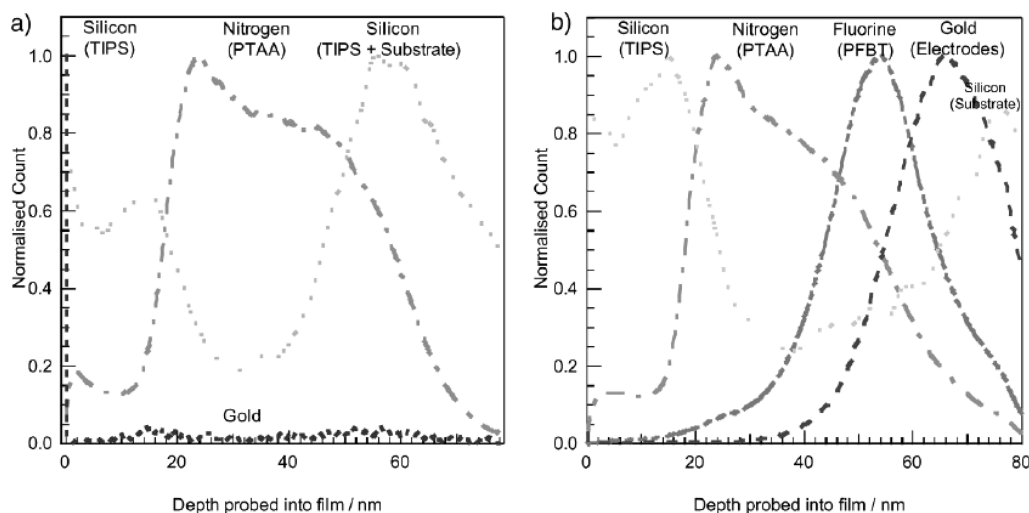
Figure 14. DSIMS depth profile of a TIPS-pentacene: PTAA film on a silicon substrate with a pentafluorobenzenethiol (PFBT)-treated gold source and drain electrodes. The graphs show the phase separation, (a) in the channel and (b) over the electrodes of the TIPS-pentacene material (as indicated by the Si signal), which is closer to the air interface than the PTAA (as indicated by the N signal). Reprinted with permission from ref 118. Copyright 2009 Wiley-VCH Verlag.

analyzing ejected secondary ions. These secondary ions are measured with a mass spectrometer to determine the elemental, isotopic, or molecular composition of the surface. In the field of surface analysis, dynamic SIMS (DSIMS) is the process involved in bulk analysis, closely related to the sputtering process, using a DC primary ion beam and a magnetic sector or quadrupole mass spectrometer. DSIMS is a most sensitive surface analysis technique and can be used to investigate the distribution of chemical species on the surfaces and composition depth profiles of device structures in OTFTs.[117,118]

For example, Hamilton and co-workers used DSIMS to confirm the distribution of the components in a TIPS-pentacene/poly[bis(4-phenyl)(2,4,6-trimethylphenyl)amine] (PTAA) blend.[118] Figure 14 shows that the first signal to appear is the Si from the silyl group on the TIPS-pentacene molecule. The nitrogen signal (from the PTAA) can be seen to reach to a maximum of approximately 20–30 nm beneath the top surface. The broadening in the F peak (which is a monomolecular layer <1 nm thick) is due to a combination of a variable rate of etching for different materials in the layer and a slight spread in the energy density of the Cs ion beam. The gold signal rises immediately afterward as the profiling reached the source and drain electrodes, and finally the Si signal rises once more indicating profiling into the glass substrate. A depth profile of an area between the source and drain electrodes showed the same distribution of TIPS and PTAA, indicating that the phase separation occurs over the entire area of the spin-coated sample.

The ability of DSIMS to examine the phase separation in molecule–polymer blends will make it increasingly popular for characterization of blended systems in OTFTs. Moreover, as DSIMS is able to detect elements present in the parts per billion range, it is recognized as a very sensitive surface analysis technique for investigation of the distribution of chemical species on a surface and is therefore a very useful source of information about the surfaces or interfaces in OTFTs. It is therefore an alternative to other techniques mentioned above for interface analysis and phase separation of blended systems in OTFTs.

2.3.5. Optical Second Harmonic Generation. Optical second harmonic generation (SHG) is a nonlinear optical process, in which photons interacting with a nonlinear material are effectively "combined" to form new photons with twice the energy, and therefore twice the frequency and half the wavelength of the initial photons. It is a special case of sum-frequency generation. In a SHG experiment, the light source is an optical parametric oscillator (OPO) pumped by the third-harmonic radiation of a Q-switched neodymium:yttrium aluminum garnet (Nd:YAG) laser. Selecting an appropriate wavelength is important in order to observe the SHG signal from a sample effectively because the SHG intensity strongly depends on the fundamental wavelength. For example, when a pentacene OTFT device was examined, the electric field induced SHG (EFISHG) spectrum of vacuum-deposited pentacene films determined that the fundamental wavelength was fixed at 1120 nm in the experiment.[119,120] Finally, a charge coupled device camera and guide laser are attached to the microscopic SHG measurement system.

Electric field induced SHG (EFISHG) is commonly used to probe the electric field distribution along the OFET channel and the process of channel formation in OTFTs, which is the first step to understanding the operation of a device.[119−121] Recently, Yamada and co-workers have used the EFISHG technique to examine the electric field distribution along the pentacene TFT channel for the off and on states of an FET.[119] Figure 15a shows that the SHG is not enhanced over the entire region under the no-bias condition. On the other hand, when $V_{ds} = -100$ V and $V_g = 0$ V (off state characteristics of the FET), the SHG is enhanced, particularly in the region near the edge of the drain electrode. However, this SHG enhancement decreases when $V_{ds} = -100$ V and $V_g = -100$ V (on state characteristics of the FET). The explanation is that when the FET is in an off state, a high lateral electric field is formed near the electrode. Consequently, SHG is enhanced near the edge of the drain electrode. In contrast, when the FET is in an on state, holes inject from the source electrode. The holes subsequently accumulate in the FET channel. These injected holes contribute to the modification of the established electric field, which decreases the SHG signal around the drain electrode.

Additionally, as a development of the EFISHG technique, the time-resolved microscopic SHG (TRM-SHG) technique has
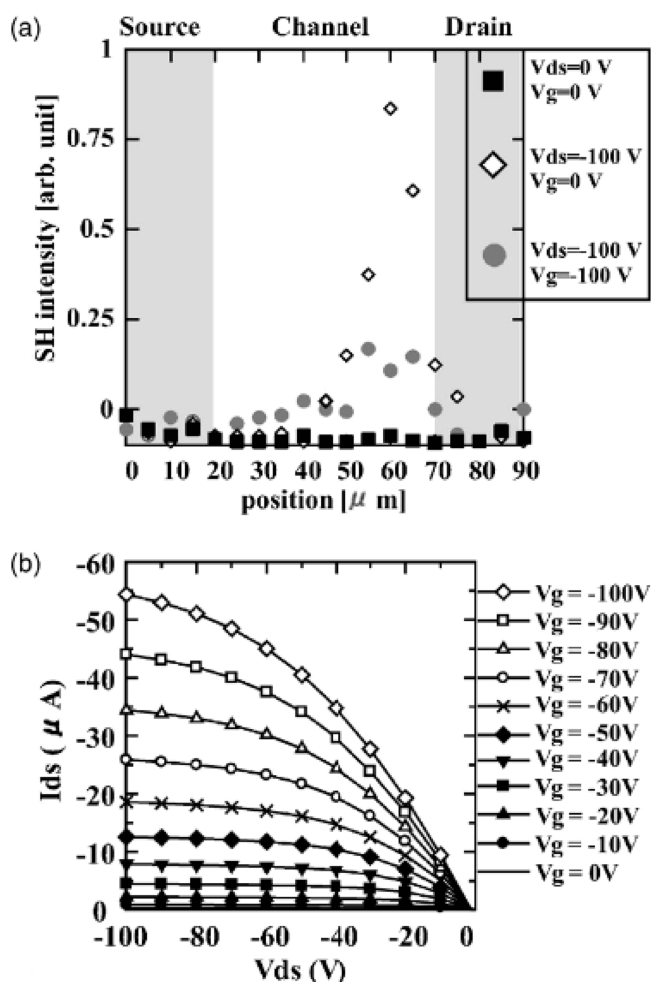
Figure 15. (a) Experimental results of an SHG experiment with a pentacene FET. Full circles, open diamonds, and squares, respectively, represent the SHG intensity for the on, off, and no-bias states. (b) Typical I_{ds}–V_{ds} characteristics of the pentacene FET. Reprinted with permission from ref 119. Copyright 2008 American Institute of Physics.

been developed to directly probe carrier behavior in OFETs. For example, the charge carrier injection mechanism in a pentacene FET was investigated by Nakao and co-workers using the TRM-SHG technique.[122] By probing SHG signals enhanced around two different top electrodes (Au and Ag), they found that charge carrier behavior was regulated by the Schottky effect. As the TRM-SHG technique can also directly probe the transient electric field distribution in the OFET channel with high temporal and spatial resolutions, Manaka and co-workers used this technique to quantitatively study migration of the peak of the electric field[123] and found this migration always follows a diffusion-like behavior under a broad range of experimental conditions.

The SHG technique has been shown to be one of the most powerful techniques for probing charge transport and injection phenomenon in OTFTs. Both EFISHG and TRM-SHG techniques can be successfully used to study OTFTs, such as for evaluating the transient change of the carrier density,[124] and indirectly evaluating the contact resistance[125] and charge carrier behavior as mentioned above. Moreover, the combination of SHG with other probe techniques will help researchers to understand the device physics of OFETs and promote the development of new techniques for probing the electric field.

2.3.6. Polarized Optical Microscopy. Polarized optical microscopy (POM) is capable of distinguishing between isotropic and anisotropic substances, exploiting the optical properties specific to anisotropy, and revealing detailed information concerning the structure and composition of materials that are invaluable for identification and diagnostic purposes. There are two polarizing filters in a polarizing microscope-termed the polarizer and analyzer. When two polarizing filters are crossed, their transmission axes are oriented perpendicular to each other and light passing through the first polarizer is completely extinguished, or absorbed, by the second polarizer, which is typically termed an analyzer. The light-absorbing quality of a dichroic polarizing filter determines exactly how much random light is extinguished when the polarizer is utilized in a crossed pair and is referred to as the extinction factor of the polarizer. Quantitatively, the extinction factor is determined by the ratio of light that is passed by a pair of polarizers when their transmission axes are oriented parallel versus the amount passed when they are positioned perpendicular to each other. In general, extinction factors between 10 000 and 100 000 are required to produce jet-black backgrounds and maximum observable specimen birefringence (and contrast) in polarized optical microscopy.

The POM technique is usually used to study the phase transitions and molecular orientations in macroscopically oriented liquid crystal (LC) films[126] or elucidate the supramolecular organization of discotic materials, which have been successfully implemented in OTFTs.[127] An and co-workers used POM to analyze the morphology and ordering of the phases in two liquid crystal materials based on a perylene diimide (PDI) core.[128] Photographs (Figure 16) of the corresponding devices reveal that the sample with higher mobility (sample PDI1) displays a texture consistent with a columnar discotic LC, while the sample with lower mobility (sample PDI2) has a completely different texture. This suggests that the LC domains in sample PDI1 are much larger than in sample PDI2; the lower mobility in sample PDI2 might then be due to a high density of grain boundaries acting as barriers to transport. Such a difference can result from small differences in the processing conditions—such as melting temperature, cooling rate, shear applied during sample assembly, etc., which in turn affect the morphology and ordering of the phases.

In conclusion, POM provides a vast amount of information about the composition and three-dimensional structure of a variety of samples in OTFTs. Virtually unlimited in its scope, the technique can reveal information about thermal history and the stresses and strains to which a specimen was subjected during formation. Useful in manufacturing and research, POM is a relatively inexpensive and accessible investigative and quality control tool, which can provide information unavailable using any other technique.

2.3.7. Transmission Electron Microscopy. Transmission electron microscopy (TEM) is a microscopy technique whereby a beam of electrons is transmitted through an ultrathin specimen, interacting with the specimen as it passes through. An image is formed from the interaction of the electrons transmitted through the specimen; the image is magnified and focused onto an imaging device. TEMs are capable of imaging at a significantly higher resolution than light microscopes, owing to the small de Broglie wavelength of electrons. This enables the instrument's user to examine fine detail—even as small as a single column of atoms, which is tens of thousands times smaller than the smallest resolvable object in a light microscope. In a TEM instrument, as
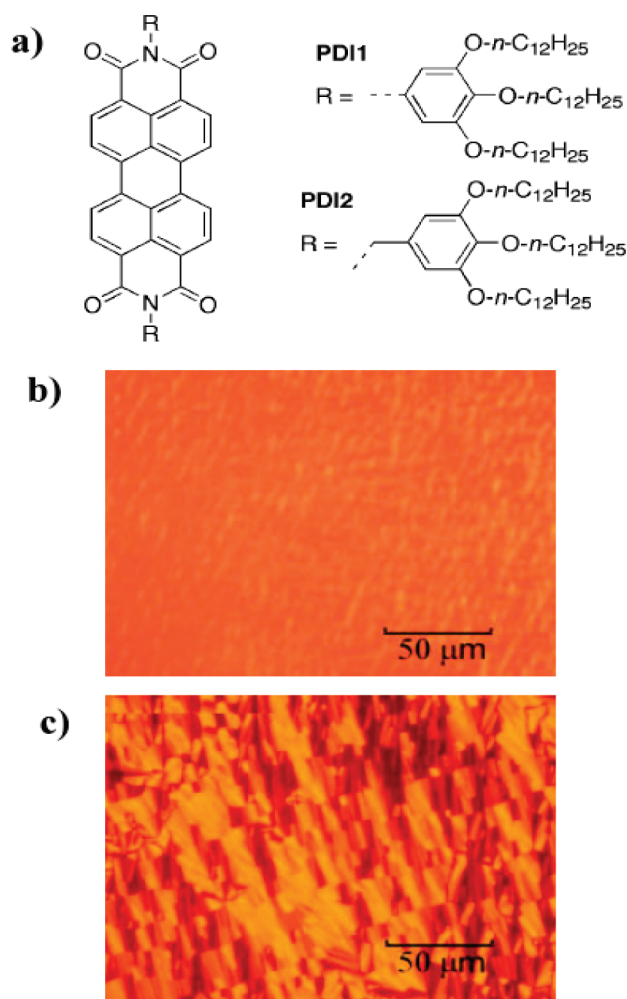
a)

PDI1

R = ⋯

O-*n*-C₁₂H₂₅
O-*n*-C₁₂H₂₅
O-*n*-C₁₂H₂₅

PDI2

R =

O-*n*-C₁₂H₂₅
O-*n*-C₁₂H₂₅
O-*n*-C₁₂H₂₅

b)

50 μm

c)

50 μm

Figure 16. (a) Generalized structure of a perylene diimide (PDI) (left) with the substituents (right) used in the experiment. Polarized optical microscopy images of (b) sample PDI1 and (c) sample PDI2 at room temperature. Reprinted with permission from ref 128. Copyright 2005 Wiley-VCH Verlag.

electron backscatter diffraction, electrons are accelerated by an electrostatic potential in order to gain the desired energy and determine their wavelength before they interact with the sample to be studied. The periodic structure of a crystalline solid acts as a diffraction grating, scattering the electrons in a predictable manner. Working back from the observed diffraction pattern, it may be possible to deduce the structure of the crystal producing the diffraction pattern.

In OTFT applications, crystal structure can be investigated by high resolution transmission electron microscopy (HRTEM). Because of its high resolution, it is an invaluable tool to study nanoscale properties of crystalline material such as semiconductors and metals. In a TEM, a thin crystalline specimen is subjected to a parallel beam of high-energy electrons. Because the wavelength of high-energy electrons is a fraction of a nanometer, and the spacings between atoms in a solid is only slightly larger, the atoms act as a diffraction grating to the electrons, which are diffracted. That is, some fraction of them will be scattered to particular angles, determined by the crystal structure of the sample, while others continue to pass through the sample without deflection. As a result, the image on the screen of

the TEM will be a series of spots, the selected area diffraction pattern (SADP), each spot corresponding to a satisfied diffraction condition of the sample's crystal structure. If the sample is tilted, the same crystal will stay under illumination, but different diffraction conditions will be activated, and different diffraction spots will appear or disappear.

Bao and co-workers used HRTEM to explore the detail microstructure within the polymer nanocrystalline before and after annealing.[129] A freestanding poly(2,6-bis(3-alkylthiophen-2-yl)dithieno[3,2-b;2′,3′-d]thiophene) (PBTDT) thin film was fabricated, and the interface surface of the film should be exposed upward where the orientation of the lamellar could be highly consistent with the edge-on orientation. Figure 17 shows the typical HRTEM images and corresponding selective area electron diffraction (SAED) patterns of PBTDT thin films delaminated from mica without and with annealing. After annealing, the crystalline structure of PBTDT thin film is highly ordered, and the π−π stacking distance is slightly smaller than normal (as shown in SAED results). The use of fast Fourier transformation (FFT) can help to obtain structure information from single-crystalline grain. The rectangular symmetry of the patterned spots in Figure 17e implies that the PBTDTT grain might be orthorhombic structure proposed hereinafter and the reflections can be indexed as (0h0) and (0h ± 3), as shown in Figure 17f.

2.3.8. Electrical Characterization Techniques. Electrical characterization techniques are the aggregate of techniques applied in OTFTs for the characterization of charge carrier traps and carrier transport peoperties in organic semiconductor materials. The material is usually processed into a very thin film through which a current passes. Thus, the ability to characterize transport properties of an organic film is of special importance in organic electronics. Time-of-flight (TOF) and space-charge-limited current (SCLC) are well-known techniques for measuring carrier mobilities in organic electronic materials.[130,131] In these experiments, the mobility measurement can be performed if the organic active layers are amorphous. In the OTFT experiment, the organic active layers are commonly thin and ordered, and other electrical characterization techniques are also well applied for the carrier measurement.

Impedance spectroscopy (IS) can measure the impedance of a system over a range of frequencies, and therefore the frequency response of the system, including the energy storage and dissipation properties, is revealed. In OFET, charge carriers are generally considered to be injected, accumulated, and transported. A device is equivalent to a circuit, which consists of small resistors (energy dissipater) and capacitors (energy storage) connected in series as a ladder. Often, data obtained by IS are expressed graphically in a Bode plot or a Nyquist plot. Bode plots are the polar representation of the Nyquist plot in frequency domain—the impedance magnitude and dielectric losses (phase). The phase diagram is very sensitive to resonance frequency of parallel RC loops, which are very commonly used in equivalent circuits for organic thin films to represent the two conduction paths—conduction and displacement current.

The Jaiswal research has shown the importance of frequency response results by impedance measurements of OFET under direct current (DC) bias.[132] Hamedi and co-workers demonstrated p-channel fiber-embedded electrolyte-gated OTFT transistors.[133] In the IS measurements, they revealed a slow but major response associated to bulk electrochemical doping in the P3HT film. In a recent work, IS has been applied on top-contact pentacene FETs for analyzing the charge injection and
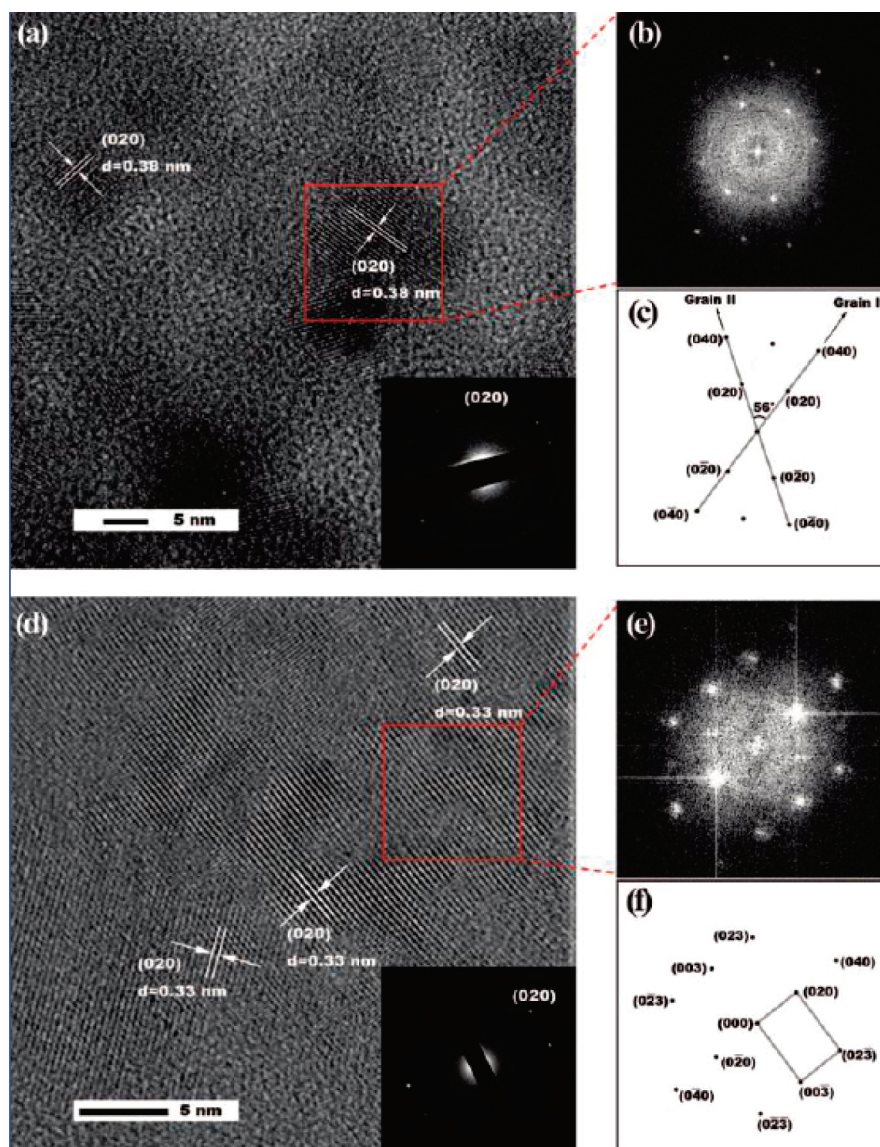
Figure 17. (a) HRTEM image of the interface of PBTDT thin film without annealing and corresponding SAED ring pattern (inset). (b) FFT pattern conducted from the square region containing two grains in panel a and the planes are indexed in panel (c). (d) HRTEM image of the interface of PBTDT thin film after annealing and corresponding SAED ring pattern (inset). (e) FFT pattern conducted from the square region in panel (d) and the planes are indexed in panel (f). Reprinted with permission from ref 129. Copyright 2008 American Chemical Society.

transport properties.[134] Two relaxation processes in the horizontal and the vertical direction of OFET were observed and analyzed by IS. The estimated mobility obtained from the IS analysis was comparable to steady-state current–voltage results. This alternative method by IS provides an additional advantage of isolating the effect of carrier concentration when evaluating the mobility of OFETs.

Lenski and co-workers have used a transmission line technique to measure the frequency-dependent complex conductivity of pentacene in a TFT configuration.[135] Results show that complex conductivity is strongly frequency dependent and follows roughly the expectations of universal dielectric response of disordered solids. In a recent paper, a dynamic infrared electro-optic (EO) technique is used to estimate the mobilies of field induced charge in TFTs.[136] By applying square-wave voltages of variable frequency to the gate or drain, one can measure the time it takes for charges to accumulate on the surface, and therefore, determine their mobility.

Some techniques are also introduced to measure the charge carrier traps in the organic thin films in FETs. For example, deep-level transient spectroscopy (DLTS) can be applied to study the characteristics of electronic charge concentrations and the interface traps of the pentacene thin films.[137] The thermally stimulated current (TSC) technique is another powerful tool used to characterize carrier traps in organic materials in FETs. Matsushima and co-workers investigated the influence of O_2 and H_2O molecules absorbed in carbon-60 (C60) films on their electron trap and n-type FET characteristics using a TSC technique.[138] The TSC results demonstrated that the absorption of O_2 and H_2O molecules in the C60 films induced an increase in the electron trap concentration, which degrades C60 FET characteristics. The annealing process can markedly lower the electron trap concentrations and lead to enhancing the C60 FET characteristics.

3. PATTERNING AND PRINTING TECHNIQUES FOR OTFTS

Organic thin-film transistors and integrated circuits will become increasingly important if low-cost, large-scale fabrication techniques become commercially available. Patterning and printing techniques represent promising fabrication techniques, some of which have been used in early stages of production such as prototype displays. Various patterning and printing techniques have been successfully implemented in the fabrication of OTFTs in research laboratories and can be categorized into several types: photolithography, soft lithography, imprint lithography, other patterning techniques, inkjet printing, and other printing techniques. Photolithography and other conventional techniques are well-developed patterning techniques used for inorganic electronic and photonic devices and have also proven useful for OTFT fabrication. However, conventional techniques all have limitations for patterning active or passive components of organic systems, such as high manufacturing costs for large-area fabrication, and their restricted applicability to many important classes of problems. Therefore, it is necessary to develop new or unconventional techniques including molding, embossing, and printing as alternative patterning techniques for organic electronics. Nowadays, these unconventional techniques are being increasingly accepted and developed in the exploratory phase of OTFT research. The following sections describe in detail various patterning and printing techniques for the fabrication of OTFT devices according to the mentioned-above categories; additional details have been described in other reviews.[139−142]

3.1. Photolithography

Photolithography, also called optical lithography, is the dominant manufacturing technique in the conventional microelectronics industry. Photolithography is widely implemented in manufacturing by virtue of several advantages, including straightforward scaling to large area substrates, parallel patterning capability, and availability of a broad basis of equipment and expertise. In addition, recent technical advances offer potential routes to high-volume production of devices with sub-50-nm resolution or patterning of minimum features below 37 nm.[140,143] However, photolithography is largely restricted by its technical disadvantages when it is used as a patterning technique for organic devices: these include degradation and delamination of the organic semiconductors caused by the solvents involved in the photopatterning process, incompatibility with patterning relatively fragile organic materials on nonplanar substrates, and high-cost and cumbersome manufacturing processes. Nevertheless, there are still many efforts to pattern organic semiconductors or conductive materials by photolithography for OTFTs, and some photolithographic techniques that have been developed as promising patterning techniques for this area are discussed in this section.

In conventional photolithography, the two most widely used ways for patterning films are subtractive and additive photolithographic patterning techniques. In the case of patterning an organic semiconductor, a photoresist is spin-coated onto the organic film (subtractive) or a substrate (additive) and is subsequently exposed to light through a photomask. Chemical changes occur in the exposed regions making the photoresist either more soluble (positive resist) or less soluble (negative resist) in a given solvent. The soluble part of the resist is then removed leaving behind a photoresist pattern. Using the remaining photoresist as a contact mask, an etching step is then used to transfer the pattern
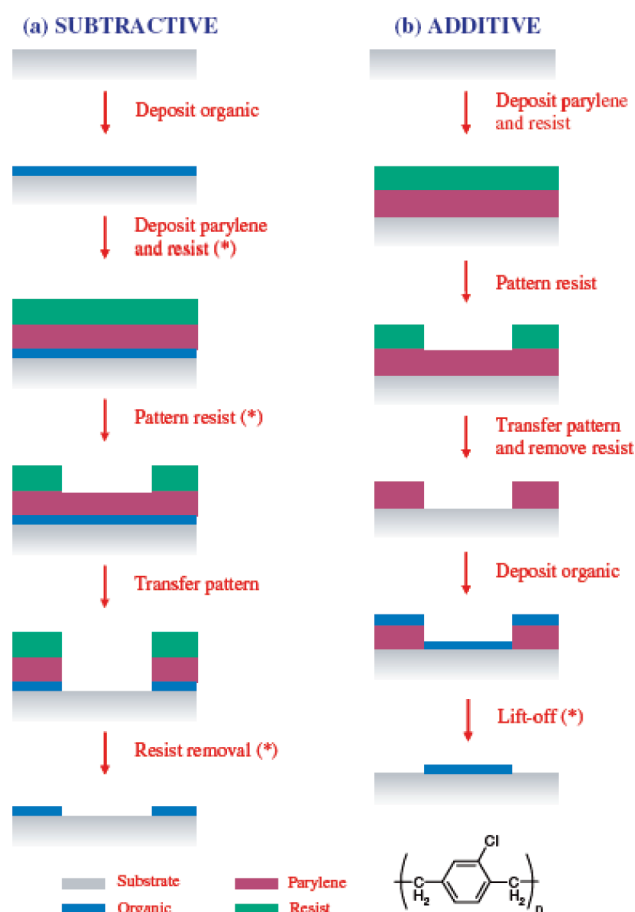

Figure 18. Subtractive (a) and additive (b) photolithographic patterning approaches for organic films. The asterisks indicate the steps where the organic film would be damaged during conventional photolithography. The chemical structure of parylene-C is shown at the bottom. Reprinted with permission from ref 144. Copyright 2006 Elsevier.

to the underlying film. Finally, the photoresist is stripped off by an appropriate solvent (subtractive). The additive photolithographic patterning process involves lift-off and dissolving the photoresist pattern to remove the active material above it giving the patterned semiconductor (a schematic illustration of these processes is shown in Figure 18). The mask can be aligned against the substrate in a contact mode, proximity mode, or projection mode. Contact mode photolithography is sometimes used in research and prototyping processes, whereas projection mode photolithography is mainly applied for high volume production. Both photolithographic patterning techniques have been successfully applied to the patterning of organic semiconductor materials and conductive materials for OTFTs.[144]

Many examples of OTFT devices have used photolithography to pattern the active layers or the electrodes. Recently, pentacene was patterned as the semiconductor layer for an OTFT backplane by photolithography and dry-etched using a dual protection layer of poly p-xylylene and an SiO_2 film, and uniform transistor performance was obtained in driving a 5.8-in. flexible color active-matrix organic light-emitting-diode display.[145] Pentacene can also be patterned by use of a photopatternable pentacene precursor, by either a polymer precursor approach[146] or a decomposition approach.[147] Other small molecules or conjugated polymers, such as P3HT, can be effectively patterned

3374

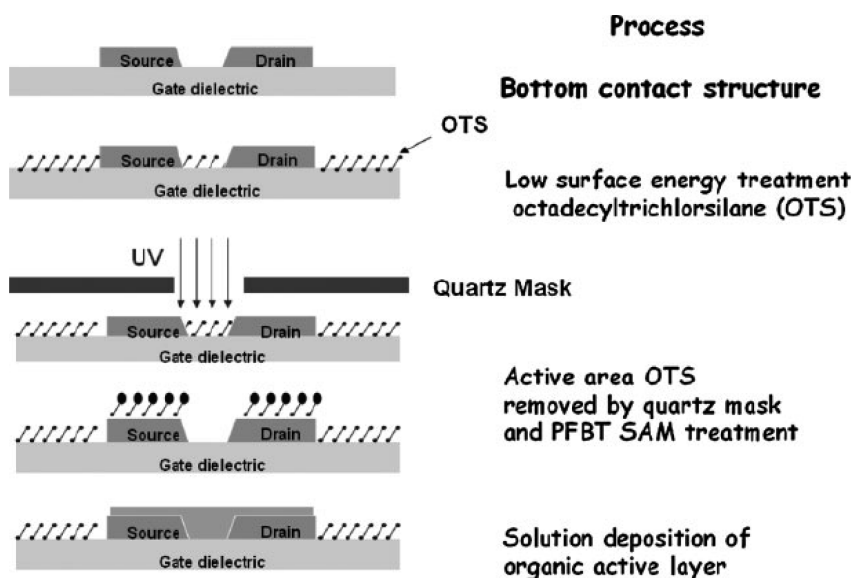dx.doi.org/10.1021/cr001904 |Chem. Rev. 2011, 111, 3358−3406

Figure 19. Process flow of a non-relief-pattern lithography process for solution-processed organic semiconductors. Reprinted with permission from ref 150. Copyright 2008 Wiley-VCH Verlag.

by improved photolithographic methods, including nondestructive photolithography[148,149] and nonrelief-pattern lithography,[150] as discussed below. As another key component, electrodes can be patterned by photolithography directly or by means of improved photolithographic methods. Metal electrodes are still widely deposited by photolithography for device research, such as charge trapping memory transistors[151] and OTFTs on paper.[152] Organic conductive materials patterned by photolithography have also been widely studied. Polyaniline (PANI) and the conducting polymer poly(3,4-ethylenedioxythiophene) are two typical examples of organic conductors photopatterned as electrodes for OTFTs and integrated circuits.[153−156] Recently, it has been shown that spin-cast photosensitive organosilver precursors can be reduced to Ag metal based on a photolithography process,[157] which facilitates the fabrication of solution-deposited electrodes.

In the conventional photolithography process for patterning organic materials, the adhesion between the active layer and photoresist can be significant however, rendering the active layer susceptible to physical damage when the photoresist is removed. To lesson this problem, DeFranco and co-workers reported a generic approach for the photolithographic patterning of organic materials with micrometer resolution.[144] They used parylene-C as an intermediary in both subtractive and additive photolithographic patterning processes (Figure 18). The parylene-C can adhere only weakly to the organic layer and so is less liable to cause damage to the active layer when it is peeled away to expose the active layer, and its use can avoid the use of aggressive reagents in the conventional lift-off process. A nondestructive and high-resolution photolithographic patterning technique was developed for P3HT-based OTFTs by Song's group.[148,149] They optimized the lift-off process by careful selection of the resist and polymer solvents, and were able to pattern organic films using subtractive photolithography without the need to expose the substrate to any chemical reagents.

Recently, Park and co-workers used an unconventional non-relief-pattern, photoresist-free photolithographic technique to fabricate solution-processed OTFTs and circuits.[150] This approach involves depositing a functional SAM onto a substrate and patterning it using deep ultraviolet (DUV) light irradiation. Low surface energy SAMs can then steer deposited liquid into areas where the SAM has been removed by the DUV processing. Direct DUV exposure of a SAM can remove most SAMs, resulting in a hydrophobic to hydrophilic transformation, and then 2,8-difluoro-5,11-bis(triethylsilylethynyl)anthradithiophene (diF-TESADT) is solution-deposited on PFBT-treated Au electrodes by use of the self-assembly properties of diF-TESADT (Figure 19). This non-relief-pattern lithography of a SAM can easily result in microstructures with good resolution, and this approach does not require the photoresist coating, development, or removal processes which are typically responsible for a large portion of manufacturing costs.

A silver-patterning method has been developed by Lee and co-workers for all-solution-processed n-type transistors.[157] This method is based on a photolithography process, in that a photosensitive organosilver precursor is spin-coated onto the top of an insoluble thermally cured organic insulator/AlNd substrate. Broadband UV irradiation of the film through a photomask produces a partially reduced and insoluble silver compound. After development with MeCN, the irradiated areas can be reduced by hydrazine hydrate to obtain pure source−drain metallic patterns (Figure 20a). The well-defined channel between the source and the drain can be seen in Figure 20b, and the low rms roughness (with a value of 4.76 nm) can be observed in Figure 20c. This soluble metal precursor route leads to devices with higher electron mobilities than those fabricated by vacuum deposition, and has the potential to allow the fabrication of low-cost, flexible integrated circuits and display backplanes.

Very recently, a simple and versatile photo-cross-linking methodology for device fabrication has been reported by Png and co-workers.[158] This method is based on the observation that sterically hindered bis(fluorophenyl azide)s (sFPAs) can generally be mixed into polymer organic semiconductors and give rise to photo-cross-linking when exposed to deep-ultraviolet light (DUV) without degrading the semiconductor. The photo-cross-linking efficiency is high and dominated by alkyl side-chain
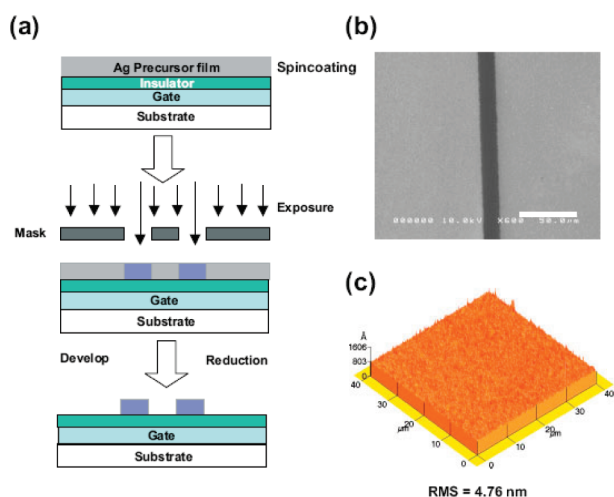
Figure 20. (a) Procedure for the deposition of patterned source−drain metal electrodes with a soluble organosilver precursor. The photosensitive organosilver precursor is spin-coated onto the top of the insoluble thermally cured organic insulator (a polyvinylphenol derivative)/AlNd gate/glass substrate. Broadband UV irradiation of the film through a photomask produces a partially reduced and insoluble silver compound. After development with MeCN, the irradiated areas can be reduced by hydrazine hydrate to obtain pure source−drain metallic patterns (70−80 nm). (b) Scanning electron microscopy image of the resulting source−drain pattern with 15 μm channel length. The scale bar is 50 μm. (c) Atomic force microscopy image of the reduced metallic patterns, showing an rms roughness of 4.76 nm. Reprinted with permission from ref 157. Copyright 2005 Wiley-VCH Verlag.

insertion reactions, which makes it possible to develop high-performance heterostructures with an unprecedented degree of control. The sFPA methodology is also compatible with the semiconductor layers used in high-performance polymer FETs, which can therefore also be photopatterned. Poly(2,5-bis(3-tetradecylthiophene-2-yl)thieno[3,2-b]thiophene)   (PBTTT) films can be photo-cross-linked as active layers, and the output and transfer characteristics of devices were found to be unchanged from those of control devices without cross-linker and DUV exposure. The hole mobility was on the order of 0.1 cm^2·V^{-1}·s^{-1}, with on/off ratios of more than 10^4.

Other promising unusual photolithographic techniques include optical soft lithography and interlayer lithography. The former approach uses conformable, elastomeric elements with relief features on their surfaces as photomasks for patterning the exposure of layers of a photoresist or other photosensitive materials.[159] The nondestructive, reversible, atomic scale contacts that can be established, without applied pressure, through generalized adhesion forces (typically van der Waals) between the mask and the resist layer (typically a solid thin film) are key to this process.[160−162] This approach provides extremely high resolution and parallel operation with inherently low-cost and simple experimental setups, and it also avoids the contact-related problems between mask and photoresist in conventional photolithography. The latter method makes use of an intermediate photoresist layer between the substrate and the organic layer to be patterned in order to minimize the lithographic processing steps.[163] The selection of the active material, the developer and photoresist are all very important for patterning organic semiconductors, conductors, and insulators on both rigid and flexible substrates. These techniques all indicate promise for specific applications in organic electronics.

3.2. Soft Lithography

Soft lithography involves a set of techniques that use a soft (elastomeric) mold, stamp, or mask to transfer the pattern by a number of different procedures, such as molding and printing. Soft lithography has rapidly developed as an alternative to photolithography and other conventional microfabrication techniques, due to its advantages in the large area and low-coat patterning of organic materials on nonplanar substrates. Elastomers are a versatile class of polymers for replication of a topographic master. The most widely implemented and successful elastomer for nanofabrication is poly-(dimethylsiloxane) (PDMS).[140,164] PDMS is highly UV-transparent and has low surface energy and low modulus which give the flexibility required for conformal contact with substrate surfaces without the risk of cracking. Additionally, this flexibility in molds facilitates easy, nondestructive removal from masters and replicates, especially of fragile organic materials. Furthermore, PDMS molds with feature sizes down to a few nanometers have been produced recently.[165,166] Other elastomers have also been developed for soft lithography to circumvent the limitations of PDMS, and some of these are comparable to, or even better than, PDMS in some cases.[141,167,168] Soft lithographic techniques based on stamps also show promise for large-area, low-cost implementation due to their simple operation and high resolution. Generally, a stamp supplies a chemical or material ("ink") to a substrate by physical contact. This transferred material acts as either a functional layer of a device, a resist for etching underlying materials, or a catalyst for directing the deposition or growth of other materials. To achieve high-quality pattern transfer, conformal contact must be established between the stamp and the substrate, preferably without external pressure, which is often achieved with the use of an elastomeric stamp, such as PDMS. Such soft lithographic techniques are also called "printing" methods. This section will concentrate on soft lithographic techniques that have been used for patterning or printing elements of OTFT devices in the laboratory.

3.2.1. Micromolding in Capillaries.
Micromolding in capillaries (MIMIC) is a molding technique that relies on the spontaneous filling of microfluidic channels by using capillarity with liquid materials, such as solutions, photo- or thermally curable prepolymers, and liquid metals. In MIMIC, a PDMS mold is often used because it is chemically inert to the abovementioned liquid materials, which allows the reversible and repeated use of a PDMS mold with topographic surfaces. This technique offers the ability to pattern organic semiconductor films as well as conductive films, to form the active layer and electrodes for OTFTs. However, the capillary filling rate can be slow, especially as the size of the fluidic channel decreases. The capillary flow can be assisted by applying a vacuum to one end of the capillaries or by heating the liquid to decrease its viscosity.[169,170]

It has been demonstrated that source and drain electrodes for OTFTs can be patterned using the MIMIC technique. Rogers and co-workers defined the source and drain electrodes by the microchannels of a PDMS mold.[171] Specifically, conductive carbon or conducting polymer electrodes with channel lengths of 25 μm were patterned on top of a P3HT layer by MIMIC, and the top-contact P3HT TFTs exhibited a charge-carrier mobility of 0.01−0.05 cm^2·V^{-1}·s^{-1}. Tunable organic transistors can be fabricated by using a conducting fluidic source and drain electrodes of mercury which flow on top of a thin film of the organic semiconductor pentacene.[172] Fluidic motion alters the

channel width of this transistor to tune the source–drain current in this type of microfluidic organic transistor. Recently, working OTFTs that use conducting single-walled carbon nanotube (SWNT) lines as source/drain electrodes patterned using the MIMIC technique have been reported by Park and co-workers.[173] The combined use of multistream laminar flow in microfluidic channels and controlled flocculation can pattern high-density SWNT networks serving as source/drain electrodes for OTFTs.

Recently, Cavallini and co-workers have demonstrated FETs where drain current flows through a precisely defined array of nanostripes made of crystalline and highly ordered molecules.[174] The molecular stripes are fabricated across the channel of the transistor by a stamp-assisted deposition of the molecular semiconductors from a solution (Figure 21). As the solvent evaporates, the capillary forces drive the solution to form menisci under the stamp protrusions. The solute precipitates only in the regions where the solution is confined by the menisci once the critical concentration is reached and self-organizes into molecularly ordered stripes 100–200 nm wide and a few monolayers high. The charge mobility measured along the stripes is 2 orders of magnitude larger than the values measured for spin-coated thin films. The deposition assisted by the stamp has both the effectiveness and the simplicity desired for a solution-based technology.

A variation of MIMIC for patterning polymer semiconductor TFT arrays was recently reported by Salleo and co-workers.[175] This technique also exploits capillary forces to pattern a solution-processable polymer semiconductor. A chemically treated PDMS stamp is placed directly on top of a substrate coated with the polymer semiconductor solution. In the regions of contact, the PDMS stamp absorbs the solvent, leaving behind a solid polymer semiconductor film between the stamp and the substrate. In the recessed regions of the PDMS stamp, the polymer semiconductor solution wicks into the stamp due to capillary forces, effectively leaving behind a clean surface in the noncontact regions. Using this stamping process, patterned arrays of poly[(9,9′-dioctylfluorene)-co-bithiophene] (F8T2) and poly-[5,5′-bis(3-alkyl-2-thienyl)-2,2′-bithiophene] (PQT-12) with features as small as 2 μm were fabricated for use in both top- and bottom-contact TFTs.

3.2.2. Soft Contact Lamination. Soft contact lamination exploits the conformal properties of PDMS, so that individual components of the device can be made separately and then laminated together in the final step. In addition, the soft contact lamination method is a noninvasive technique and has several advantages for fabricating organic devices, such as high performance, nanoresolution, and flexible nature. These features are particularly useful for assembling OTFTs considering the chemical and mechanical fragility of organic semiconductors.

One important advantage of the lamination technique for OTFT fabrication is that this method can be used to manufacture OTFTs at low cost with high-volume processing. It is often combined with other printing and patterning techniques such as microcontact printing[176] or dry transfer methods[177] in the manufacture of OTFTs and plastic circuits in order to enhance the mechanical flexibility and compatibility. Soft contact lamination methods can give lower contact resistances than those obtained with evaporated source and drain contacts.[178] Lamination of a stamp prepared with an integrated gate metal and elastomeric gate against a fully fabricated pentacene top-contact device produces a double-gate structure for simultaneous study
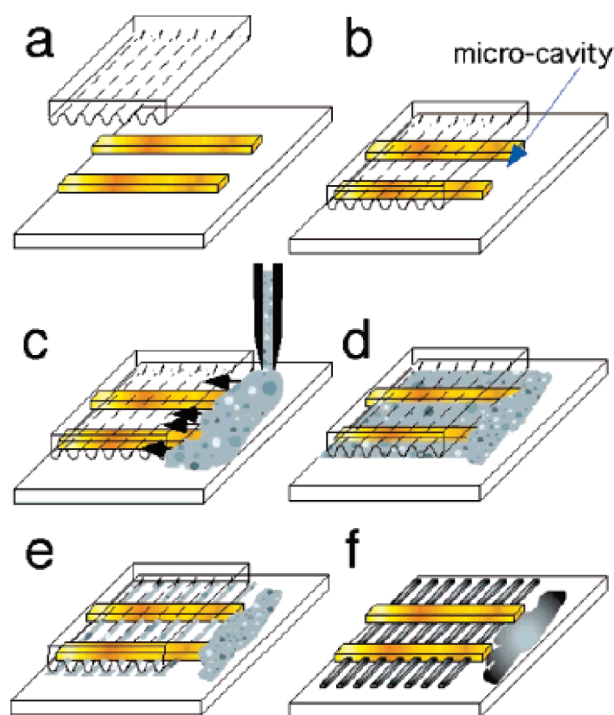

Figure 21. Schematic representation of the deposition process of a precisely defined array of nanostripes made of crystalline and highly ordered molecules, showing the steps related to micromolding in capillaries (a–d) and the steps related to lithographically controlled wetting (e and f). Reprinted with permission from ref 174. Copyright 2005 American Chemical Society.

of transport properties through field-effect measurements on both the bottom and top interfaces of the organic semiconductor.[179]

The lamination method can also be used to study the effects of processing conditions on polymer films and should aid in the study of organic semiconductor–dielectric interfaces.[180] This technique has advantages over other methods because the films do not need to be exposed to a solvent for transfer, the process can be done at room temperature without pressure, and it enables good electrical contacts to be formed with the films. Soft contact lamination can be used to assess the effects of varying the angle of the periodic groove patterns on pentacene thin film transistors with a 140 nm periodic groove patterned dielectric layer.[181] In this technique, thin metal electrodes are deposited onto an elastomeric stamp, and the stamp is then brought into contact with the substrate (Figure 22). As the angle was decreased from 90° to 0°, the current output and carrier mobility increased and the threshold voltage of the device was shifted. It was concluded that the molecular orientation of pentacene on the patterned dielectric layer was mainly responsible for variations in the output current, charge carrier mobility, and threshold voltage.

3.2.3. Microcontact Printing. Microcontact printing (μCP) is a stamp-based soft lithographic technique that offers a simple and low-cost surface patterning methodology with high versatility and submicrometer accuracy. In a typical μCP process, the PDMS stamp is inked with a solution typically containing molecules or colloids in order to transfer inks onto a hard silicon master or any solid patterned surface or flexible polymer substrate. By bringing the inked stamp in conformal contact with the surface through van der Waals forces, the ink is
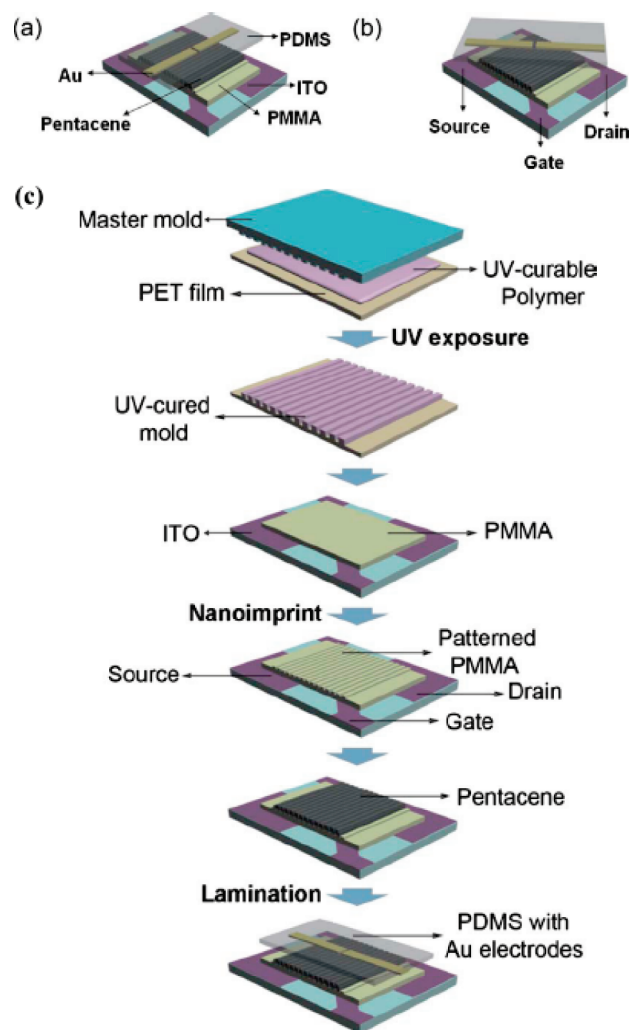
Figure 22. Pentacene TFTs with a Au deposited PDMS mold by soft contact lamination. (a) Current direction is parallel to groove direction and (b) a certain angle is formed between current direction and groove direction. (c) Schematic illustration of the fabrication of pentacene TFTs by soft contact lamination. Reprinted with permission from ref 181. Copyright 2010 American Institute of Physics.

transferred to the surface. Automated printing using a micro-contact printer has been recently demonstrated.[182] Because of the patterned structure of the stamp, only the areas with protrusions are able to contact the surface, and the ink is area-selectively transferred according to the pattern of the template. The inks commonly employed in μCP are chosen for their ability to form SAMs during the μCP process and include alkanethiols and organosilanes.[183] Recently, stamps for μCP were rapidly produced by injection molding a commercial polyurethane resin, using a silicon master as the mold insert; these exhibited excellent replication of the sub-micrometer linear features of the micromold.[184] The use of injection molding as a standard method for the production of stamps for microcontact printing has been proposed and may have advantages for future nano-technology applications that require mass production of stamps. Despite a wide variety of new stamp materials, PDMS remained the cheapest and easiest stamp material to use, and has the advantage that many surface-treatment techniques can be used to change the hydrophobicity of a PDMS stamp.[185]

μCP and subsequent etching are usually used to fabricate source and drain electrodes for OTFTs. Since the source and drain electrodes are defined prior to the deposition of the chemically and mechanically fragile organic semiconductor, the resulting OTFTs are therefore built in the bottom-contact geometry. Leufgen and co-workers fabricated bottom-contact OTFTs with channel lengths as small as 100 nm using μCP and etching.[186] To achieve sub-micrometer features, they carefully controlled the contact pressure, the contact time, and the concentration of the molecular inks during printing. OTFT structures with channel lengths down to 100 nm were fabricated by μCP when the process conditions were optimized. Rogers and co-workers demonstrated a reel-to-reel process for fabricating gold electrodes for bottom-contact P3HT TFTs using a cylind-rical PDMS stamp.[187] These bottom-contact P3HT TFTs ex-hibited an average charge-carrier mobility of 0.02 cm$^2 \cdot$V$^{-1} \cdot$s^{-1}, similar to those of typical bottom-contact P3HT TFTs.

Zschieschang and co-workers used μCP and electroless plat-ing techniques to deposit a fluorinated SAM (FSAM) on a hydrophilic flexible polyethylene naphthalate (PEN) substrate.[188] The patterned substrate was then activated in a palladium bath; the palladium catalyst was only adsorbed in the hydrophilic, unstamped regions. Subsequent electroless plating resulted in the selective deposition of nickel only in the hydrophilic regions, and not in the regions stamped with FSAM. The electroless-plated nickel electrodes served as the gate electrode in flexible pentacene TFTs. Parashkov and co-workers have developed a process for the fabrication of OTFTs and integrated circuits, employing a combination of high-resolution μCP and selective or diffusion electropolymerization.[189] An alkylthiol template was microcontact-printed onto a gold-coated glass substrate for the selective growth of poly(3,4-ethylenedioxythiophene)-polystyr-ene sulfonate (PEDOT-PSS). To transfer PEDOT-PSS patterns from the gold surface, polyimide (PI) was cast and cured directly on the PEDOT-PSS patterned substrate. Peeling the PI substrate removed the PEDOT-PSS features from the gold surface. Bottom-contact OTFTs were fabricated and had a charge-carrier mobility of 0.02 cm$^2 \cdot$V$^{-1} \cdot$s^{-1}. It should be noted that the solutions required for chemical or electrochemical polymerization are gen-erally not compatible with the organic semiconductors of OTFTs. As a consequence, the application of these procedures is also limited to the fabrication of bottom-contact devices.

A "stamp-and-spin-cast" method was developed for direct patterning of conducting polymer electrodes for OTFTs.[190] To fabricate the PANI source and drain electrodes, Lee and co-workers microcontact-printed octadecyltrichlorosilane (OTS) on oxidized silicon wafers. Subsequent spin-coating of an aque-ous PANI dispersion on the patterned substrate created con-ductive PANI patterns in the hydrophilic regions (Figure 23). Bottom-contact pentacene TFTs with PANI features as small as 5 μm were fabricated, which exhibited an average charge-carrier mobility of 0.016 $\pm$ 0.008 cm$^2 \cdot$V$^{-1} \cdot$s^{-1} and on/off current ratios as high as 10^4. Briseno and co-workers have employed μCP and dewetting methods to transfer unreacted low molecular weight (LMW) siloxane oligomers from freshly prepared "dry" PDMS stamps for patterning organic semiconductors and con-ducting polymers into functional devices.[191] This simple method can be used to pattern organic semiconductors from solution with resolutions as small as 1 μm and does not require any ink. It can be easily scaled to a very large area on various substrates with potential applications where large-area printing is required for fabricating organic electronic devices.
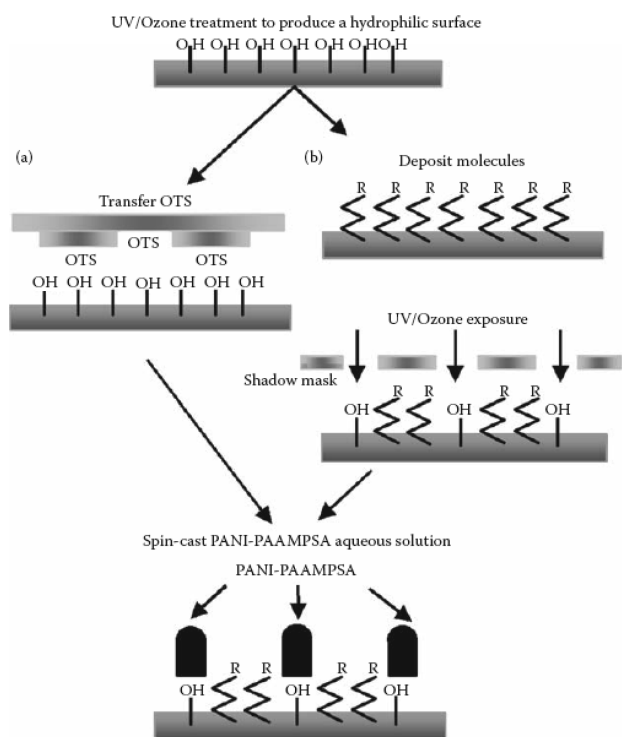
3378

dx.doi.org/10.1021/cr1001904 |*Chem. Rev.* 2011, 111, 3358–3406

Figure 23. Schematic illustration of the "stamp-and-spin-cast" method. Hydrophobic patterns are created by (a) μCP or (b) subtractively removing hydrophobic molecules by UV-ozone irradiation through a shadow mask. An aqueous PANI dispersion is spin-coated onto the patterned substrate. PANI features selectively deposit in the hydrophilic regions immediately after the spin-coating. Reprinted with permission from ref 190. Copyright 2005 American Institute of Physics.

3.2.4. Transfer Printing. Transfer printing is a direct patterning technique that can transfer a solid film from a stamp with patterned features to a substrate. Although patterns can be transferred from either rigid stamps or soft stamps, here we focus on the use of soft elastomers (e.g., PDMS) to print functional solid materials for OTFT devices. The PDMS stamp ensures conformal contact between the stamp and substrate via van der Waals interactions, resulting in high-quality printed patterns. This technique avoids the etching processing step in μCP, which is limited to the fabrication of bottom-contact devices due to incompatibility problems, and the printing process often requires no solvent. Moreover, transfer printing occurs under ambient conditions, and pattern features have levels of resolution that exceed those possible with traditional μCP over large areas on both rigid and flexible substrates. The process allows for direct patterning of three-dimensional and multilayer structures without additional processing steps, and a variety of single- and multilayer conductors, semiconductors, and dielectrics can be transfer-printed for organic electronic systems.[192−195]

The transfer printing process relies on interfacial chemistry to transfer the solid material from a PDMS stamp to a substrate. Transfer printing based on covalent interactions includes surface condensation reactions between surface-bound silanols (Si—OH), titanols (Ti—OH), and thiol—metal reactions.[195−197] In this way, transfer printing can provide a nondestructive method for making electrical contact with a molecular layer, avoiding the penetration of, and/or damage by, metal during evaporation. Therefore, the performance of devices fabricated by printing

metals directly from a stamp is usually better than that of those obtained by shadow-mask evaporation. A noncovalent transfer process was recently demonstrated by Hur and co-workers for patterning gold and gold/titanium multilayers.[198] This procedure does not rely on the formation of specific covalent bonds for pattern transfer, but noncovalent surface forces are employed to print electrodes directly on top of the organic semiconductor thin films without prior modification or surface treatment. The on/off ratios of these P3HT devices produced by noncovalent transfer-printed electrodes are significantly higher than those of devices prepared using shadow-mask evaporation techniques, possibly due to improved channel definition.

A simple metal transfer printing technique has been employed in the fabrication of OTFTs.[199] This method is a purely additive process using mechanical adhesion as the patterning driving force, and large areas can be rapidly patterned in a single step in air. These advantages allow the technique to be adapted for reel-to-reel fabrication. Additionally, a conducting polymer PEDOT-PSS has been patterned as the source and drain electrodes for OTFTs by using the polymer inking and stamping technique.[200] A PDMS stamp with spin-coated PEDOT was placed on a Si/SiO$_2$ substrate to make a conformal contact. The assembly of the PDMS mold and the substrate was baked on hot plate at 80 °C for 2 min. Finally, the PDMS stamp was removed from the substrate, leaving positive PEDOT patterns on the substrate (Figure 24a). This technique is fully compatible with patterning on flexible substrates, and both top-contact and bottom-contact OTFTs demonstrate excellent electrical characteristics. Field-effect mobilities and on/off current ratios in the saturation regime as large as 0.7 cm$^2 \cdot$V$^{-1} \cdot$s^{-1} and 10^6, respectively, were obtained.

Organic semiconductors, small molecules, or polymers can also be transfer-printed using stamps. Pentacene and P3HT are typical examples that have been deposited by transfer printing technique for use in OTFT devices.[201,202] These materials can be patterned without the need for solvents that can interfere with the delicate chemistry and physical structure of the device components, and therefore these devices demonstrate quality comparable to, or better than, those fabricated using standard techniques. For example, by printing P3HT onto smooth polyimide surfaces prepared by spin-coating, OTFTs with mobility of 0.02 cm$^2 \cdot$V$^{-1} \cdot$s^{-1} and on/off current ratios of 10^3 or 10^4 can be fabricated. Recently, Kim and co-workers have developed a simple but robust process—plasma enhanced polymer transfer printing—for fabricating micropatterns of P3HT thin films.[203] This method is based on transferring a thin P3HT film spin-cast directly on a prepatterned PDMS mold. Printing is accomplished by the application of oxygen plasma to both the P3HT film and the substrate giving surface energy modulation under ambient conditions without additional pressure. Control of the relative interfacial surface energy by the plasma enables a wide range of polymers from P3HT to conventional insulating ones to be micro/nanopatterned on various substrates including Si, glass, and polymers over large areas. A bottom contact OTFT with the printed P3HT patterns using PEPTP exhibited a carrier mobility of approximately 0.02 cm$^2 \cdot$V$^{-1} \cdot$s^{-1} with a relatively high on/off current ratio of 6×10^3.

3.3. Imprint Lithography

Imprint lithography is a nonconventional lithographic technique for high-throughput patterning of nanoscale structures at high resolution and at low cost. Unlike traditional lithographic approaches, which form a pattern using photons or electrons to
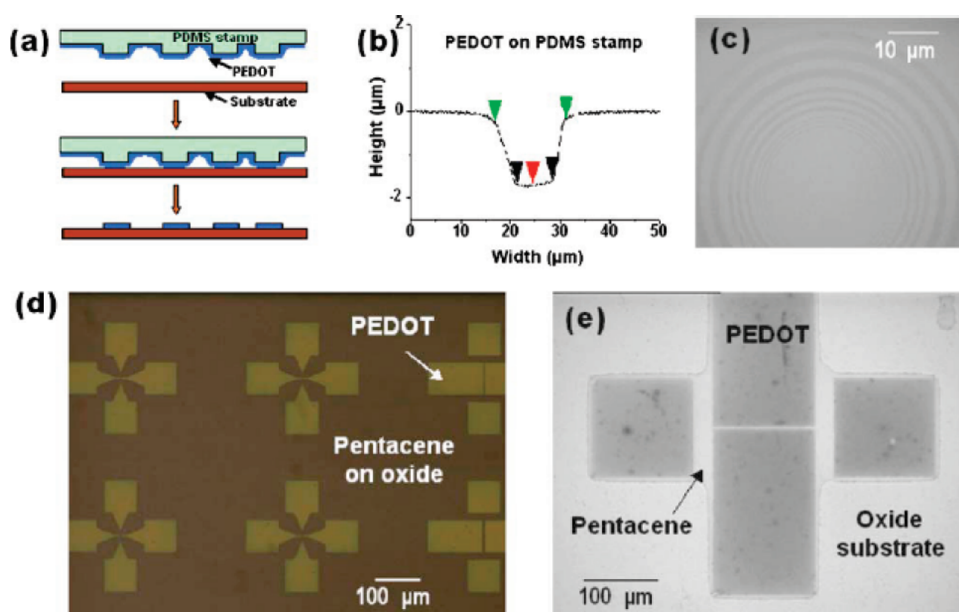
Figure 24. (a) Schematic illustration of polymer inking and stamping processes for patterning a PEDOT conducting polymer. (b) Cross-sectional AFM image of PEDOT on a PDMS stamp. (c) Concentric ring patterns transferred onto a PES flexible substrate. (d) PEDOT electrode patterns transferred onto a SiO$_2$ substrate for use in bottom-contact OTFTs, with gap widths from 2 to 10 μm. (e) PEDOT electrode patterns transferred onto a pentacene thin film surface for use in top-contact OTFTs, with W/L = 140 μm/2 μm. Pentacene outside the PEDOT electrode pads adheres to the stamp and is removed when the PMDS stamp is peeled off from the substrate. Reprinted with permission from ref 200. Copyright 2006 American Institute of Physics.

modify the chemical and physical properties of the resist, imprint lithography creates features by a direct mechanical deformation of the resist shape using a mold and can therefore achieve resolutions beyond the limitations set by light diffraction or beam scattering that are encountered in conventional techniques.[204] Furthermore, for the manufacture of semiconductor integrated circuits (IC), imprint lithography has the potential to be a next-generation lithography tool for creating all feature nodes all the way down to 5 nm, without having to change the lithography tools, resists, and masks, as is required in conventional lithography. Imprint lithography is already established as a research tool in organic electronics and, in some cases, also is already being explored for commercial manufacturing in photonics, data storage, and certain segments of microelectronics.

Three imprint lithographic techniques are commonly used in laboratory research, namely, nanoimprint lithography (NIL), step-and-flash imprint lithography (S-FIL), and soft imprint lithography (SIL). NIL refers to the pressure-induced transfer of a topographic pattern from a rigid mold (typically silicon) into a thermoplastic or thermally curable polymer film heated above its glass transition temperature. During NIL, the resist is in a flowable liquid state after the heating process and becomes solidified after the deformation.[205] The imprint mold is rigid, so feature collapse and deformation during imprinting are eliminated. Although this approach can work well, several challenges still need to be addressed before the technique can be implemented in large-area, flexible electronics: these include the high temperature and pressure required during the imprinting process, contamination and the limited useful lifetime of the mold during repeat processing, thermal expansion effects of the resist materials with suitable physical properties including low viscosity and low glass transition temperatures, and the need for overlay accuracy, large-area uniformity, and low defect density. This technique however still remains a powerful patterning tool for applications in OTFT fabrication.

NIL is often used to define the source and drain electrodes of OTFT devices. Austin and co-workers used NIL to pattern gold source and drain contacts for P3HT OTFTs with channel lengths from 1 μm down to 70 nm with high yields.[206] As the channel length was decreased, short-channel effects were clearly visible and the performance of these devices was reduced. All-polymer FETs have been fabricated by combining NIL and inkjet printing, and trenches with hydrophilic bottoms confined by hydrophobic walls with considerable heights can be patterned by NIL.[207] Devices with channel lengths of 250−300 nm with good performance have been demonstrated in top-gate all-polymer FETs. To improve the functionality of imprinted bottom-gate OTFTs, a novel thermally initiated radical polymerization-based nanoimprint lithography process (TIP-NIL) has been recently developed for the patterning of sub-micrometer-spaced contacts, used as source and drain electrodes in downscaled OTFTs.[208] The method is based on thermally initiated radical polymerization of a novel imprint resist whose outstanding chemical and physical properties are responsible for the excellent results in processability and structure transfer (Figure 25). In combination with a pretreated stamp, the thermally curable resist enables residue-free imprinting, thus making etching obsolete. In addition, this process requires only moderate temperatures and it is ecofriendly due to a water-based lift-off. Pentacene OTFTs obtained using this method show excellent transistor behavior parametrized by a high on/off current ratio of greater than 10^5 and a high charge carrier mobility (0.25 cm$^2 \cdot$V$^{-1} \cdot$s^{-1}).

By means of nanoconfinement during nanoimprinting, Zheng and co-workers demonstrated the uniaxial alignment of a liquid-crystalline conjugated polymer, poly(9,9-dioctylfluorene-*co*-benzothiadiazole) (F8BT).[209] The orientation of the conjugated backbones was parallel to the nanolines imprinted into the polymer film. An ambipolar polymer FET in a top-gate configuration with aligned F8BT as the active semiconducting layer
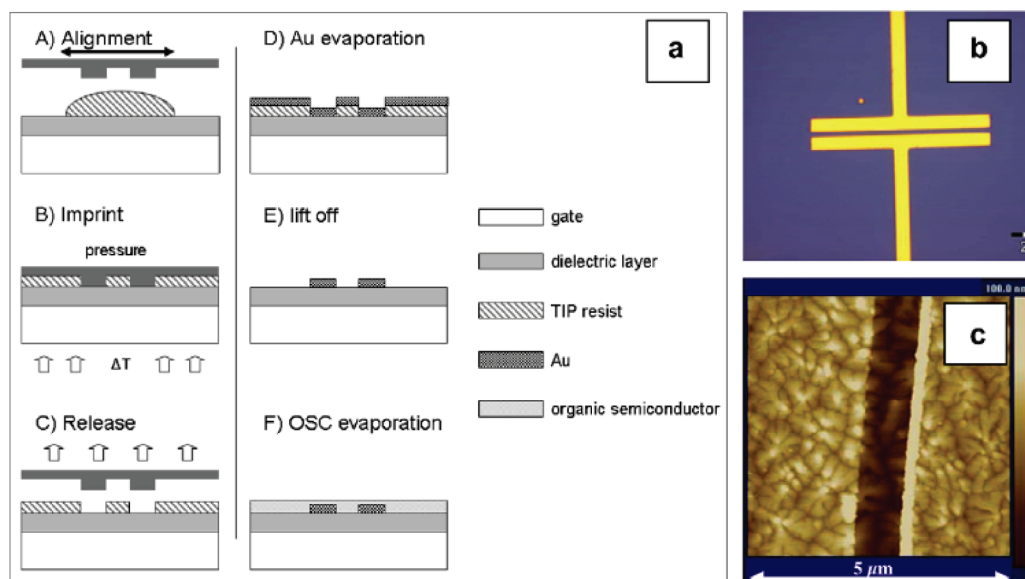
3380

dx.doi.org/10.1021/cr1001904 |*Chem. Rev.* 2011, 111, 3358–3406

Figure 25. (a) Schematic illustration of the TIP-NIL process: A silicon stamp containing the source—drain structures is roughly aligned onto the substrate (A). The stamp is pressed into the resist thus completely displacing the resist under the source—drain structures (B). Subsequently, the resist is cured by thermally initiated polymerization. After the stamp removal (C), the source—drain material is evaporated onto the substrate (D). The imprint resist is dissolved with water, which leaves the metal source—drain electrodes well preserved (E). Finally, the sample is covered by the organic active layer, pentacene (F). (b) Image of the source and drain structures after the lift-off. (c) AFM topographic image ($5 \times 5\,\mu$m) of the pentacene layer formed on top of the contacts and in the channel (L = 900 nm). Reprinted with permission from ref 208. Copyright 2010 Elsevier.

showed mobility enhancement when the chains were aligned parallel to the transport direction. Mobility anisotropies for hole and electron transport were 10−15 and 5−7, respectively, for current flow parallel and perpendicular to the alignment direction.

Similar to NIL, S-FIL has the potential to be a high-throughput, low-cost technique for fabricating nanoscale features. In S-FIL, a low-viscosity, photocurable liquid or solution is used to fill the void spaces of a quartz mold. The solution consists of a low-molecular-weight monomer and a photoinitiator. Illumination of the mold and resist with UV radiation initiates polymerization, creating a replica of the mold. Removing the mold leaves a topographically patterned (inverse) replica on the substrate. Because of the low viscosity of the resist, external pressure is not required for imprinting. Furthermore, this lithographic technique is also insensitive to the effects of pattern density seen in NIL. This approach has the potential for large-area, low-cost fabrication on both flat and nonflat substrates with low pressure and at room temperature.

Soft imprint lithography (SIL) is an appealing nanoimprinting technique using soft molds for nanoscale patterning and electronics. A soft mold such as PDMS is used instead of a rigid mold (e.g., silicon or quartz) and has the advantages of ease of replication of the original master structure, gas permeability for the evaporation of organic solvents during the nanoimprinting process, an easy demolding process and lower sensitivity to the contaminants on a sample surface due to its flexibility. Therefore, the ultimate limit in the resolution of SIL is on a smaller length scale than those of NIL and S-FIL which involve rigid molds. For example, SIL with soft molds demonstrates good lithographic fidelity down to relief heights of several nanometers, and with some capabilities at the level of ~1 nm.[210] The advantages of SIL make it suitable for many practical applications, for example, direct metal patterning on a flexible substrate[211] and alignment of

layers for functional devices.[212] It may also provide an opportunity to form surface relief structures that could serve as engineered sites for molecular recognition.[210]

Recently, Lin and co-workers used molecular-scale SIL to form oriented features of relief with dimensions as small as ~1 nm and then employed these structures as alignment layers for liquid crystal devices.[210] Several polymer formulations for molds and molded materials and process conditions were described, indicating that this molecular scale fidelity in replication can be used to produce surfaces that will effectively align liquid crystal molecules. SIL has also been used to align pentacene molecules for OTFTs.[212] This technique can precisely control the distribution and size of the micro- and nanometer-scale substrate relief and hence control the morphology and orientation of the pentacene. The nanometer-scale groove patterns, with 70 nm lines and 130 nm spaces, have been shown to lead to the in-plane orientation of the pentacene molecules. Compared to pentacene films that are not aligned, an enhanced field effect mobility of 1.67 cm$^2 \cdot$V$^{-1} \cdot$s^{-1} has been achieved when the optimal π-orbital overlap direction is parallel to the direction of the current flow. SIL with a PDMS mold is superior to other methods in that it allows for the mass production of large-area patterns with excellent lateral resolution.

Gold source and drain electrodes on a flexible polymer substrate can also be fabricated by SIL. Recently, Park and co-workers demonstrated a high-throughput and ultrafine patterning of metallic micro- and nanostructures for electronics on flexible substrates via a direct nanoimprinting process of metallic nanoparticles.[211] A metal nanoparticle solution was dispensed on a flexible substrate and imprinted by using a PDMS stamp at low pressure and low temperature, which is compatible with the temperature restrictions of flexible substrates (Figure 26). OTFTs were fabricated by using an air-stable semiconducting polymer and nanoimprinted gold source−drain electrodes on a
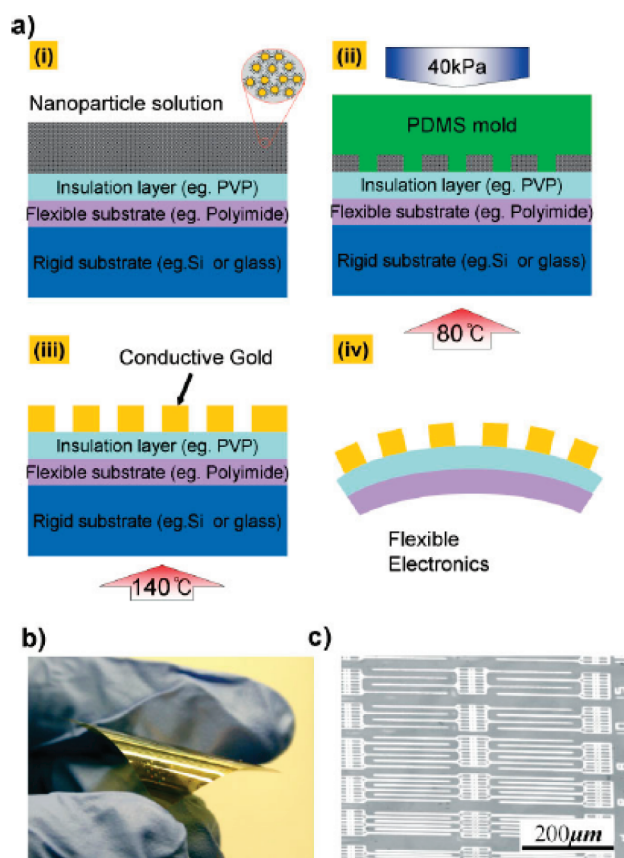
Figure 26. Overview of direct nanoimprinting of gold nanoparticles: (a) Procedure for direct nanoparticle nanoimprinting: (i) fix a clean flexible substrate onto a rigid substrate and dispense the nanoparticle solution (the inset picture is a magnified schematic view of SAM-protected Au nanoparticles), (ii) nanoimprinting with a PDMS stamp, (iii) nanoparticle melting process, (iv) release of the flexible substrate; (b) photograph of electrical devices nanoimprinted on a polyimide substrate. (c) Optical micrograph of microscale electrical structures (source—drain electrodes for multichannel transistors) on a polyimide substrate fabricated by direct nanoimprinting of a gold nanoparticle solution. Reprinted with permission from ref 211. Copyright 2008 Wiley-VCH Verlag.

flexible polymer substrate with good output and transfer characteristics. Also, OTFT devices on flexible substrates showed no significant changes in their performance after bending cycles. It is expected that SIL can provide a very simple and effective nanoscale patterning tool for a variety of functional nanoparticles and enable extremely low-cost, high-throughput, ultrafine resolution manufacturing on flexible substrates.

3.4. Other Patterning Techniques

The semiconductor industry has been pushing high-precision nanoscale lithography as a way to manufacture ever-smaller transistors and higher-density integrated circuits (ICs). Critical issues, such as resolution, reliability, speed, and overlay accuracy, all need to be addressed in order to develop new lithography methodologies for such demanding, industrially relevant processes. To fabricate low-cost and flexible organic electronic devices, inexpensive, noninvasive processing technologies that are physically and chemically compatible with electrically active organic materials need to be developed to lower fabrication costs and maximize device performance. This section will focus on a

range of patterning techniques that are, in principle, suitable for the fabrication of working OTFT devices, which involve other conventional or improved lithographic and nonlithographic patterning techniques that are not described above.

Scanning beam lithography is a serial process, most often used to produce photomasks for projection lithography rather than for actual device fabrication, which can usually generate high-resolution features with arbitrary patterns relative to photolithography. Therefore, high-resolution patterning techniques such as electron beam lithography are still used for organic-based device fabrication.[213,214] Although focused laser beam scanning has a lower resolution than focused electron beam and focused ion beam scanning, it is the least expensive. The two leading methods are laser ablation and selective laser polymerization. Organic materials from selected regions can be locally removed in order to pattern the organic layers in OTFTs.[215,216] However, a number of factors should be taken into consideration in order to achieve a good pattern resolution, since this determines the device performance and processing speed. Focused laser beam-induced photochemical reactions can pattern organic materials as active layers for OTFTs.[217] For example, high-resolution of source and drain patterns with PEDOT-PSS were clearly defined by maskless laser direct patterning.[218] Furthermore, solution-processable OTFTs with 10-μm channel lengths were successfully achieved by focusing a Nd:YAG laser beam onto spin-coated PEDOT-PSS films and developing with deionized water.

A gentle, simple, and yet effective photoinduced and resist-free subtractive method has been developed for the efficient patterning of films of organic semiconductors and the merits of the method demonstrated for the highly soluble fullerene [6,6]-phenyl C61-butyric acid methyl ester (PCBM).[219] The patterning technique is notably straightforward as it requires no photoresist material and encompasses only two steps: (i) exposure of selected film areas to visible laser light during which the PCBM monomer is photochemically converted into a dimeric state, and (ii) development via solvent washing after which the nonexposed portions of the PCBM film are selectively removed (Figure 27). Functional arrays of micrometer-sized PCBM FETs can be fabricated by this technique, which leaves the electronic properties of the remaining patterned organic material unaffected. Soluble organic materials can also be patterned by a new technique termed lithographically controlled wetting.[220] A stamp is placed in contact with a liquid thin film, and capillary forces drive the liquid to distribute only under the protrusions of the stamp. As the solvent evaporates, the deposited solute forms a pattern on the surface with the same length scale as the stamp. The procedure is single-step, cheap, versatile, and reproducible and allows one to transfer motifs on the nanometer scale from a mold to a molecular thin film.

Two simple methods employing selective physical delamination instead of chemical patterning or etching processes have been recently introduced for clean patterning of semiconducting polymers for use in TFTs without compromising device performance.[221] The first process is based on differential adherence as shown in Figure 28a. Semiconducting polymers adhere more strongly to high-energy, hydrophilic surfaces than to lower-energy, hydrophobic surfaces. When the polymer is deposited onto a substrate with a pattern of hydrophilic and hydrophobic surface regions, delamination of the PMMA film will peel off the polymer film from the hydrophobic areas but leave the polymer film on the hydrophilic areas. In principle, this method is similar to conventional selective dewetting techniques based on

substrates with patterned wettability,[222] but this method can yield a better uniformity and better yield of the patterned features. The second method utilizes a patterned solid film as a sacrificial layer to peel off the semiconducting polymers from the undesired areas on the substrates. The process is a solid-state analogue of a conventional lift-off patterning process (Figure 28b). This method allows semiconducting polymers to be patterned on hydrophobic surfaces and can be applied more flexibly without being limited by the constraints imposed by the surface-energy prepatterning. These two simple methods can be easily integrated into the device fabrication process without
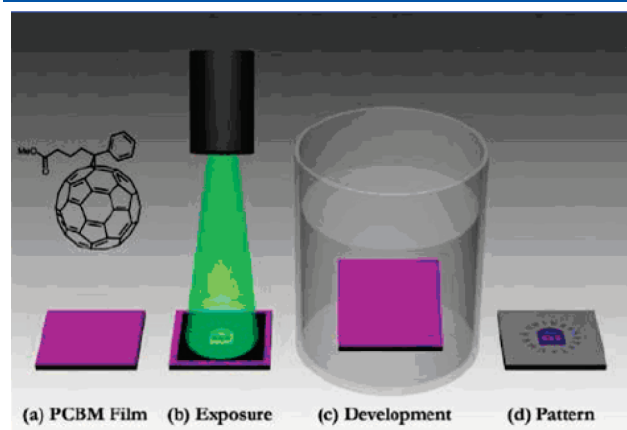

Figure 27. Schematic illustration of the process flow diagram for one representation of the photoinduced and resist-free imprinting (PRI) of a PCBM film. (a) Solution-processed PCBM film on a substrate. (b) Laser-light exposure of the film through a (black) shadow mask, which transforms the exposed PCBM molecules into a low-solubility (dimeric) state. (c) Solution development of the exposed PCBM film, which selectively removes the nonexposed portions of the film. (d) Resulting pattern of electronically active PCBM. Reprinted with permission from ref 219. Copyright 2009 American Chemical Society.

degradation of device performance for either top-gate or bottom-gate device configurations. These two patterning methods might provide high-resolution but low-cost patterning of high-performance polymer semiconducting films for a range of practical applications.

Organic semiconductor thin-films can also be patterned by a dry-taping approach reported by Liu and co-workers.[223] In this method, Scotch tape is gently pressed onto the surface of an organic thin film that has been previously deposited on a substrate bearing a patterned Au film. When the tape is peeled off, the semiconductor material directly above the Au pattern and the Au film itself are selectively removed, while those portions of semiconductor material sitting directly on the substrate remain, resulting in the formation of patterned organic semiconductors on substrates. On the basis of this approach, the patterning of a variety of solution- and vapor-deposited organic small-molecule semiconductors on different surfaces has been demonstrated. This patterning technique allows the direct fabrication of large arrays of bottom-contact pentacene FETs with high performance. Patterned devices exhibited mobilities as high as 0.65 cm$^2 \cdot$V$^{-1} \cdot$s^{-1} and on/off ratios of $10^6 - 10^7$.

Cold welding is a derivative transfer printing technique that can be used to define source and drain electrodes for top-contact OTFT devices.[224] Cold welding differs from transfer printing in that it relies on the formation of metallic bonds between two metal surfaces of similar composition for pattern transfer. Cold welding can occur between gold on the raised regions of a silicon hard stamp and a gold strike layer on the substrate at room temperature under applied pressure. However, the high contact pressure and the subsequent etching process may damage the active layer of OTFTs, and therefore a highly conformable (e.g., PDMS) stamp is needed for cold welding at ambient pressures. An underetching technique in combination with low resolution lithography and simple lift-off processing enables the efficient fabrication of OTFTs with controllable channel lengths.[225] Device structures with self-aligned buried gate and channel

Figure 28. (a) Schematic process flow for patterning PBTTT polymer films by using a PMMA dielectric film as a sacrificial layer and 3 M Scotch tape to selectively delaminate the PBTTT/PMMA films from OTS-covered, hydrophobic areas of the substrate that were prepatterned using a photoresist pattern defined by photolithography. (b) Schematic process flow for lift-off patterning of PBTTT film on OTS-treated surface areas using 3 M Scotch tape to strip off the PBTTT and an underlying patterned PI film from the hexamethyldisilazane (HMDS)-treated surfaces. Reprinted with permission from ref 221. Copyright 2009 Wiley-VCH Verlag.

3383

dx.doi.org/10.1021/cr1001904 |Chem. Rev. 2011, 111, 3358–3406

lengths below 0.4 μm can also be fabricated on polymer substrates. An electrode-peeling transfer method was developed for fabrication of flexible OTFTs; this method is compatible with other patterning techniques, such as microcontact printing and transfer printing.[226] The method involves the use of a SAM as a connecting buffer layer between the electrodes and the dielectric layer. An adhesive Scotch tape substrate was attached on the top of the gate electrode and was then peeled off from the glass substrate together with the source–drain electrodes/dielectric layer/gate electrode multilayer.

The soft molding in reverse (SMIR) technique can be used to pattern not only the polymer active area for polymer TFTs but also the channel at the same time.[227] It is a parallel process where the polymer being patterned is put under similar conditions as in drop casting, such that molecular ordering of the polymer can take place. The key step in SMIR is to place a PDMS mold with the polymer solution onto the polymer gate dielectric layer, and then the solvent in the polymer solution starts evaporating in the void and permeates out of the PDMS walls, slowly thickening and solidifying providing, in the process, a sufficient period of time for orientation of the molecules. The pattern-formation process is the same as for soft molding, only this time in reverse, that is, while the mold is in place. The channel can be finally defined by simply carrying out a blanket metal deposition as the solution thickens and solidifies. The ability of this technique to define the channel length in the process of patterning the active area is a distinct advantage that is quite useful in studying and fabricating polymer TFTs.

Many other patterning techniques based on new mold materials have also been employed for creating micropatterns to fabricate OTFTs. For example, a simple and direct patterning method has been introduced for patterning pentacene OTFTs that involves a blanket deposition of pentacene on a mold followed by transfer of the pentacene on the mold onto the active area of the OTFT.[228] A UV-curable poly(urethaneacrylate) (PUA) mold is sufficiently hard and yet flexible enough for the patterning. The hardness of the mold makes it possible to fabricate sub-100 nm patterns, while the flexibility of the mold allows for conformal contact and reduces processing pressure. The electrical performance of an OTFT fabricated by this method was similar to that of an OTFT fabricated by the conventional shadow-mask technique. While this method is simple, the surface on which the pentacene can be deposited is limited to that of the mold material, and thus the freedom to choose a surface giving larger pentacene grain size is lost. To remove this restriction, a gate dielectric of choice needs to be coated onto the PUA mold and pentacene then deposited on the coated dielectric for fabrication of top gate pentacene TFTs.[229]

A technique known as "hot lift-off" was developed by Wang and co-workers to fabricate an array of 7- by 7-μm organic semiconductor squares.[230] In this technique, a partially cured epoxy stamp is conformally contacted against an organic semiconductor with an applied pressure in order to induce local fracture of the organic semiconductor along the patterned edges of the stamp. This process is similar to other patterning techniques, such as cold welding[224] and microcutting.[231,232] Because the work of adhesion between the epoxy and the organic semiconductor is greater than the work of adhesion between the substrate and the organic semiconductor, the organic semiconductor can peel off with the epoxy stamp in the regions of contact, leaving behind a patterned organic semiconductor in the noncontact regions on the substrate. The method can be used to rapidly pattern large areas at one time in the open air, which makes it an attractive alternative approach to conventional organic semiconductor microcrystalline patterning techniques which offers great promise for the fabrication of organic integrated devices.

3.5. Patterning by Inkjet Printing

Print technology borrowed from the graphic arts and newspaper industry can be adapted in principle to the production of large-volume organic electronics. In particular, inkjet printing is facilitating initial exploration of various aspects of printed electronics in a laboratory setting. Inkjet printing is an attractive patterning technique because it requires no physical mask, has digital control of ejection, and provides good layer-to-layer registration. This technology is compatible with flexible substrates, and can be adapted to high-throughput manufacturing processes, such as roll-to-roll printing methods. The initial impetus to create jet-printing technology came from display manufacturing based on the deposition of polymer light-emitting diodes (PLEDs), and now inkjet printing has been developed as a potential manufacturing method for broad applications, such as organic TFT active matrix backplanes, large-area wireless power-transmission sheet, solar cells, conductive structures, memory devices, sensors, and biological/pharmaceutical tasks.[233−235] This section will focus on the development of its use in the fabrication of OTFTs and organic circuits; other reviews on inkjet printing provide additional details.[234,236,237]

Inkjet printing is a material-conserving deposition technique used for liquid phase materials. These materials, or inks, consist of a solute dissolved or otherwise dispersed in a solvent. A drop-on-demand (DOD) piezoelectric inkjet printing system is most commonly used due to its high placement accuracy, controllability, and efficient usage of materials. The piezo actuator is outside the print-head cavity and does not interact directly with the printing ink, whereas in thermal jet printers the ink is heated to vaporization and requires inks that are not damaged by this process. Piezo actuation also provides greater control over droplet ejection because the waveform that drives the actuator can be tuned for different materials and to control the ejection velocity. One limitation of the resolution for thermal and piezo-electric inkjet printing is the size of the nozzle. To increase the resolution of printed features, an electrohydrodynamic jetting (EHJ) technique to achieve submicrometer resolution has been developed by Park and co-workers,[238] resulting in feature sizes in the range 240 nm to 5 μm.

For example, the feasibility of employing inkjet technology with sub-femtoliter droplet volumes has been demonstrated, which allows definition of metal contacts with single-micrometer resolution on the surface of organic semiconductors to create high-performance OTFTs and low-power complementary circuits.[239] The use of the sub-femtoliter inkjet system for printing Ag nanoparticles is illustrated in Figure 29. The amount of organic solvent dispensed during subfemtoliter inkjet printing is extremely small, and the Ag nanoparticle calcination temperature after subfemtoliter inkjet printing is low (130 °C); therefore, the morphology of the organic semiconductor is not disturbed. However, the main limitation of the sub-femtoliter inkjet system is the relatively small throughput, which is a consequence of the time required to cover large areas with multiple printing passes.

Other high resolution inkjet printing techniques have also been developed for definition of electrode gaps on a 100 nm scale.[240−242] A novel bottom-up self-aligned printing (SAP) technique with two simple additive printing steps has recently

3384

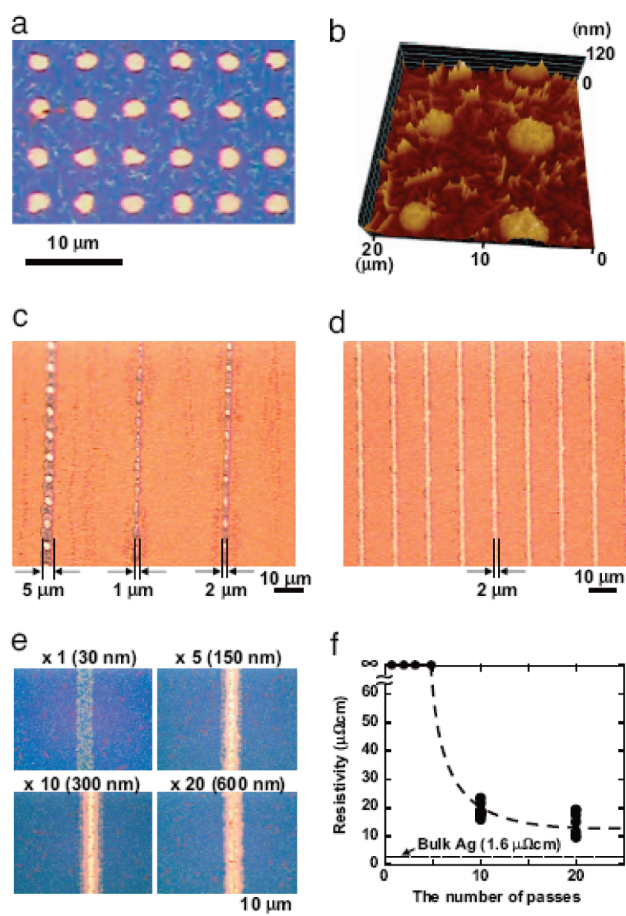dx.doi.org/10.1021/cr1001904 |Chem. Rev. 2011, 111, 3358–3406

Figure 29. Printed Ag nanoparticles using a sub-femtoliter inkjet. Optical microscope image (a) and atomic force microscope (AFM) image (b) of fine dots of Ag nanoparticles deposited by sub-femtoliter inkjet printing on the surface of a thin pentacene film after calcination at 130 °C. The diameter of the dots is ~2 μm, and the thickness is 30 nm. The dots were formed with a single printing pass. (c) Optical microscope image of inkjet-printed Ag lines after a single printing pass before calcination. Linewidths between 1 and 5 μm were obtained in a controlled manner by adjusting the electric field inside the inkjet nozzle. (d) Optical microscope image of inkjet-printed Ag lines after a single printing pass and after calcination at 130 °C. Lines with a line width down to 2 μm are uniform and continuous over large areas. (e) Optical microscope image showing the effect of multiple-pass printing on the evolution of the morphology of an inkjet-printed Ag line after calcination. The effective thickness of the line increases from 30 nm after a single pass to 600 nm after 20 passes. (f) Evolution of the electrical resistivity of inkjet-printed Ag lines with the number of passes after calcination at 130 °C for 1 h in nitrogen. Reprinted with permission from ref 239. Copyright 2008 PNAS.

been demonstrated that is capable of 100 nm resolution while preserving high yield and uniformity.[241] The SAP technique is based on printing a first PEDOT-PSS electrode pattern, subjecting its surface to a carbon tetrafluoride (CF_4) plasma treatment so that it becomes repulsive to the ink, and then printing a second PEDOT-PSS electrode pattern along the edge of the first electrode, such that the ink droplets flow off the first conductive electrode and dry in close proximity to, but not in electrical contact with, the first printed electrode (Figure 30a). However, in this device configuration, in which the two linear electrodes printed from multiple droplets run parallel to each other, a
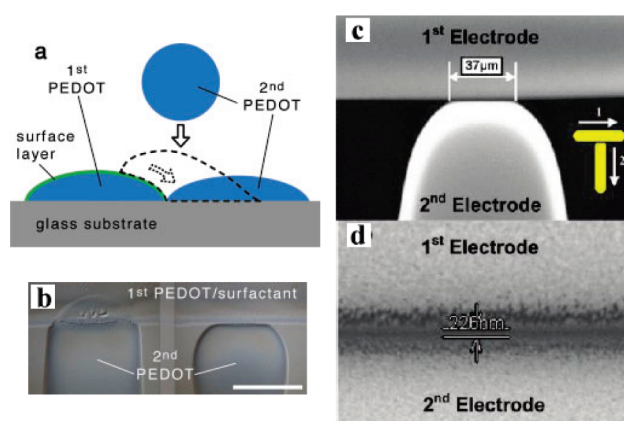

Figure 30. (a) Schematic diagram of the self-aligned printing (SAP) process. The dashed line indicates the initial position of printed PEDOT-PSS before dewetting from the hydrophobic surface layer. (b) Optical micrograph illustrating dewetting of pure PEDOT-PSS layer from benzalkonium chloride surfactant-modified PEDOT-PSS. Left: incomplete dewetting and pinning without postprinting anneal of the first pattern. Right: complete dewetting after postprinting anneal. Reprinted with permission from ref 241. Copyright 2005 Wiley-VCH Verlag. (c) SEM images of "T-shaped" SAP gold electrodes, where the second contact is printed at an angle of 90° with respect to the first one and the channel width is defined by a single droplet. The naturally rounded shape of the droplet conforms to the edge of the first electrode and is deformed into a straight line along the edge of the first contact. In this region, a sub-micrometer electrically insulating gap is created. This is magnified in panel (d), where a clear gap of ~200 nm can be observed. Reprinted with permission from ref 243. Copyright 2010 American Chemical Society.

significant number of devices are shorted. Therefore, a new configuration based on T-shaped single droplet contacts has been developed very recently which, by favoring a better understanding and control of the SAP process, allows the achievement of a surprisingly high device yield of 94–100% on arrays with very low leakage currents.[243] In the T-shaped architecture, the channel formation is determined by the fluid dynamics and dewetting of a single droplet only and allows easier optimization than for two parallel printed electrode lines, resulting in high yields of electrically insulating electrode gaps without shorts (Figure 30c).

Acoustic inkjet printing has been used to deposit a polymeric semiconductor onto patterned metal source–drain contacts.[244] In brief, a high-frequency transducer attached to the back of an acoustic lens launches an acoustic wave through the lens. The lens focuses the acoustic energy, forming a pressure wave that overcomes the surface tension of the liquid standing over the lens and expels a drop from the surface. The nozzleless design minimizes clogging of the ejector, a common problem with thermal or piezo inkjet printers. The resulting P3HT TFTs in a coplanar device geometry exhibited a mobility of 0.1 $cm^2 \cdot V^{-1} \cdot s^{-1}$ and on/off current ratios of ~10^6.

Inkjet printing can work well with a range of metal nanoparticles, such as gold and silver, which are useful for low-cost OTFTs.[245–248] For example, silver nanoparticles stabilized with poly(vinyl pyrrolidone) (PVP) can be utilized as inkjet-printable precursors for fabricating source–drain electrodes for organic transistor devices.[248] The transistors prepared with inkjet-printed source–drain electrodes not only exhibit better FET characteristics than transistors based on vacuum-evaporated

silver electrodes, but they also reveal a temperature-dependent annealing behavior. Surface dangling oxygen atoms of PVP induce an interface dipole, which causes an increase in the work function of the printed electrodes, thus facilitating the injection of charge carriers into the organic semiconductor.

Inkjet printing can also be employed with organic semiconductors, via-hole interconnections, and resistors for OTFTs and organic circuits.[249−252] Polymeric semiconductors are most suitable for inkjet printing since their physical properties may be tailored by simple material design. For example, polymer segment length—which is directly related to the molecular weight and, hence, viscosity—has a critical impact on the flow properties of dilute polymer solutions in the inkjet printing process. Inkjet printing of active layer inks, such as a regioregular polythiophene (PQT-12), F8T2, and P3HT, have been demonstrated. There are also several examples of small molecules deposited by inkjet printing, such as TIPS-pentacene, other pentacene precursors, and oligothiophenes. Recently, top-gate OTFTs have been fabricated on plastic substrates with the n-channel polymers deposited by inkjet printing.[253] These inkjet-printed TFTs showed electron mobilities >0.1 $cm^2 \cdot V^{-1} \cdot s^{-1}$ and acceptable device characteristics.

3.6. Patterning by Other Printing Techniques

Other printing techniques refer to methods in which patterns of materials are applied to a substrate simply by physical contact or exposure through the use of nozzles or masks. The components of OTFTs, from the metal contacts to the insulating elements to the active transport layers, can be patterned by various printing methods, whether these electronic materials are supplied in vapor, liquid, or solid form. Depending on the characteristics of the techniques involved, experimental demonstrations of discrete OTFT devices or circuits have been achieved by these methods, either independently or in combination with other patterning techniques.

Materials can also be deposited in the vapor phase using organic vapor jet printing (OVJP), which can provide an alternative to shadow masking for defining patterns using scanned, small-diameter nozzles.[254,255] In OVJP, organic molecules are sublimed into a hot inert carrier gas and expanded through microscopic nozzles forming a highly collimated gas jet. The jet impinges on the cooled substrate, forming well-defined thin film deposits. Pattern resolution and printing speed are controlled by the nozzle diameter, nozzle-to-substrate distance, downstream pressure, and molecular mass of the carrier gas. This direct, mark-and solvent-free printing technique has been successfully employed for patterning of pentacene for low-cost OTFT applications. Pentacene transistors were grown[255] using OVJP at local pentacene deposition rates of 700 Å/s, having an effective channel hole mobility of 0.25 $cm^2 \cdot V^{-1} \cdot s^{-1}$ and on/off current ratios of 7×10^5.

The shadow-mask patterning technique, which has been demonstrated for the use of commercial organic light emitting diode (OLED) displays, can also pattern the electrodes and organic semiconductors in OTFTs. In this process, metals or small molecules emerge in a directed flux from a source in a physical vapor deposition system and travel through openings in masks placed near the surface of the substrate.[256] The high vacuum under which the deposition is carried out ensures that the mean free path of the evaporated species exceeds the distance between the source and substrate, and finally the evaporated materials travel in a directional manner through the gaps in the

mask and onto the substrate. An advantage of shadow-mask patterning is that, in principle, the masks can be placed and aligned within the deposition system without breaking the vacuum. In fact, the shadow-mask technique is still one of the most common methods for patterning source−drain electrodes of organic transistors.[257] However, shadow-mask approaches have disadvantages that include moderate resolution, inefficient materials utilization, requirement for a high vacuum environment, and patterned areas which are limited by the size of the chamber and of the mask. Polymeric shadow masks have recently been used to fabricate pentacene TFTs and circuits, due to their mechanical flexibility and high resolution.[258] Pentacene-based integrated RF-ID circuits have been powered by near-field coupling at radio frequencies of 125 kHz and above 6 MHz.

Laser-based printing refers to methods that allow a laser to direct the deposition of templates or functional materials onto a device substrate. These techniques include laser-induced thermal imaging (LITI),[259] laser-induced forward transfer (LIFT),[260] and selective laser sintering,[261] which have been used for patterning organic components of fully operative OTFTs. Blanchet and co-workers used LITI to pattern conducting polymer electrodes on flexible substrates for pentacene TFTs.[259] LITI is a solventless thermal imaging technique and is based on the thermal effect of a continuous wave laser, carefully imaged on a donor substrate, by which a material is transferred from a donor to an acceptor substrate placed in contact (Figure 31a). Bottom-contact pentacene TFTs with printed PANI/SWNT electrodes showed charge-carrier mobility of 0.3 $cm^2 \cdot V^{-1} \cdot s^{-1}$, which is twice as high as that of OTFTs with gold electrodes (0.15 $cm^2 \cdot V^{-1} \cdot s^{-1}$).

Both metal contacts and organic semiconductors can be patterned using LIFT for the fabrication of OTFTs.[260] Under the action of a single laser pulse of a Nd:YAG picosecond laser at 355 nm, a small portion of the desired material was transferred from a donor to an acceptor substrate, placed in close proximity, and a square mask was used to select a homogeneous part of the beam, which was imaged on the donor thin layer using a converging lens. Both bottom- and top-contact OTFT devices were fabricated by LIFT in this way, in which source and drain electrodes were deposited from silver nanoparticle ink and copper phthalocyanine (CuPc) was used to form the active layer. The challenge with this method is to transfer very thin layers of functional materials and to obtain well-resolved deposit patterns, which is particularly critical in the case of the electrodes, in order to control the OTFT channel dimensions.

Low-cost and high-resolution carbon electrodes can be easily achieved by selective laser sintering of carbon films formed from carbon solution.[261] This method has been used to pattern carbon-paste electrodes in a process whereby the laser-irradiated region of the solution-processed carbon film remains, and the other parts are washed away (Figure 31b). The resulting carbon electrodes are compatible with most organic solvents and give high performance pentacene TFTs with channel lengths down to 2 μm, owing to the low carrier injection barrier at the carbon/organic interface. Advantages of this technique include the achievement of transparent carbon electrodes without using a vacuum process or lithography and the easy realization of programmable pattering.

Screen printing is a printing technique that uses a mesh to support an ink-blocking stencil. The attached stencil forms open areas of mesh that transfer ink as a sharp-edged image onto a substrate. A squeegee is moved across the screen stencil, forcing
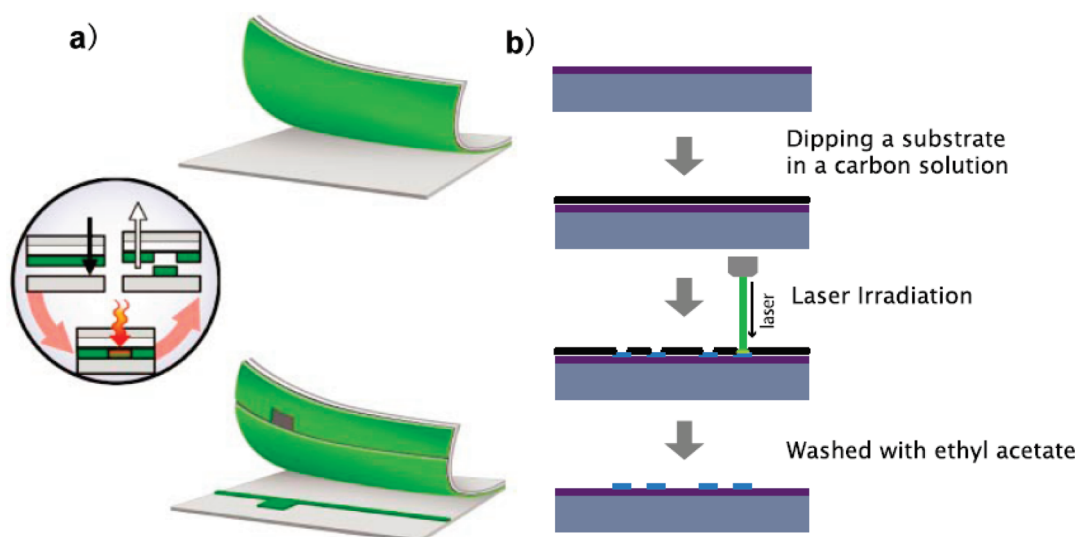
3386

dx.doi.org/10.1021/cr1001904 |Chem. Rev. 2011, 111, 3358–3406

Figure 31. (a) Illustration of the laser-based printing processes. (a) Two flexible films, a multilayer donor and an acceptor are held together by a vacuum. The laser beam is focused onto a thin absorbing layer that converts light into heat, an optional ejection layer is placed directly underneath, and a DNNSA−PANI/SWNT conducting layer coated on top. The heat generated at the metal interface decomposes the surrounding organic material creating a gas bubble that expands and propels the conducting layer onto the receiver. After imaging is completed, the donor and receiver films are separated. Reprinted with permission from ref 259. Copyright 2003 American Institute of Physics. (b) Fabrication of the carbon electrode pattern. Reprinted with permission from ref 261. Copyright 2009 American Institute of Physics.

solution-based ink past the threads of the mesh in the open areas. Removing the screen leaves a pattern of ink in the geometry of the openings in the mesh. Screen printing is more versatile than traditional printing techniques for several reasons: it is compatible with a variety of organic materials as inks, it is a simple process carried out at ambient pressure (unlike lithography), and it enables low-cost printing on flexible substrates. An obvious disadvantage of this technique is the relatively low resolution (~75 μm), especially for forming the critical dimensions in transistors. However, recent improvements have indicated that features as small as 30 μm can be achieved.[262] OTFTs and inverters were fabricated using screen-printed electrodes. The screen printing ink was formulated with silver nanoparticles, which have high conductivity, and carbon black, which has a high work function, in the ratio of 30: 70 wt.%. However, further increases in resolution are required in order to be able to define the channel lengths in transistors.

So far, the traditional technologies of offset, gravure, and flexographic printing with state of the art resolutions in the range of 20 μm have only been optimized for visual image properties. For polymer electronics, however, the focus of printing is now shifting from visuality to functionality. The successive deposition of the different layers required for polymer FETs remains a challenge as a result of the stringent requirements on the apparatus as well as ink chemistry and rheology. There have been some efforts to pattern the source and drain electrodes by using a laboratory scale offset or flexographic printing.[263−266] Recently, integrated circuits were successfully fabricated solely by means of these mass-printing techniques.[265] The source−drain electrodes, polymeric semiconductor, and dielectric were patterned by using offset, gravure, and flexographic printing, respectively, and the circuits were completed by flexographic printing of the gate electrodes in a fast, continuous mass-printing process. The gate electrode and scan bus lines of OTFT-backplane can be printed by combining screen printing and reverse offset printing with Ag ink as a conducting ink. In the printing process, screen

printing was applied to uniformly deposit Ag ink thin film over the entire area of substrate, and then etching resist was deposited and patterned by reverse offset printing. The final gate electrodes were obtained through etching Ag ink layer in the exposed areas. By using this process, the line feature of 50 um was easily obtained.[267]

The use of gravure for the printing of organic electronic devices is very attractive due to its very high throughput, optimal control of feature size, ability to use any substrate, ability to independently vary printing plate/ink/substrate temperature, and its ability to use a very wide range of potentially aggressive inks, solvents, and particulates.[268] The gravure printing process uses a metallic roll, in which the images to be printed have been etched or engraved into its surface. The patterns are filled with ink, and any excess is subsequently wiped off using a blade which is tightly pressed against the roll, the doctor blade. The inked and wiped surface of the roll then comes into contact with the substrate, which is pressed against the gravure roll with the use of an imprint roll, and the ink is transferred from the rolls' patterns to the substrate, completing the print. The resolution of the print is highly dependent on the quality of the patterns on the roll, and the surface and shape properties of the nonpatterned areas. The minimum size of printed features is determined by the size of the patterns on the roll, the amount of ink they deposit, and the wetting properties of the ink. In printed electronics, minimizing feature sizes is critical to enabling high performance, low power, and low cost. A recent work has combined the mass printing techniques (flexography and gravure printing) for the realization of source/drain electrodes by employing effects of surface wetting and dewetting on heterogeneous substrates. OFETs with a channel length of 10 um were produced solely by means of highly productive methods.[269]

The mass production technique of gravure contact printing is used to fabricate state-of-the-art P3HT FETs.[270] Gravure contact printing is a fast and simple technique traditionally with the highest throughput in comparison to other mass printing

3387

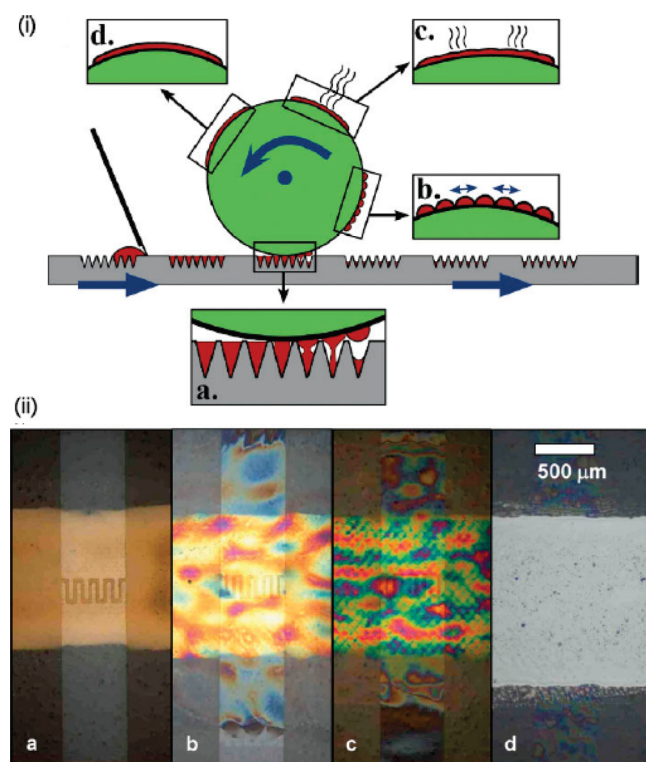dx.doi.org/10.1021/cr1001904 |*Chem. Rev.* 2011, 111, 3358–3406

Figure 32. (i) Schematic of the gravure printing process with the planar cliché used in this work (industrial roll-to-roll gravure uses a cylindrical cliché). The substrate is fixed to a cylinder which is free to rotate. The cliché moves from left to right. The doctor blade on the left of the figure scrapes ink into the cells as the cliché moves. Insets: (a) ink transfer from the cliché cells to the substrate; (b) spreading of the ink to form a uniform film; (c) solvent evaporation; and (d) deposited thin film. (ii) Sequential gravure printing of the transistor: P3HT (3% by wt in Indan) (iia); after the addition of poly(2-hydroxyethyl methacrylate) (PHEMA) (iib), of cross-linked XL-PHEMA (a cross-linkable version of PHEMA) (iic), and of Ag ink gate (iid). Reprinted with permission from ref 270. Copyright 2010 Wiley-VCH Verlag.

techniques. The gravure contact printing process is illustrated in Figure 32i. As the cliché (printing plate) moves from left to right, ink deposited at one end of the cliché is scraped by the fixed doctor blade into the cells, and any surplus is removed. A drum, which is synchronized with the cliché motion, is pressed down onto the cliché and picks up the ink in the cells as the plate passes underneath it. For successful ink transfer, the surface energy and wetting behavior of the substrate must be more favorable to the ink than those of the cliché (Figure 32i, inset a). Also, the shear forces, dependent on the printing speed and ink shear behavior, must allow the ink to be pulled onto the substrate. The ink droplets transferred from the cells must then flow together to form a continuous pattern (Figure 32i, inset b), and the solvent then evaporates (Figure 32i, inset c) leaving behind a layer of material in the print pattern (Figure 32i, inset d). FETs were sequentially fabricated using gravure-printed P3HT, two insulator layers, and an Ag ink top metal gate (Figure 32ii). Printing in ambient and using this bottom-contact/top-gate geometry, an on/off ratio of $>10^4$ and a mobility of 0.04 $cm^2 \cdot V^{-1} \cdot s^{-1}$ are achieved. This rivals the best top-gate polymer FETs fabricated with these materials.

A roll with more than 50 000 transistors has been produced completely by means of gravure printing. A special printing

layout was developed in order to avoid register problems in print direction. Upon using this layout, contact pads for source/drain electrodes of the transistors are printed together with the gate electrodes in one and the same printing run.[271] The principle suitability of the gravure printed transistors for integrated circuits has been shown by the realization of 5-stage ring oscillators. It has been recently demonstrated that screen printing and gravure printing may be highly versatile and could be very appropriate to deposit organic semiconducting layers.[272] These fast "single step" processes combined with amorphous semiconducting polymers give thin, uniform, and reproducible layers. The performances of printed or spin-coated films are similar and lead to robust and reliable full printed transistors and logic functions.

Polymeric transistors and functional integrated circuits can also be fabricated by combining pad printing and blade coating.[273] In pad printing, a flexible pad picks up the ink from a pattern engraved into a plane plate and transfers it to the substrate. In blade coating, a blade is moved over a substrate (with a small blade—substrate gap) and spreads a liquid in front of it to form a film. Both methods combine what is needed for polymer electronics production: fine patterning and thin film capability. The laboratory equipment is able to be used in a batch process which should enable scaling up of the process to a roll-to-roll process with a continuously moving substrate.

4. OTFT FABRICATION METHODS

4.1. Introduction to OTFT Constitution and Device Design

A typical OTFT consists of the following elements: electrodes (gate, drain, and source), a dielectric layer, and an organic semiconductor layer (Figure 33). There are three popular geometries used for OTFTs, as shown in Figure 33: bottom gate, top contacts (BG−TC); bottom gate, bottom contacts (BG−BC); top gate, bottom contacts (TG−BC). For the BG−TC geometry, excellent electrode/organic layer contact and high performance transistors can be obtained and this geometry is usually used for research aimed at developing new materials for OTFTs. Although the BG−BC geometry is a more feasible configuration for many practical applications, unfortunately, this geometry commonly results in much lower device performance due to the poor contacts. The TG-BC geometry is considered to be a potentially promising configuration for large area printed electronics and also ensures good dielectric/single-crystal contact for single-crystal FETs.

Engineering of the transistor structure can lead to improved device performance and stability of organic systems on flexible substrates that are presently the subject of widespread research and commercialization efforts, because of the advantages that they offer in terms of durability, weight, and ease of transport/ use. For example, a 19-by-37 cell organic transistor-based stretchable active matrix has been fabricated by combining printing, vacuum evaporation, and mechanical processes by taking full advantage of an SWNT-based elastic conductor and paste.[10] A few steps toward integration of new architectural possibilities in organic electronics have also been made. Cylindrical OFETs have been obtained starting from a metallic fiber used in textile processes (Figure 34a), which paves the way toward innovative applications of textile electronics.[274] Vertical FETs, where the channel length is determined by the film thickness, have been shown to be a promising means of dramatically increasing the current in an organic transistor by considerably reducing the channel length. Vertical FETs can be
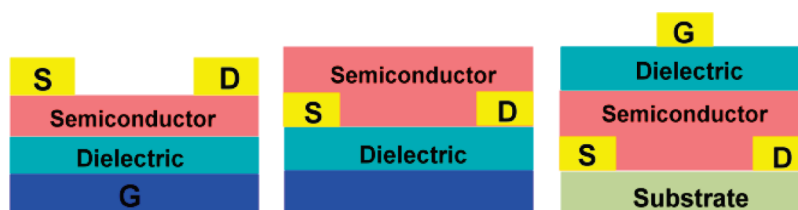
3388

dx.doi.org/10.1021/cr1001904 |*Chem. Rev.* 2011, 111, 3358–3406

Figure 33. Three common geometries of organic thin-film transistors. From left to right: bottom gate, top contacts (BG–TC); bottom gate, bottom contacts (BG–BC); top gate, bottom contacts (TG–BC). S: source; D: drain; G: gate.
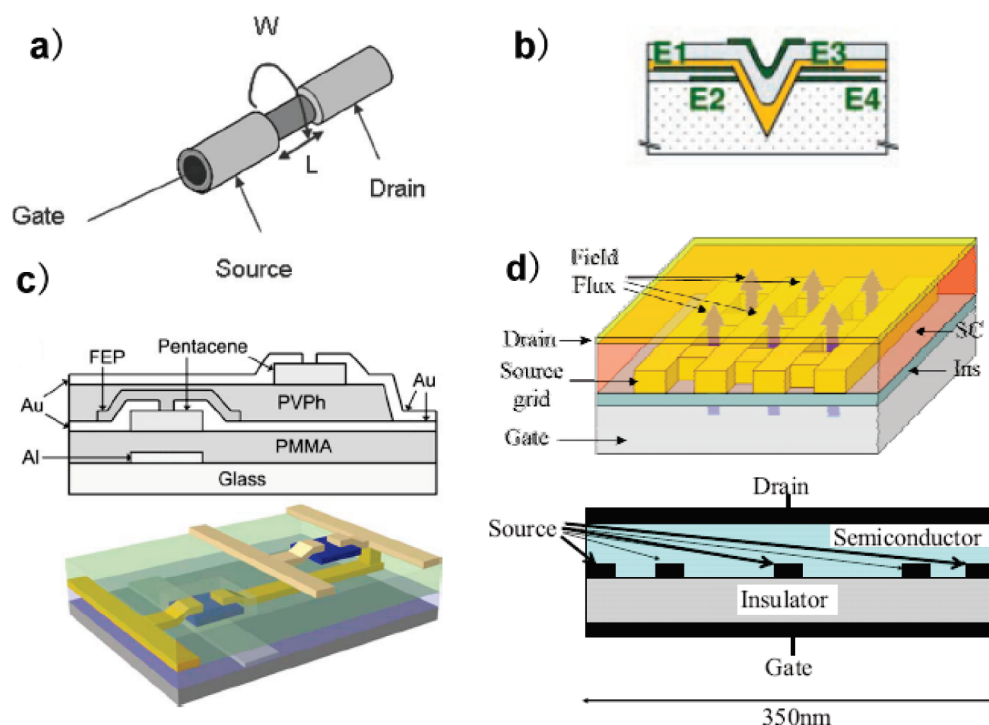

Figure 34. (a) Structure of a cylindrical OFET. Reprinted with permission from ref 274. Copyright 2006 American Institute of Physics. (b) Vertical-channel FETs with source–drain electrodes for two submicrometer, E1-E2 and E3-E4 (two planar source–drain pairs). Reprinted with permission from Science (http://www.aaas.org), ref 232. Copyright 2003 American Association for the Advancement of Science. (c) Schematic representation of an inverter with vertically stacked pentacene thin film transistors. Reprinted with permission from ref 277. Copyright 2009 American Institute of Physics. (d) Schematic illustration and side view of a grid-patterned source electrode vertical FET. Reprinted with permission from ref 278. Copyright 2009 American Institute of Physics.

fabricated by means of solid-state embossing (Figure 34b),[232] excimer laser treatment,[275] photolithography,[276] and nanoscale self-assembled templates (Figure 34c).[277] A vertical organic inverter can also be introduced that consists of two p-channel transistors. The structure of the vertical inverter involves one pentacene transistor stacked on top of another pentacene transistor, and the two transistors have different polymer dielectrics (Figure 34d).[278] Utilization of two different dielectrics enables each of the two transistors to behave as a drive and load transistor for the inverter.

In addition to the three conventional configurations shown in Figure 33, an encapsulation layer is often used in the device architecture to protect the functional devices. For example, a TiO_x layer acts as a scavenging and passivation layer for removing O_2 and H_2O from semiconducting polymers and prevents penetration of O_2 and H_2O, and thereby leads to a significant improvement in the lifetime of OTFTs when they exposed to air.[279] As the thin TiO_x layer is flexible and can be deposited from

solution, its use can reduce the air sensitivity of flexible organic electronic devices to the point where low-cost encapsulation materials should be capable of generating sufficiently long operating lifetimes to be used in commercial products. Self-encapsulation of polymer TFTs by depositing a blend of semiconductor and encapsulant from solution provides an alternative way to minimize damage to the semiconductor layer by exposure to the environment.[280] Alternatively, combining a Teflon passivation layer with Teflon electrets can allow functionalization of the protective capping layer as a second gate in order to control the threshold voltage of transistors.[281]

4.2. Deposition of Organic Semiconductors

The development of OTFTs has largely depended on progress in the deposition techniques and molecular design of organic semiconductors, which are a key component in OTFTs. New organic semiconductors with desirable properties have been synthesized by materials chemists, but new deposition
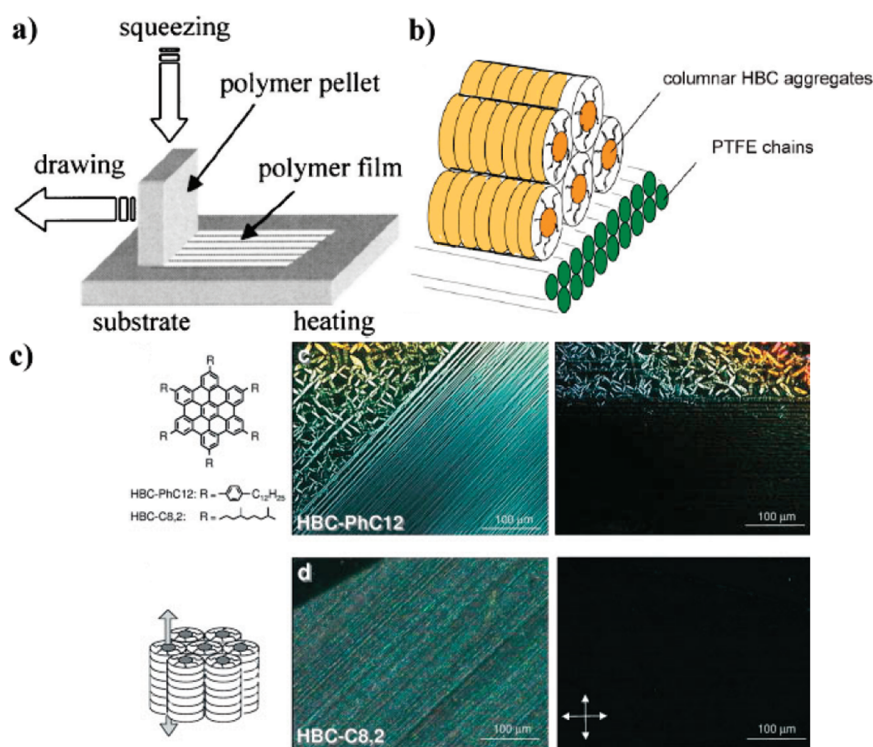
Figure 35. (a) Schematic illustration of the friction-transfer process. Reprinted with permission from ref 284. Copyright 2004 American Institute of Physics. (b) Schematic view of a parallel arrangement of the columnar HBC stacks with respect to the underlying PTFE polymer chains. (c) Molecular and supramolecular structures of the hexa-*peri*-hexabenzocoronene (HBC) derivatives (left). Optical microscopy images under cross polarizers of aligned HBC films on oriented PTFE. Transmitted-light-intensity maxima were observed for films positioned with the alignment direction ±45° to the polarizers (middle), and minima for films oriented parallel or perpendicular to the alignment direction (right). Reprinted with permission from ref 286. Copyright 2003 Wiley-VCH Verlag.

techniques are still required for low-cost, large-area manufacturing processes; these require initial development and optimization in the laboratory. Many experimental techniques for patterning and printing of organic semiconductors have been reviewed in the above sections, and this section will focus on deposition techniques for the alignment of organic semiconductors, although other new deposition methods are also discussed.

4.2.1. Friction-Transfer Technique. The friction-transfer technique was proposed by Wittmann and Smith for preparation of a highly oriented poly(tetrafluoroethylene) (PTFE) film.[282] The PTFE film can be deposited on clean metal or glass surfaces by squeezing and drawing a PTFE block on suitable substrates. The friction-transfer technique offers attractive advantages for polymer film preparation since no solvents are required and it is therefore independent of solubility considerations. Many conjugated polymer films can be prepared by this technique and have been used as the active component in OTFTs. For example, the chain axis of P3HT strongly tends to align along the PTFE friction-transfer direction when P3HT is solvent-cast on a PTFE layer.[283] The field effect mobility is highly anisotropic, with the higher mobility along the friction-transfer direction of PTFE. The origins of the anisotropic properties of this film are likely to be its intrinsic properties as well as its topography.

Well-aligned, highly crystallized conjugated polymer thin films can also be prepared by a drawing method without using solvents and without using underlying alignment layers.[284] In this case, a pellet made by compressing a powdered conjugated polymer is drawn on the substrate (Figure 35a). Regioregular poly(3-dodecylthiophene) (P3DDT) and P3HT thin films have been

prepared for use in polymer FETs, and a mobility enhancement was observed for current flow along the friction-transfer direction. In the case of P3DDT-based devices, hole mobilities along the drawing direction were enhanced by a factor of 20−70 compared with conventional spin-coated films. This mobility enhancement arises from the molecular alignment of the polymer.

Small molecules such as pentacene[285] and hexa-peri-hexabenzo-coronene (HBC) derivatives[286] can also orient uniaxially on PTFE alignment layers. It was observed that the field-effect mobility of pentacene along the molecular columns was 4.2×10^{-1} cm$^2 \cdot$V$^{-1} \cdot$s^{-1}, which was about 100 times higher than that along the friction direction.[285] From electron diffraction and polarized absorption measurements, it was concluded that pentacene molecules adsorb in an edge-on geometry on the PTFE layer, with molecular columns aligned normal to the sliding direction, resulting in the opposite results of the previous P3DDT devices. For HBC derivatives, the columnar stacks in HBC films were oriented parallel to the underlying PTFE chains (Figure 35b).[286] From the optical images, it can be seen that well-aligned HBC films were grown on the PTFE surface, while randomly oriented morphologies were observed on substrates where the alignment layer was absent (Figure 35c). Devices with the channel parallel to the columnar pathway exhibited higher field-effect mobilities than those of devices with columns perpendicular to the channel.

4.2.2. Rubbing Alignment Technique. Rubbing alignment has already widely applied in the display industry: for example, a rubbing alignment brushing prototype machine has been recently used to brush large-area substrates for liquid crystal displays.[287] Application of rubbing alignment in the fabrication

3390

dx.doi.org/10.1021/cr1001904 |*Chem. Rev.* 2011, 111, 3358–3406

of OTFTs was first reported by Sirringhaus and co-workers and afforded enhanced mobility in polymer FETs through the alignment of liquid-crystalline polymers.[288] The enhanced mobility of F8T2 FETs was explained in terms of alignment of the polymer chains parallel to the transport direction with the help of a rubbed polyimide layer. High mobilities of $0.01-0.02$ cm$^2\cdot$V$^{-1}\cdot$s^{-1} were found along the rubbing direction for F8T2 in the nematic glassy phase. The rubbing alignment technique can therefore be used to prepare surfaces with aligned features, and polyimide and poly(vinylalcohol) (PVA) are commonly used as the rubbed polymer alignment layer for OTFTs.

Other liquid-crystalline semiconductors aligned on rubbed surfaces, such as a liquid-crystalline oligofluorene semiconductor in the nematic phase,[289] and derivatives of the liquid-crystalline semiconductor 5,5″-bis(5-alkyl-2-thienylethynyl)-2,2′:5′,2″-terthiophene,[290] have also been demonstrated. Small molecules are another class of semiconductor materials that can be prepared on rubbed alignment layers. For example, the optical anisotropy of a pentacene film on a rubbed PVA layer has been reported and the electrical performance of the resulting pentacene FETs depends on the direction of a current flow.[291] The electrical performance of an OFET with a parallel-rubbed PVA layer was enhanced compared to the performance of an OFET with a perpendicular-rubbed PVA layer or a nonrubbed PVA layer, although the morphological effects such as the grain size and surface roughness were indistinguishable from the OFET on the untreated PVA layer. A variety of organic semiconductors, such as p-sexithiophene (α-6T), p-sexiphenyl (α-6P), pentacene, CuPc, and copper hexadecafluorophthalocyanine (F$_{16}$CuPc) can also be aligned by rubbing.[292] The resulting mobilities were anisotropic with ratios in the range of $15-100$, where higher mobilities were obtained along the rubbing direction.

4.2.3. Photoalignment Technique. The photoalignment technique differs from the rubbing technique and gives a high possibility of producing an easy-orientation axis onto the polymer surface in the liquid crystal cell on irradiation by polarized ultraviolet light. The liquid crystals in an illuminated region can be oriented perpendicularly to the direction of the polarized ultraviolet light, and therefore many liquid crystals can be aligned by such a photoalignment technique. This technique avoids many of the drawbacks associated with the traditional rubbing technique for liquid crystal alignment, such as sample contamination, static charge generation, and scratches.[293,294] The photoalignment layers for liquid crystals can be polyimide-based materials[295] or poly(4-cyano-4′-methacryloyloxyazobenzene) (pCNAz).[296] In the case of F8T2, a mobility as high as 0.02 cm$^2\cdot$V$^{-1}\cdot$s^{-1} has been achieved by aligning the polymer chain parallel to the charge transport direction on a light induced pCNAz layer. Using another liquid crystal semiconductor, 5,5′-bis(4-octyloxyphenyl)bithiophene (P2TP), an enhanced mobility of 0.05 cm$^2\cdot$V$^{-1}\cdot$s^{-1} was obtained by alignment of the $\pi-\pi$ intermolecular packing direction parallel to the charge-transport direction.[296]

Apart from liquid crystal materials, pentacene is the most popular molecular material for alignment by photoalignment techniques for fabricating OTFTs with anisotropic electronic properties. A photoaligned polyimide layer is often used to control the orientation of pentacene, thus producing films with strong anisotropic field-effect mobility.[293,297] For example, a polyamic acid containing azobenzene in the backbone structure (Azo-PAA) was used to induce preferential orientation of pentacene molecules. The orientation of the Azo-PAA backbone

was achieved via random rotation of azobenzene accompanied by angular selective photoisomerization cycles. By thermally imidizing the photoaligned Azo-PAA film, a stable polyimide film was obtained with excellent capability for aligning liquid crystal molecules. In this process, the charge carrier mobility of pentacene FETs along the polyimide alignment direction was about twice that of the perpendicular direction.

Other photoalignment materials can also be used for pentacene FETs. A series of highly soluble maleimide-based polymers with photoreactive pendant groups have been synthesized and used as a gate dielectric insulator and, at the same time, as an alignment layer for pentacene FETs.[298] Photopolymerization of polymer-coated OTFTs with linearly polarized UV radiation resulted in anisotropy in field-effect mobility. The observed field-effect mobilities and on/off ratios were in the range $0.12-0.3$ cm$^2\cdot$V$^{-1}\cdot$s^{-1} and 10^3-10^4, respectively.

4.2.4. Other Alignment Techniques. Magnetic alignment of an anisotropic molecule originates from the diamagnetism of organic molecules. A magnetic moment induced by a uniform magnetic field will interact with this magnetic field and the molecule will acquire extra energy, which depends on its orientation with respect to the magnetic field direction. This results in an orientational force that drives the molecule to align with its axis of smallest susceptibility along the field direction.[299,300] In comparison with other alignment techniques, magnetic alignment has several advantages, since the field exerts a well-defined, contact-free, torque force on all the molecules and can therefore be used for thin films as well as bulk samples. Low molecular weight liquid crystals or liquid-crystalline polymers can be aligned in magnetic fields,[301] and on the basis of this technique, solution-processed OFETs have been constructed with a HBC derivative with charge carrier mobilities of up to 10^{-3} cm$^2\cdot$V$^{-1}\cdot$s^{-1}, which are significantly enhanced with respect to the unaligned material.[302] Exceptionally high mobility anisotropies of $25-75$ for current flow parallel and perpendicular to the alignment direction have been measured as a function of the channel length. Atomic force microscopy performed on the FET structures revealed fibril superstructures that are oriented perpendicularly to the magnetic field direction, consisting of molecular columns with a slippage angle of 40° between the molecules (Figure 36A). For channel lengths larger than 2.5 μm, the fibrils are smaller than the electrode spacing, which adversely affects the device performance.

The epitaxial growth of organic thin films for OTFTs has also been studied as a way of achieving molecular alignment. OFETs can be prepared from an epitaxially grown film fabricated by a wet-transfer process.[303,304] Planar molecules of 2,3,7,8,12,13,17,18-octaethyl-21H,23H-porphyrin platinum(II) (PtOEP) were aligned orthogonally on KBr crystal surfaces along the [110] direction with an edge-on orientation to the surface normal direction. The epitaxial film was transferred onto a SiO$_2$/Si surface immediately after removing the KBr on the water surface to produce the OFETs. A weak epitaxial growth (WEG) approach has been developed by Wang and co-workers,[305] which produces highly oriented and continuous organic thin films of disk-like phthalocyanine compounds with the intermolecular $\pi-\pi$ interaction direction parallel to the substrate, leading to a significant improvement of the carrier transport in OTFTs.

The Langmuir–Blodgett (LB) technique has also been used for the alignment of HBCs, triphenylenes, phthalocyanines, and polymers. For example, HBC molecules formed well-defined LB films when spread from a solution at the air–water interface.[306]
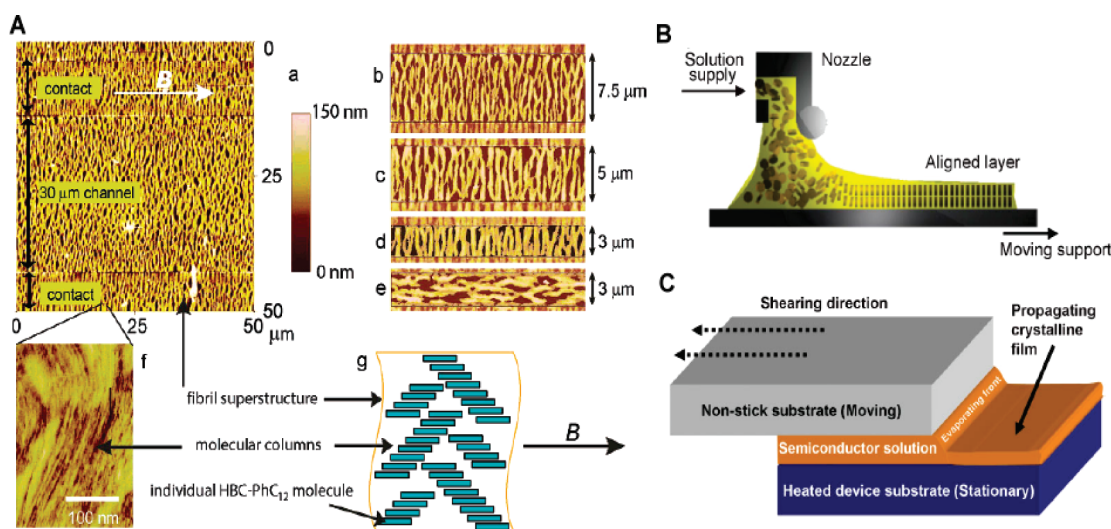
3391

dx.doi.org/10.1021/cr1001904 |*Chem. Rev.* 2011, 111, 3358–3406

Figure 36. (A) AFM images of magnetically aligned substituted HBC-based FETs for different channel lengths L and a schematic representation of the fibril superstructure consisting of molecular columns. (a) $L = 30$ μm, (b) $L = 7.5$ μm, (c) $L = 5$ μm, (d) $L = 3$ μm, (e) $L = 3$ μm for the opposite orientation. (f) Internal structure of a fibril, showing evidence for unidirectionally aligned columnar stacks at 40° to the magnetic field. (g) Schematic representation (top view) of the fibril superstructure, aligned perpendicularly to the magnetic field. The fibrils consist of molecular columns (at 40° to the field), with the individual molecules aligned along the field with the discs in an edge-on arrangement. The films in (a−d) were fabricated in a horizontal magnetic field (denoted by the black arrow). In (e), the magnetic field direction points upward. Reprinted with permission from ref 302. Copyright 2005 American Chemical Society. (B) Schematic presentation of the zone-casting technique. Reprinted with permission from ref 308. Copyright 2005 Wiley-VCH Verlag. (C) Schematic illustration of the solution-shearing method. Reprinted with permission from ref 312. Copyright 2008 Wiley-VCH Verlag.

Regioregular P3HT can be aligned by the LB technique giving[307] polymer FETs with mobilities as high as 2×10^{-2} cm$^2 \cdot$V$^{-1} \cdot$s^{-1}. Preferential alignment of the polymer backbones within the LB films was detected by polarized UV−visible absorption, but no significant anisotropic mobility was measured.

The zone-casting technique has been developed to achieve highly ordered thin films, which allow fabrication of OTFT devices with improved performance. As schematically presented in Figure 36B, a solution of organic material is deposited by a nozzle onto a moving support.[308] In this arrangement, a concentration gradient is formed between the nozzle and the support. At the critical concentration, the material is nucleated from the solution onto the moving support as an aligned thin layer. On the basis of this processing technique, both HBC derivatives and pentacene can be successfully aligned into highly ordered surface layers.[308−311] Recently, Duffy and co-workers[311] fabricated zone-cast pentacene FETs with high field-effect mobilities up to 0.4−0.7 cm$^2 \cdot$V$^{-1} \cdot$s^{-1} and on/off ratios of 10^6−10^7. Well-aligned pentacene films were made by zone-casting from a solution of unsubstituted pentacene molecules in a chlorinated solvent. A high degree of structural alignment was confirmed by this study, with out-of-plane 00n reflections up to at least the seventh order, and a pronounced in-plane anisotropy with the a-axis of the triclinic unit cell predominantly aligned parallel to the zone-casting direction and the ab-plane parallel to the substrate. These results indicate that zone-casting is a powerful technique for the solution deposition of aligned films of small-molecule organic semiconductors.

Small-molecule semiconductors can also be aligned by a facile solution-shearing technique.[312] The solution-shearing process is illustrated schematically in Figure 36C. A small volume of an extremely dilute organic solution is sandwiched between two preheated silicon substrates that move relative to each other at a controlled speed. The bottom wafer is the device substrate, and the top wafer acts as the shearing tool, and its surface is modified to cause dewetting of the solution. The motion of the wafers exposes a liquid front that rapidly evaporates to produce a seeding film containing multiple crystal grains. These crystals act as nucleation sites for the remaining molecules in solution and thus propagate along the direction of the shearing. Top-contact OTFTs prepared with solution-sheared semiconductors have mobilities that are comparable and, more often, superior to those of drop-cast devices.

Homeotropic alignment of a calamitic liquid crystal can be simply induced by treating the substrate with a silanizing agent such as OTS,[313] or by simple melt-processing.[314] For example, a simple melt-processing technique was recently developed to induce homeotropic alignment of 5,5′-bis(4-hexylphenyl)-2,2′-bithiophene (DH-PTTP) in the channel of an OTFT; this allowed the thin-film morphology to be controlled leading to an improved charge mobility. On the basis of the thermal behavior of DH-PTTP, an OTS-treated glass cover was used to confine the material on the substrate and prevent dewetting in the melt. DH-PTTP was either placed as a powder in the channel of a transistor and an OTS-treated glass cover placed on top, or the glass cover was placed directly on top of the gold electrodes and the DH-PTTP powder placed along one edge. The device was then placed in a hot stage under nitrogen and heated above the melting point of DH-PTTP. A molten film was formed between the coverslip and the substrate because of the weight of the glass cover or by capillary filling from the edge of the cover. The device was finally completed by cooling at various rates to room temperature under nitrogen. Bottom-contact OFETs with mobilities up to 2.6×10^{-2} cm$^2 \cdot$V$^{-1} \cdot$s^{-1} were fabricated using this technique.

4.2.5. Other Deposition Techniques. Besides conventional deposition techniques such as spin-coating and drop-casting, some new deposition techniques have also been
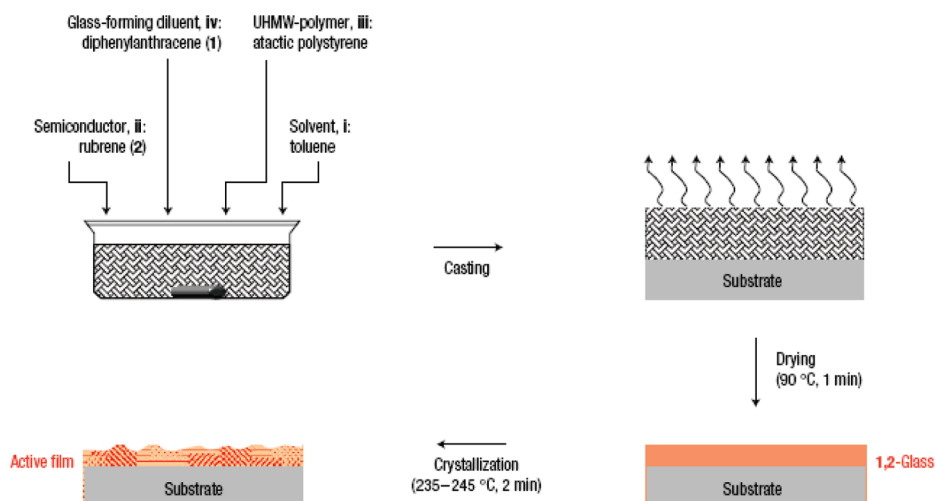
Figure 37. Schematic illustration of the process incorporating a glass-inducing diluent, 5,12-diphenylanthracene. The vitreous nature of the as-cast films allows, in a subsequent fabrication step, controlled crystallization of the active, semiconducting species rubrene at convenient temperatures that are more than 100 °C below its melting temperature. Reprinted with permission from *Nature* (http://www.nature.com), ref 316. Copyright 2005 Nature Publishing Group.

developed for the fabrication of OTFTs. Recently, a novel and simple contact-film-transfer method was used for the fabrication of high-performance polymer TFTs using the polymer/air interface as a charge-transport layer; this allowed the fabrication of ambipolar OTFTs free from the constraints of conventional solution-based processes.[315] A single drop of water was placed on the edge of stacked glass/PEDOT-PSS/P3HT substrates. The water selectively penetrated into the PEDOT-PSS layer. After the PEDOT-PSS layer was completely dissolved, the glass substrate was easily detached from the organic layer, resulting in the transfer of the P3HT film from the glass to the PCBM transistors. The transistors exhibited balanced electron and hole mobilities of 2.1×10^{-2} and 1.1×10^{-2} cm$^2 \cdot$V$^{-1} \cdot$s^{-1}, respectively. Complementary inverters based on two identical ambipolar transistors showed good performance with a gain of 14.

A general route for facile fabrication of thin-film devices from solution, which differs from existing vapor-phase and solution-based deposition techniques, has been described.[316] The process is illustrated in Figure 37. The key beneficial feature of the process is the incorporation of a glass-inducing diluent that enables controlled crystallization from an initial vitreous state of the organic semiconductor, formed in a selected area of the phase diagram of the two constituents. The vitrifying diluent did not adversely affect device performance and stable, discrete rubrene-based transistors were fabricated, with saturated mobilities of up to 0.7 cm$^2 \cdot$V$^{-1} \cdot$s^{-1}, and on/off ratios of $\geq 10^6$. The device mobility was nearly temperature-independent, indicative of the high crystalline quality of the solution-processed, rubrene-based films. Inverter and ring-oscillator structures were also demonstrated.

The controlled phase separation method combined with a surface energy patterning process has been used for spontaneous assembly of thin-film circuits from solution.[317] The polymer blends employed included PQT-12 as the semiconductor and poly(methyl-methacrylate) (PMMA) as the insulator. OTS was patterned to control surface energy. Phase separation on OTS-treated surfaces can occur via surface-directed spinodal decomposition: as PQT-12 is less soluble than PMMA in dichlorobenzene, and solvent evaporation from the top-surface of the film is faster than solvent diffusion through the film, PQT-12 is

therefore rejected toward the solvent-rich part of the film. The three-component solution is strongly quenched in the miscibility gap near the substrate due to the increased PQT-12 concentration, forming a transient PQT-12 wetting layer. The performance of the devices made by phase separation is identical to that of devices made by conventional means, with the median mobility of 0.04 cm$^2 \cdot$V$^{-1} \cdot$s^{-1}. In addition, the solution blend technique is effective for optimizing the electronic properties of devices[318,319] and is a promising method for all-solution-processable fabrication OTFTs.

The grain size in solution-processed organic semiconductor thin films can be tuned over 3 orders of magnitude.[320] This process involves the addition of fractional quantities of fluorinated 5,11-bis(triethylsilylethynyl) anthradithiophene (FTES-ADT), that are capable of seeding the crystallization of triethylsilylethynyl anthradithiophene (TES-ADT). In this unique case, fractional quantities of FTES-ADT were homogeneously incorporated in TES-ADT and no phase separation is observed. This method is simple and requires no additional processing steps in device fabrication. Mobilities, ranging from 0.005 cm$^2 \cdot$V$^{-1} \cdot$s^{-1} to 0.36 cm$^2 \cdot$V$^{-1} \cdot$s^{-1}, showed a strong dependence on grain size.

4.3. Modification of the Dielectric Surface

The properties of the semiconductor/dielectric interface determine the molecular structure and morphology of the organic semiconductor, as well as the motion of the mobile charge carriers in the conduction channel. Therefore, modification of the dielectric surface is an important experimental technique in OTFT research. Tuning of the interfacial surface can be achieved using SAMs, bilayer polymeric dielectrics, plasma treatment, or by insertion of insulating layers between the interfaces. Such modification can affect the uniformity, packing, conformation, polarity, and charge density of the surface, leading to control over the OTFT performance. Introduction of dielectric materials in OTFTs is discussed in recent reviews,[321−323] and here we focus on advances in modification of the dielectric surface.

4.3.1. SAM-Based Modifying Techniques.
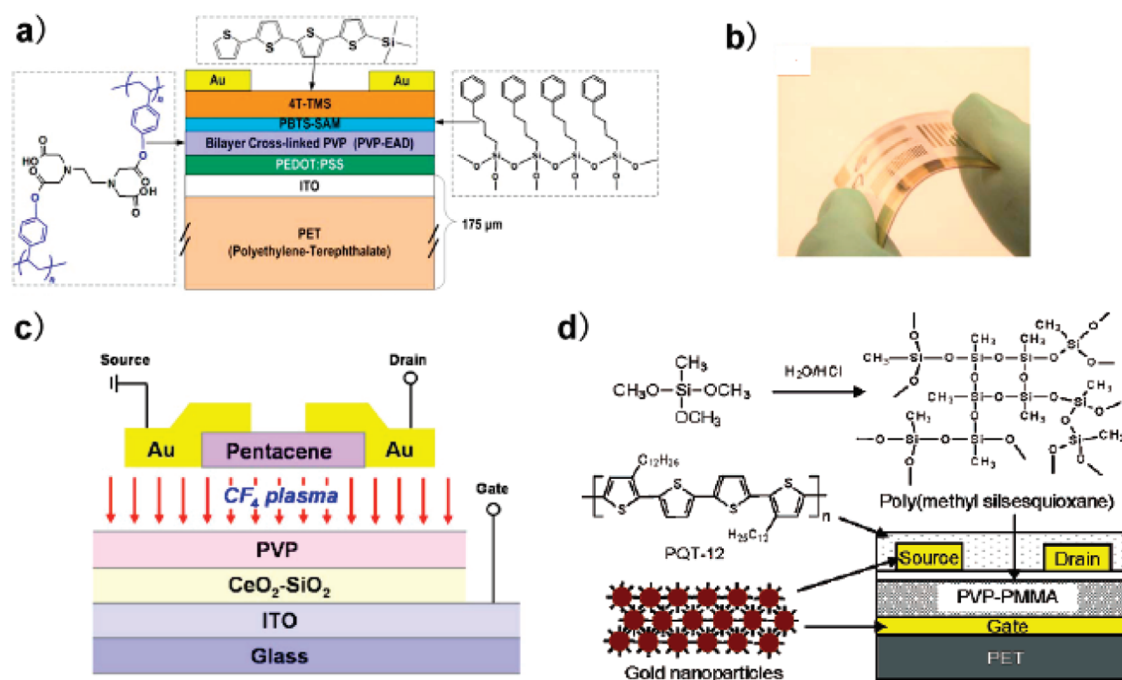One of the major motives for modifying the dielectric surface is to

3393

dx.doi.org/10.1021/cr1001904 |*Chem. Rev.* 2011, 111, 3358–3406

Figure 38. (a) Device structure and (b) photograph of flexible trimethyl-[2,5′5′,2″,5″,2″]quarter-thiophen-5-yl-silane (4T-TMS) solution-processed OFETs. Reprinted with permission from ref 330. Copyright 2009 American Institute of Physics. (c) Schematic structure of fabricated top-contact pentacene TFTs obtained after CF$_4$ plasma treatment. Reprinted with permission from ref 331. Copyright 2007 American Institute of Physics. (d) Schematic depiction of the formation of poly(methyl silsesquioxane) from methyltrimethoxysilane and its incorporation as a dielectric top layer in an all-solution processed OTFT device on PET. Reprinted with permission from ref 333. Copyright 2006 American Chemical Society.

significantly reduce the OFET operating voltage. It has been widely shown that a powerful way to do this is by using a SAM, due to the high density of −OH groups on the surface of conventional inorganic gate dielectrics.[324] Much effort has been carried out to control the dielectric surface using SAMs, such as OTS, hexamethyldisilazane,[325] fluorinated silanes,[326] and alkyl-phosphonic acids.[327] For example, anthryl-alkylphosphonic acid (π−σ-PA) SAMs were fabricated on top of aluminum oxide as the gate dielectrics for low-voltage driven OTFTs which showed small leakage current densities and subthreshold slopes.[327]

The physical interactions at the semiconductor/gate dielectric (SiO$_2$) interface can be controlled by inserting hydrophobic organoalkylsilanes with an alkyl chain length of C8, C12, C16, or C18.[328] Depending on the physical structure of the dielectric surface, which was found to depend on the alkyl chain length of the SAM (ordered for C18 and disordered for C8), ultrathin pentacene films adopt different nanostructures near the interface. The field-effect mobilities of the resulting FET devices varied by more than a factor of 3 depending on the alkyl chain length of the SAM, reaching values as high as 0.6 cm^2·V^{-1}·s^{-1} for the disordered SAM-treated dielectric. This enhancement of the electrical properties can be attributed to laterally well-ordered crystallites and large grains in the pentacene submonolayer in the system with an organosilane SAM with short alkyl chains; this results from a higher lateral diffusion mobility of pentacene molecules on the SAM-treated dielectric surface during the deposition.

In a recent paper, Virkar and co-workers have shown the importance of phase and order of the organic dielectric surface modification layer in achieving two-dimensional (2-D) growth of subsequently vacuum-deposited organic semiconductors in pentacene and C$_{60}$.[329] The LB technique was employed to systematically vary the organization and density of the OTS monolayers. In this process, amphiphilic OTS molecules were compressed by applying a lateral pressure to the monolayer film at the air−water interface. With increasing applied lateral pressure, the film underwent a transition from a 2-D gas to a 2-D liquid and finally to an ordered 2-D solid. As a result of the increase in density of the OTS, a substantial improvement in the charge-transport characteristics was obtained, with mobilities as high as 5.3 and 2.3 cm^2·V^{-1}·s^{-1} for C$_{60}$ and pentacene, respectively.

SAMs can also modify the polymer dielectric and form bilayer polymeric dielectrics for use in flexible OTFTs. A low interface trap density was achieved by modifying a cross-linked PVP surface with a phenyl-terminated SAM from 4-phenylbutyltri-chlorosilane (PBTS).[330] The device stacking architecture is shown in Figure 38a, with a conducting polymeric gate and a double layered dielectric composed of low-temperature cross-linked PVP and PBTS SAMs. Through the optimized solution-shearing process, controlled crystallization of a small-molecule organic semiconductor film was obtained with favorable charge transport microstructure and a low bulk trap density. Low-voltage, solution-processed organic transistors can be fabricated on rough plastic substrates (Figure 38b), with a carrier mobility over 0.2 cm^2·V^{-1}·s^{-1}, and a turn-on voltage of near 0 V under ambient conditions.

4.3.2. Other Modifying Techniques. Plasma treatments have been widely used to modify surfaces or define patterns in organic polymer films. The surface wettability or surface energy of the dielectric surface can often be tuned to match those of organic semiconductors by this technique. Recently, low-k and high-k hybrid gate dielectrics for pentacene TFTs were modified by CF$_4$ plasma treatment.[331] After CF$_4$ plasma treatment,

3394

dx.doi.org/10.1021/cr1001904 |*Chem. Rev.* 2011, 111, 3358–3406

fluorine atoms diffuse into the interior of the low-k polymer and eliminate ionic impurities which reduce the leakage current density and overall pentacene initial growth on the superhydrophobic surface is significantly improved (Figure 38c). Excellent device performance was obtained, with maximum field-effect mobility of 1.41 cm$^2 \cdot$V$^{-1} \cdot$s^{-1}, a low threshold voltage of +1 V, and on/off current ratios of 10^5. Appropriate surface treatment of oxygen plasma-enhanced chemical vapor deposited (PECVD) silicon nitride (SiN$_x$) and silicon oxide (SiO$_x$) as gate dielectrics can also be used to improve the performance of solution-processed OTFTs, and integration of OTFT circuits targeted for flexible and lightweight applications.[332]

A class of polysiloxanes, poly(methyl silsesquioxane) (pMSSQ), has been used as a modification agent for the gate dielectric surface in OTFTs.[333,334] pMSSQ is solution-processable and its solution viscosity in various organic solvents can be tuned by varying the cross-link density to suit common solution deposition processes. It is also self-cross-linkable at a temperature that is compatible with the use of common plastic substrates, thus enabling fabrication of flexible OTFTs (Figure 38d).[333] This polymer modification approach leads to significantly improved performance of polythiophene-based FETs. The beneficial effects on transistor performance of surface modification with pMSSQ are often significantly greater than those obtained using other silane SAMs.

Dielectric surfaces can also be modified with polymer insulators as bilayer dielectrics for OTFTs. By using this technique, the air stability of n-channel OTFTs based on N,N'-dioctyl-3,4,9,10-perylene tetracarboxylic diimide was improved.[335] The hydrophobic nature of the polymer surface inhibited protonation of the siloxyl groups on the SiO$_2$ surface, leading to fewer SiO$^-$ groups that can behave as electron traps. Among the polymer insulators tested, the devices modified with hydroxyl-free polymers exhibited the best air stabilities. The electron trapping effect of the SiO$_2$ layer can also be effectively suppressed by inserting an alkane layer.[336] A hydroxyl-free insulating material, a long-chain alkane, tetratetracontate (TTC, C$_{44}$H$_{90}$) layer was coated on the SiO$_2$ surface. After the insertion of TTC on the SiO$_2$ interface, the operating mode for a pentacene FET with Al electrodes was switched from p-type to n-type.

4.4. Contact Engineering

Contact engineering involves the modification of the interface between source−drain electrodes and the semiconductor, and deposition of various promising electrode materials by new experimental techniques. In an ideal OFET, the source and drain contacts are ohmic, meaning the value of the contact resistance is negligibly small in comparison with the electrical resistance of the semiconductor (i.e., the channel resistance). However, many studies on real devices have shown significant nonohmic behavior at the metal−organic contacts. Especially when downscaling the device, the channel-length independent contact resistance acts as a "bottleneck" that limits the performance of the transistor. It is therefore necessary to reduce contact effects by means of contact engineering. This section will discuss the contact engineering of three kinds of contact materials, namely, metal materials, organic conductive materials, and carbon-based materials.

4.4.1. Metal Electrodes. One of the simplest modification techniques to reduce contact resistance is to form a SAM on top of the metallic contacts. In the bottom contact OTFT architecture, increased contact resistance arising from interfacial charge
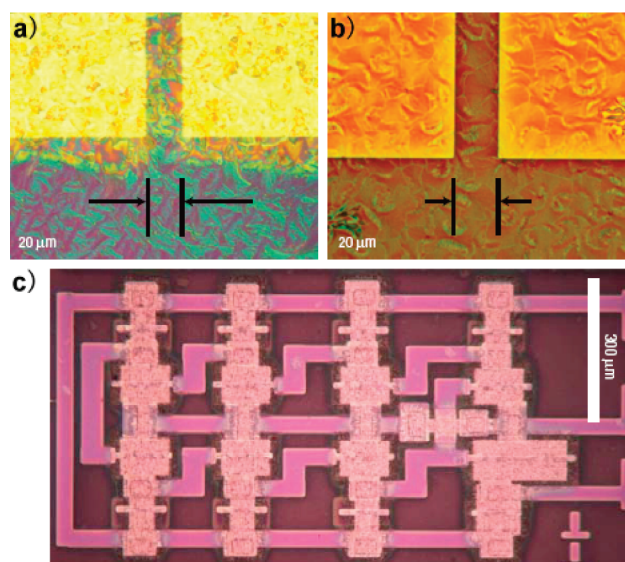

Figure 39. (a) Film spin-cast at 1000 rpm from 2 wt% solutions in warm toluene onto substrates with PFBT-treated source and drain contacts. (b) Film spin-cast at 1000 rpm from a 2 wt% solution in room-temperature toluene onto substrates with untreated source and drain contacts. Images were taken using differential interference contrast with channel lengths of 20 μm. (c) An optical micrograph of a seven-stage ring oscillator. The different microstructures in the PFBT-treated electrodes and polyimide field regions can be easily seen. Reprinted with permission from *Nature* (http://www.nature.com), ref 340. Copyright 2008 Nature Publishing Group.

migration, surface dipoles, the insulating nature of the side chains, or physical delamination is much more significant than in the top contact OTFT geometry. Improved charge injection and quality of the semiconductor film on top of bottom contacts can be realized by treating the contacts chemically by means of SAMs prior to deposition of the semiconductor. In the simplest case, one can use thiol-terminated SAMs to adsorb onto gold electrodes, which can effectively improve the contact and lower the contact barrier for use in high-performance OTFTs.[337,338] Our research group used sulfur to modify gold top-contact electrodes resulting in significant increases in the performance of n-channel OTFTs based on N,N'-dioctylperylene diimide (PDI-C8) and N,N'-ditridecylperylene diimide (PDI-C13).[339] The highest mobilities (ca. 0.80 and 0.87 cm$^2 \cdot$V$^{-1} \cdot$s^{-1} for PDI-C8 and PDI-C13, respectively) were obtained for sulfur-modified devices fabricated by optimized growth rates under ambient conditions in the dark. This result demonstrates that the contact resistance at the gold−organic interface is a major limiting factor for PDI-C8/13-based OTFTs, and effective modification can be a good method to improve the gold−organic interface.

A low-cost approach has been reported recently for controlling the microstructure of solution-cast acene-based organic thin films through modification of interfacial chemistry.[340] In this process, pentafluorobenzenethiol (PFBT) was used as a contact-treatment SAM to chemically and selectively tailor the source−drain contact interface, which then initiated the crystallization of soluble organic semiconductors, leading to the growth on opposing contacts of crystalline films that extend into the transistor channel (Figure 39a,b). High-performance OTFTs and circuits can be fabricated by this technique (Figure 39c) and used as a tool to determine the influence of the microstructure on

the device characteristics. The use of the contacts to induce crystallinity in the channel region of OTFTs opens the way to novel room-temperature, low-cost, self-patterning techniques for manufacturing high-channel-mobility OTFTs and flexible circuits.

An interlayer can be often introduced between the metal electrode and organic semiconductor layers in order to reduce contact resistance.[341] For example, improved injection was achieved by introducing an electron injection layer using solution-processable titanium suboxide (TiO_x). The enhanced performance of fullerene n-channel FETs was achieved by using a TiO_x injection layer.[341] The electron mobilities of OTFTs using Al as source−drain electrodes after this modification were comparable to those obtained with OFETs using Ca as the source−drain electrodes. This study demonstrated that the TiO_x layer can reduce the electron injection barrier because of the relatively strong interfacial dipole of TiO_x. The insertion of an organic interlayer between the gold electrode and the pentacene layer has also been demonstrated to lead to a simultaneous improvement in adhesion and reduction in contact resistance.[342] In this study, a newly synthesized organic material, oligo(3-methylsulfanylthiophene) (OMST), was applied as an adhesive interlayer in order to effectively improve the adhesion and device characteristics of flexible, bottom-gated, pentacene TFTs. Cyclic bending tests also showed that the electrical properties of devices with the thermally evaporated interlayer were more stable than those of the device with no interlayer.

Optimization of the contact resistance has also been realized by surface treatment in short-channel bottom-contact pentacene FETs.[343] In order to reduce the contact resistance, the Au source−drain contacts were subjected to a special UV/ozone treatment, which induced the formation of a thin AuO_x layer. This technique is very effective in that it can not only decrease the hole-injection barrier between Au and pentacene but also improve the morphology of pentacene on top of the Au contacts and thus reduce the access resistance of carriers to the channel. Devices with UV/ozone treated contacts of very low resistance exhibited a charge carrier mobility up to 0.4 $cm^2 \cdot V^{-1} \cdot s^{-1}$, which was independent of the channel length.

4.4.2. Electrodes Based on Organic Conductive Materials.
Besides metal and metallic nanoparticles, highly conductive organic materials can also be used as source−drain electrodes in OTFTs, such as polypyrrole,[344] PEDOT-PSS,[345] and the organic charge-transfer salts (tetrathiafulvalene)(tetracyanoquinodimethane) $[(TTF)(TCNQ)]$[346] and $[(BO_9)(C_{14}\text{-}TCNQ)_4]$ $[BO_9 = $ bis(ethylenedioxy)tetrathiafulvalene and $C_{14}\text{-}TCNQ = $ tetradecyltetracyanoquinodimethane].[347] For example, the water-based conductive polymer, PEDOT-PSS, has received much attention as an inkjet printable electrode for polymer TFTs, although the electrical properties of devices with printed PEDOT-PSS electrodes have generally been inferior to those of devices with evaporated metal electrodes. Recently, Lim and co-workers reported that addition of dimethyl sulfoxide (DMSO) into the PEDOT-PSS solution increased the conductivity of the inkjet-printed PEDOT electrodes, thus significantly reducing the contact resistance of the electrodes.[345] The lower contact resistance of the DMSO-treated PEDOT electrode compared to the corresponding electrode without DMSO treatment may be due to enhanced interfacial stability at the contact between the printed PEDOT electrodes and the semiconductor layers. This demonstrates that the electrical properties of polymer TFTs can be
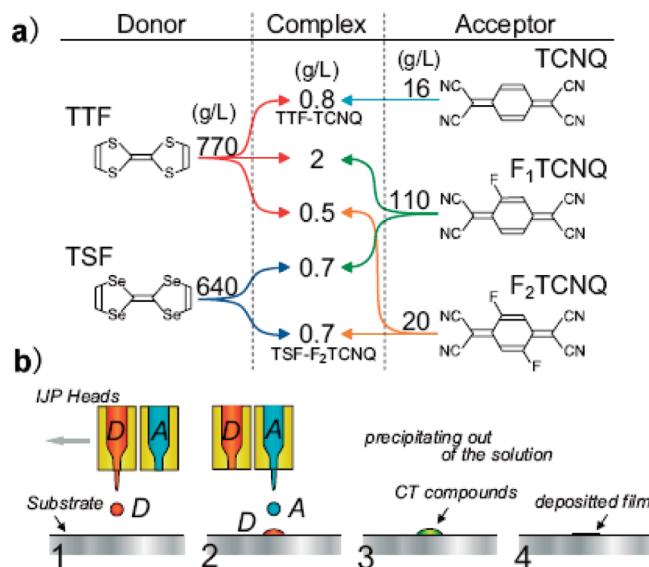

Figure 40. (a) Solubilities of organic donor and acceptor molecules before and after formation of charge-transfer complexes. Solubility in DMSO is shown for the donors (TTF and TSF), acceptors (TCNQ, F_1TCNQ, and F_2TCNQ), and their donor−acceptor complexes. (b) Illustration of the steps involved in the double-shot inkjet printing process. Reprinted with permission from ref 349. Copyright 2007 Wiley-VCH Verlag.

enhanced by controlling the solvent properties of a PEDOT-PSS solution used as the inkjet-printed source and drain electrodes.

Using a metallic organic charge-transfer salt $[(TTF)(TCNQ)]$ as source−drain electrodes can also give a drastic reduction in the contact resistance of OTFTs. A recent study demonstrated that $[(TTF)(TCNQ)]$ is an excellent electrode material for bottom-contact transistors, with a performance which is comparable to that of top-contact Au transistors.[348] $[(TTF)(TCNQ)]$ can be deposited by evaporation or inkjet printing. Recently, a double-shot inkjet printing (DS-IJP) technique was developed for deposition of the sparingly soluble $[(TTF)(TCNQ)]$.[349] This method is based on the fact that the individual component donor and acceptor molecules generally show much higher solubilities than do their complexes. Figure 40a illustrates the solubilities of some donors and acceptors and their charge-transfer (CT) complexes in DMSO. Microscale liquid intermixing of dense droplets of inks containing donors and acceptors on substrates resulted in the instantaneous formation of CT complexes that form high-quality synthetic metal films without postprocessing annealing. In the process of drop-on-demand inkjet printing, a first drop of the donor ink is overprinted by a second drop of the acceptor ink at an identical position within 2 s to form a mixed droplet on the substrate before the solvent is fully evaporated (Figure 40b). Source−drain contacts produced from the inkjet printed $[(TTF)(TCNQ)]$ films afforded high-performance pentacene TFTs that showed sharp on/off switching at low gate voltages.

4.4.3. Carbon-Based Electrodes.
Carbon-based electrodes can be also be used as source−drain electrodes for OTFTs. Single-walled carbon nanotubes (SWNTs) have been recently used as quasi-one-dimensional (1-D) source−drain electrodes to construct OFETs with molecular-scale widths (∼2 nm) and channel lengths (down to 1−3 nm).[350] The process involves
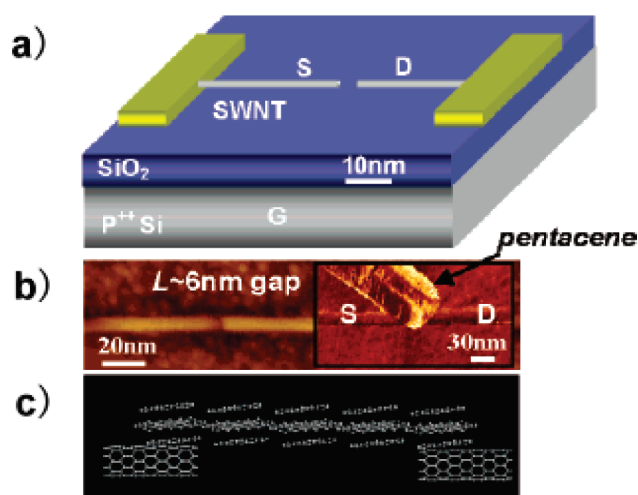
Figure 41. (a) Schematic drawing of a cut SWNT with a sub-10 nm gap to be used as source (S) and drain (D) electrodes of an organic FET. The doped Si serves as a back gate (G), and the SiO_2 thickness t_{ox} = 10 nm. (b) AFM image of a cut SWNT (diameter = 2 nm, gap size L measured to be ~6 nm after correction for the tip size effect). Right inset: AFM image of a vapor-deposited pentacene crystallite bridging a cut SWNT. (c) Drawing of a pentacene crystallite bridging two SWNT electrodes. Reprinted with permission from ref 350. Copyright 2004 American Chemical Society.

cutting metallic SWNTs to form small gaps within the tubes with control over the gap size down to ~2 nm. The cutting relies on electrical breakdown of individual SWNTs between two metal electrodes (Figure 41a), and the size of the cut was found to be controllable by varying the lengths of the SWNTs. The favorable gate electrostatics associated with the sharp 1-D electrode geometry allows for room temperature conductance modulation by orders of magnitude for organic transistors that are only several molecules in length, with switching characteristics superior to devices with lithographically patterned metal electrodes. Similar work has been carried out by Nuckolls's group who used an oxidative cutting of individual metallic SWNTs to give source−drain electrodes for chemoresponsive monolayer transistors,[95] and this new method can also applied to create point contacts for molecular electronic devices.[351]

Multiwalled carbon nanotubes (MWNTs), composed of coaxially arranged single-walled carbon nanotubes of different radii, are also good candidates for electrodes in OTFTs. However, their applications are limited by their poor solubility and low work function. A simple technique was recently used to solve this problem[352] whereby MWNTs were solubilized in water by simply wrapping them noncovalently with poly(4-styrene sulfonate) (PSS). The wrapping of the MWNTs with the water-soluble polymers is thermodynamically driven by the loss of the hydrophobic interface between the tubes and the aqueous medium. TIPS-pentacene FETs fabricated using the PSS-wrapped MWNTs as source−drain electrodes had a field-effect mobility of 0.043 $cm^2 \cdot V^{-1} \cdot s^{-1}$, which is four times higher than that of similar FETs containing gold electrodes (0.011 $cm^2 \cdot V^{-1} \cdot s^{-1}$).

Recently, Wada and co-workers have reported solution-processed carbon-paste OFETs patterned by "surface selective deposition" using self-assembled monolayers.[353] The process is illustrated in Figure 42a, where a carbon-paste solution is deposited on the region in which the self-assembled monolayers are removed by ultraviolet light irradiation. The resulting carbon film shows good mechanical and thermal stability, and the bottom-contact pentacene
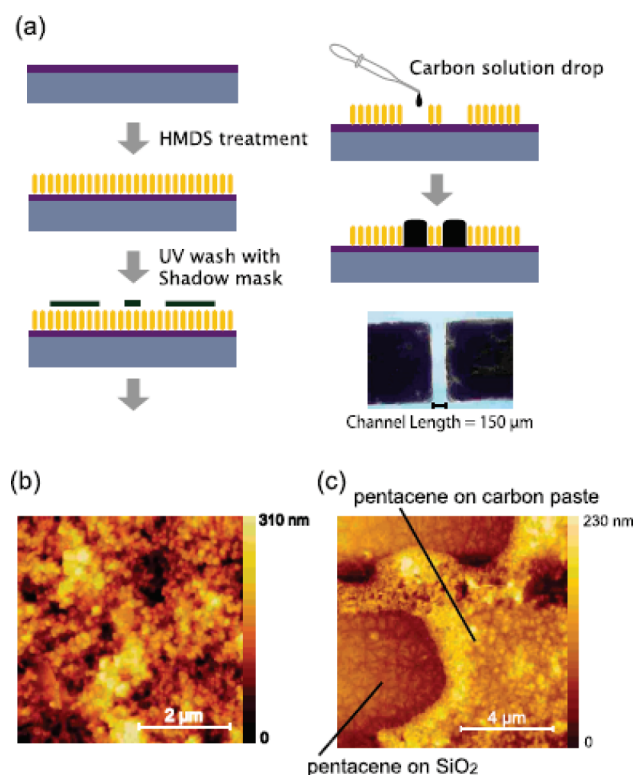

Figure 42. (a) Fabrication of a carbon-paste electrode pattern and the resulting electrodes. (b) AFM image of the carbon film. (c) Pentacene morphology around the carbon electrode. Reprinted with permission from ref 353. Copyright 2008 American Institute of Physics.

transistor shows a high performance of 1.0 $cm^2 \cdot V^{-1} \cdot s^{-1}$ and has the additional advantages of easy and low-cost fabrication. This method can also be applied to solution-processed polythiophene transistors as well as n-channel materials.

Graphene is another new promising graphite-based material for use as source−drain electrodes in OTFTs due to its unique properties, such as low resistivity, high chemical stability, and mechanical strength. For example, Cao and co-workers used cut graphene sheets as 2-D contacts for OTFTs.[354] These contacts were produced by oxidative cutting of individual 2-D planar graphene by electron beam lithography and oxygen plasma etching. Nanoscale organic transistors based on graphene contacts showed high-performance FET behavior with bulk-like carrier mobility, high on/off current ratio, and high reproducibility.

A novel approach for the preparation of regular graphene patterns has been recently reported by Pang and co-workers.[355] The process is shown in Figure 43: a key step is that the sample was exposed to an oxygen plasma to remove the graphene regions not covered by the aluminum (Figure 43e). The aluminum served as a "sacrificial" metal, protecting the covered graphene from ablation by the plasma. Using P3HT as the semiconductor, the field-effect mobilities in graphene-contacted OFETs were comparable to, or even higher than, those of similar devices with gold source−drain electrodes, demonstrating that oxygen-plasma etching of a graphene film with sacrificial aluminum contact patterns is an effective method for accurately controlling the size of graphene electrodes, and that graphene is a potential substitute for gold in hole-injecting contacts in organic electronics.

Our group has recently developed a simple way to obtain interdigital graphene source−drain electrodes on SiO_2/Si
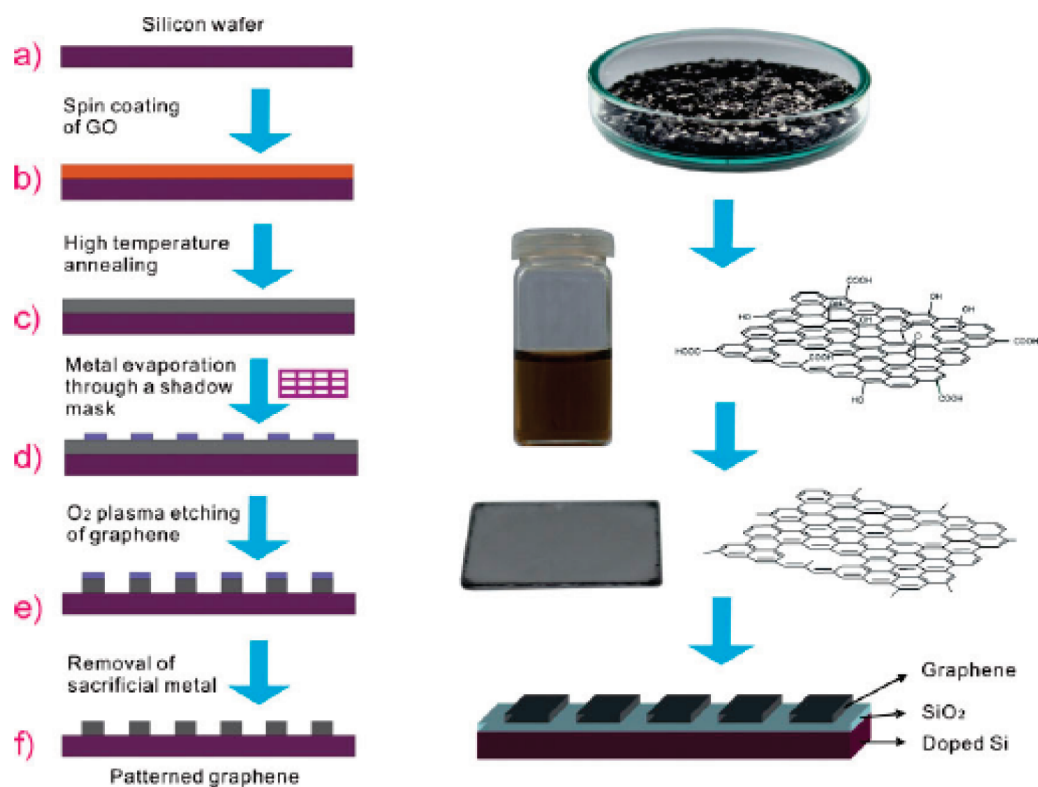
Figure 43. Schematic illustration of process for fabrication of patterned graphene electrodes. Reprinted with permission from ref 355. Copyright 2009 Wiley-VCH Verlag.

substrates.[356] A graphene film was grown on Cu and Ag electrodes that were patterned on a highly n-doped silicon wafer with a thermally oxidized SiO_2 dielectric layer. Ethanol was used as the carbon source, with Cu or Ag as the catalyst, and H_2/Ar as the carrier gas. Ethanol was placed in a low temperature zone, while the substrate with the patterned metal layers was heated to 700–800 °C. The graphene layers were obtained only on the patterned Cu or Ag layer. The pattern of the graphene layer depends on the shape of the patterned metallic catalyst. Therefore, it is easy to pattern the graphene layer. The graphene electrodes showed excellent electrode/organic interface contacts and low injection barriers, confirming that high-performance OFETs can be fabricated based on low-cost graphene source–drain electrodes.

5. CONCLUSION

Recent innovations in experimental techniques have created great opportunities for the development of OTFTs and integrated circuits. The microelectronics industry and the need for low-cost, flexible electronic devices have further pushed this development during the last decades. In this review, we have systematically categorized experimental techniques into three classes: characterization techniques, patterning and printing techniques, and deposition techniques. The latter two classes constitute fabrication or processing techniques, and complement each other in the fabrication of the key components of organic devices. All techniques described here have their own specificity and in many cases do not cover the entire spectrum of fabrication needs. In addition, most of the reported techniques still remain at the proof-of-principle stage, and extending their use to real and large-scale manufacture still represents a big challenge. A powerful set of tools is now available to characterize the optical, electronic, and microscopic structure and

composition of materials, and the intrinsic properties of films, as well as to study fundamental questions of charge injection, trapping, and transport. Such advanced characterization techniques are necessary to establish the relationships between the primary properties of semiconductors, processing of films, and performance of devices. These characterization techniques allow researchers to achieve a deep understanding of the optoelectronic properties of organic electronic devices on the nanoscale, and a better knowledge of the principles and functions of these characterization techniques will stimulate future progress in both organic electronics and instrumentation for characterization. The most commonly used characterization techniques have been described in this review, with an emphasis on how they can complement each other in building up a full understanding of structure and its relationship with performance. For example, information about the microstructure, which may be correlated to fundamental electronic properties or device performance, can be obtained by AFM which provides a local probe of nanometer-scale morphology, as well as GIXD which provides a whole-film measurement of unit cell dimensions and preferential orientation in crystalline regions. The aim of this review is to encourage the wide application of complementary characterization techniques in the study of OFETs, including electron energy loss spectroscopy,[357] low frequency noise characterization,[358] and microwave and optical spectroscopy.[359] The detailed study of organic electronic materials using advanced characterization techniques is still a young and growing area of science and much work remains to be done in order to fully understand the principles of these techniques and their applications across all length scales, but we believe that the wider availability of these techniques and the growing interest in organic electronics will encourage more groups to enter this field.

3398

dx.doi.org/10.1021/cr1001904 |*Chem. Rev.* 2011, 111, 3358–3406

Practical implementation of OFETs in electronic applications will ultimately depend on the ability to produce devices and circuits in a low-cost, large-area manufacturing process. Much work must be done before such an ambitious goal can be realized, and many innovative techniques need first to be developed in the laboratory before they find their way into a manufacturing environment. The fabrication techniques presented in this review are diverse in their operational characteristics, and most of them are novel and remain in an exploratory research phase. Some techniques have already been implemented for manufacturing in other areas, however, for example, inkjet printed display prototypes based on emissive polymers, or in the case of small molecules, vacuum deposition through shadow masks resulting in full color displays. However, further development of low-cost fabrication techniques is still needed to develop a viable strategy for manufacture of OFETs. One approach is to make use of novel techniques applied for other organic electronic systems, with careful consideration of the potential advantages of these techniques for OTFT systems. Another approach that mixes and matches different existing techniques is attractive because it exploits the various strengths of the different techniques. For the key components of OTFT devices, that is, electrodes, dielectrics, and semiconductors, it still necessary to develop new classes of materials which are compatible with promising techniques such as inkjet printing,[360,361] and the traditional high-volume technologies such as offset, gravure, and flexographic printing. The ability to use these very high-volume techniques could usher in a whole range of cheap, large area devices and structures, allowing this technology to finally reach its full potential. For example, the use of semiconducting carbon nanotubes provides a low-cost route to the fabrication of electronic inks for use in commercial electronic devices,[362] and bottom-contact monolayers or bulky FET devices with patterned graphene electrodes show very high performance even on a simple SiO_2 dielectric surface.[363] As the more advanced and versatile methods currently being developed in the laboratory make their way into manufacturing processes, we will one day realize an entirely new generation of low-cost, large-area, and flexible electronic devices and circuits.

AUTHOR INFORMATION

Corresponding Author
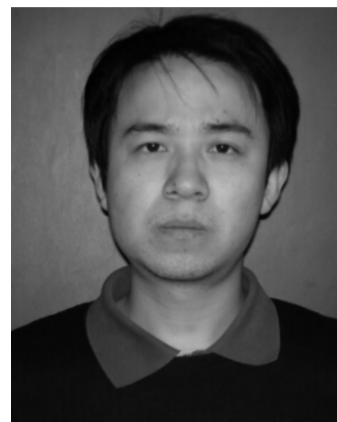*E-mail: liuyq@iccas.ac.cn.

BIOGRAPHIES

Yugeng Wen received his B.S. degree in chemistry from Ocean University of China in 2006. Since September 2006, he has been a Ph.D. student at the Institute of Chemistry, Chinese Academy of Sciences (CAS). His research interest includes fabrication, characterization, and optimization of organic field-effect transistors.

Yunqi Liu was born on April 1, 1949, in Jiangsu province, China. He graduated from the Department of Chemistry, Nanjing University in 1975, and received a doctorate from the Tokyo Institute of Technology, Japan in 1991. Presently, he is a Professor in the Institute of Chemistry, CAS, China. His research interests include synthesis of molecular materials including π-conjugated small molecules/polymers, carbon nanotubes and graphenes, fabrication of related devices including light-emitting diodes, field-effect transistors and molecular electronics, and investigation of their electronic properties. He has published over 400 peer-reviewed papers with more than 7000 citations and edited one book. He is also coauthor of 14 book chapters and coinventor on over 40 patents. His achievements have been recognized with several awards including the 2007 National Natural Prize.

Yunlong Guo was born in Hebei, China, in 1982. He received his B.S. degree in chemistry from Hebei Normal University (2005) and received his Ph.D. in chemistry from the Institute of Chemistry, CAS (2010). He was appointed to the position of Assistant Professor in 2010. His research interest includes fabrication, characterization, and optimization of organic field-effect transistors and functional organic field-effect transistors.

3399

dx.doi.org/10.1021/cr1001904 |*Chem. Rev.* 2011, 111, 3358–3406

Gui Yu was born in Changchun, China, in 1965. He graduated from Jilin University in 1988 and received his M.S. (1993) and Ph.D. (1997) degrees from Changchun Institute of Physics, CAS. After completing his Ph.D., he went to the Institute of Chemistry, CAS, as a postdoctoral worker. He was appointed to the position of professor in 2007. His research interests focuses on synthesis, structures, electronic and optical properties, and theoretical investigation of novel organic semiconductors.

Wenping Hu was born on May 14, 1970. He is a professor in the Institute of Chemistry, Chinese Academy of Sciences. He received his Ph.D. from the Institute in 1999, and then worked in Osaka University and Stuttgart University as a research fellow supported by the Japan Society for the Promotion of Science and the Alexander von Humboldt Foundation, respectively. In 2003, he returned to the Institute of Chemistry from Nippon Telephone and Telegraph. He focuses on molecular electronics and has more than 150 refereed publications which have been cited over 1400 times.

REFERENCES

(1) Vaidya, V.; Soggs, S.; Kim, J.; Haldi, A.; Haddock, J. N.; Kippelen, B.; Wilson, D. M. *IEEE Transact. Circuits Syst. I* **2008**, *55*, 1177.

(2) Lee, S.; Koo, B.; Park, J.-G.; Moon, H.; Hahn, J.; Kim, J. M. *MRS Bull.* **2006**, *31*, 455.

(3) Nakajima, Y.; Takei, T.; Tsuzuki, T.; Suzuki, M.; Fukagawa, H.; Yamamoto, T.; Tokito, S. *J. Soc. Inf. Display* **2009**, *17*, 629.

(4) Tano, T.; Tomono, H.; Onodera, A.; Yutani, K.; Murakami, A.; Suzuki, K.*NIP 25: International Conference on Digital Printing Technologies and Digital Fabrication 2009*; Louisville, KY, September 20, 2009; The Society for Imaging Science and Technology: Springfield, VA, 2009; Vol. 25, p 631.

(5) Zhou, L. S.; Wanga, A.; Wu, S.-C.; Sun, J.; Park, S.; Jackson, T. N. *Appl. Phys. Lett.* **2006**, *88*, 083502.

(6) (a) Someya, T.; Kato, Y.; Sekitani, T.; Iba, S.; Noguchi, Y.; Murase, Y.; Kawaguchi, H.; Sakurai, T. *Proc. Natl. Acad. Sci. U.S.A.* **2005**, *102*, 12321. (b) Guo, Y. L.; Yu, G.; Liu, Y. Q. *Adv. Mater.* **2010**, *22*, 4427.

(7) Someya, T.; Dodabalapur, A.; Huang, J.; See, K. C.; Katz, H. E. *Adv. Mater.* **2010**, *22*, 3799.

(8) Kato, Y.; Sekitani, T.; Noguchi, Y.; Yokota, T.; Takamiya, M.; Sakurai, T.; Someya, T. *IEEE Trans. Electron. Devices* **2010**, *57*, 995.

(9) Roberts, M. E.; Mannsfeld, S. C. B.; Queraltó, N.; Reese, C.; Locklin, J.; Knoll, W.; Bao, Z. N. *Proc. Natl. Acad. Sci. U.S.A.* **2008**, *105*, 12134.

(10) Sekitani, T.; Noguchi, Y.; Hata, K.; Fukushima, T.; Aida, T.; Someya, T. *Science* **2008**, *321*, 1468.

(11) Cantatore, E.; Geuns, T. C. T.; Gelinck, G. H.; Veenendaal, E.; Gruijthuijsen, A. F. A.; Schrijnemakers, L.; Drews, S.; de Leeuw, D. M. *IEEE J. Solid-State Circuits* **2007**, *42*, 84.

(12) Rotzoll, R.; Mohapatra, S.; Olariu, V.; Wenz, R.; Grigas, M.; Dimmler, K.; Shchekin, O.; Dodabalapur, A. *Appl. Phys. Lett.* **2006**, *88*, 123502.

(13) Steudal, S.; de Vusser, S.; Myny, K.; Lenes, M.; Genoe, J.; Heremans, P. *J. Appl. Phys.* **2006**, *99*, 114519.

(14) Street, R. A. *Adv. Mater.* **2009**, *21*, 2007.

(15) Kim, D.-H.; Rogers, J. A. *Adv. Mater.* **2008**, *20*, 4887.

(16) (a) Singh, T. B.; Sariciftci, N. S. *Annu. Rev. Mater. Res.* **2006**, *36*, 199. (b) Zhang, L.; Di, C.-a.; Zhao, Y.; Guo, Y. L.; Sun, X. N.; Wen, Y. G.; Zhou, W. Y.; Zhan, X. W.; Yu, G.; Liu, Y. Q. *Adv. Mater.* **2010**, *22*, 3537. (c) Wu, W. P.; Liu, Y. Q.; Zhu, D. B. *Chem. Soc. Rev.* **2010**, *39*, 1489. (d) Wen, Y. G.; Liu, Y. Q. *Adv. Mater.* **2010**, *22*, 1331.

(17) (a) Shaheen, S. E.; Ginley, D. S.; Jabbour, G. E. *MRS Bull.* **2005**, *30*, 10. (b) Di, C.-a.; Lu, K.; Zhang, L.; Liu, Y. Q.; Guo, Y. L.; Sun, X. N.; Wen, Y. G.; Yu, G.; Zhu, D. B. *Adv. Mater.* **2010**, *22*, 1273. (c) Di, C.-a.; Yu, G.; Liu, Y. Q.; Guo, Y. L.; Wang, Y.; Wu, W. P.; Zhu, D. B. *Adv. Mater.* **2008**, *20*, 1286. (d) Di, C.-a.; Yu, G.; Liu, Y. Q.; Zhu, D. B. *J. Phys. Chem. B* **2007**, *111*, 14083. (e) Sun, Y. M.; Liu, Y. Q.; Zhu, D. B. *J. Mater. Chem.* **2005**, *15*, 53.

(18) Arias, A. C.; MacKenzie, J. D.; McCulloch, I.; Rivnay, J.; Salleo, A. *Chem. Rev.* **2010**, *110*, 3.

(19) Pingree, L. S. C.; Reid, O. G.; Ginger, D. S. *Adv. Mater.* **2009**, *21*, 19.

(20) Bao, Z. N.; Locklin, L. *Organic Field-Effect Transistors*; CRC Press Taylor and Francis Group: Boca Raton, FL, 2007.

(21) Oliver, R. A. *Rep. Prog. Phys.* **2008**, *71*, 076501.

(22) Kalinin, S.; Gruverman, A. *Scanning Probe Microscopy: Electrical and Electromechanical Phenomena at the Nanoscale*; Springer: New York, U.S.A. 2007.

(23) Bonnell, D. A. *Scanning Probe Microscopy and Spectroscopy*; Wiley-VCH: New York, U.S.A. 2001.

(24) Dinelli, F.; Murgia, M.; Levy, P.; Cavallini, M.; Biscarini, F.; de Leeuw, D. M. *Phys. Rev. Lett.* **2004**, *92*, 116802.

(25) Kim, C.; Facchetti, A.; Marks, T. J. *Science* **2007**, *318*, 76.

(26) Lee, H. S.; Kim, D. H.; Cho., J. H.; Hwang, M.; Jang, Y.; Cho, K. *J. Am. Chem. Soc.* **2008**, *130*, 10556.

(27) Ruiz, R.; Nickel, B.; Koch, N.; Feldman, L. C.; Haglund, R. F.; Kahn, A.; Scoles, G. *Phys. Rev. B* **2003**, *67*, 125406.

(28) Ruiz, R.; Nickel, B.; Koch, N.; Feldman, L. C.; Haglund, R. F.; Kahn, A.; Family, F.; Scoles, G. *Phys. Rev. Lett.* **2003**, *91*, 136102.

(29) Yang, H. C.; Shin, T. J.; Ling, M.-M.; Cho, K.; Ryu, C. Y.; Bao, Z. N. *J. Am. Chem. Soc.* **2005**, *127*, 11542.

3400

dx.doi.org/10.1021/cr1001904 |*Chem. Rev.* 2011, 111, 3358–3406

(30) Oh, J. H.; Sun, Y.-S.; Schmidt, R.; Toney, M. F.; Nordlund, D.; Könemann, M.; Würthner, F.; Bao, Z. N. *Chem. Mater.* **2009**, *21*, 5508.

(31) Yang, S. Y.; Shin, Y.; Kim, S. H.; Jeon, H.; Kang, J. H.; Yang, H. C.; Park, C. E. *J. Phys. Chem. B* **2006**, *110*, 20302.

(32) Kelley, T. W.; Granstrom, E. L.; Frisbie, C. D. *Adv. Mater.* **1999**, *11*, 261.

(33) Yang, H. C.; Yang, C.; Kim, S. H.; Jang, M.; Park, C. E. *ACS Appl. Mater. Interfaces* **2010**, *2*, 391.

(34) Salomon, A.; Cahen, D.; Lindsay, S.; Tomfohr, J.; Engelkes, V. B.; Frisbie, C. D. *Adv. Mater.* **2003**, *15*, 1181.

(35) Engelkes, V. B.; Beebe, J. M.; Frisbie, C. D. *J. Am. Chem. Soc.* **2004**, *126*, 14287.

(36) Kelley, T. W.; Frisbie, C. D. *J. Phys. Chem. B* **2001**, *105*, 4538.

(37) Chwang, A. B.; Frisbie, C. D. *J. Appl. Phys.* **2001**, *90*, 1342.

(38) Mélin, T.; Diesinger, H.; Deresmes, D.; Stiévenard, D. *Phys. Rev. B* **2004**, *69*, 035321.

(39) Zdrojek, M.; Mélin, T.; Diesinger, H.; Deresmes, D.; Stiévenard, D.; Gebicki, W.; Adamowicz, L. *Phys. Rev. Lett.* **2006**, *96*, 039703.

(40) Lei, C. H.; Elliott, A. D. M.; Macdonald, J. E. *Appl. Phys. Lett.* **2003**, *83*, 482.

(41) Lmimouni, T. H. K.; Vuillaume, D. *Nano Lett.* **2004**, *4*, 2145.

(42) Muller, E. M.; Marohn, J. A. *Adv. Mater.* **2005**, *17*, 1410.

(43) Jaquith, M.; Muller, E. M.; Marohn, J. A. *J. Phys. Chem. B* **2007**, *111*, 7711.

(44) Hassenkam, T.; Greve, D. R.; Bjornholm, T. *Adv. Mater.* **2001**, *13*, 631.

(45) Heim, T.; Mélin, T.; Deresmes, D.; Vuillaume, D. *Appl. Phys. Lett.* **2004**, *85*, 2637.

(46) Nichols, J. A.; Gundlach, D. J.; Jackson, T. N. *Appl. Phys. Lett.* **2003**, *83*, 2366.

(47) Puntambekar, K. P.; Pesavento, P. V.; Frisbie, C. D. *Appl. Phys. Lett.* **2003**, *83*, 5539.

(48) Bürgi, L.; Richards, T. J.; Friend, R. H.; Sirringhaus, H. *J. Appl. Phys.* **2003**, *94*, 6129.

(49) Bürgi, L.; Sirringhaus, H.; Friend, R. H. *Appl. Phys. Lett.* **2002**, *80*, 2913.

(50) Teague, L. C.; Hamadani, B. H.; Jurchescu, O. D.; Subramanian, S.; Anthony, J. E.; Jackson, T. N.; Richter, C. A.; Gundlach, D. J.; Kushmerick, J. G. *Adv. Mater.* **2008**, *20*, 4513.

(51) Mathijssen, S. G. J.; Cölle, M.; Mank, A. J. G.; Kemerink, M.; Bobbert, P. A.; de Leeuw, D. M. *Appl. Phys. Lett.* **2007**, *90*, 192104.

(52) Ikeda, S.; Shimada, T.; Kiguchi, M.; Saiki, K. *J. Appl. Phys.* **2007**, *101*, 094509.

(53) Tal, O.; Rosenwaks, Y.; Roichman, Y.; Preezant, Y.; Tessler, N.; Chan, C. K.; Kahn, A. *Appl. Phys. Lett.* **2006**, *88*, 043509.

(54) Charrier, D. S. H.; de Vries, T.; Mathijssen, S. G. J.; Geluk, E.-J.; Smits, E. C. P.; Kemerink, M.; Janssen, R. A. J. *Org. Electron.* **2009**, *10*, 994.

(55) Stöhr, J. *NEXAFS Spectroscopy; Springer Series in Surface Sciences 25*; Springer-Verlag: Berlin, 1992.

(56) Delongchamp, D. M.; Sambasivan, S.; Fischer, D. A.; Lin, E. K.; Chang, P.; Murphy, A. R.; Fréchet, J. M. J.; Subramanian, V. *Adv. Mater.* **2005**, *17*, 2340.

(57) Yuan, Q.; Mannsfeld, S. C. B.; Tang, M. L.; Roberts, M.; Toney, M. F.; Delongchamp, D. M.; Bao, Z. N. *Chem. Mater.* **2008**, *20*, 2763.

(58) Chung, D. S.; Park, J. W.; Kim, S.-O.; Heo, K.; Park, C. E.; Ree, M.; Kim, Y.-H.; Kwon, S.-K. *Chem. Mater.* **2009**, *21*, 5499.

(59) Delongchamp, D. M.; Ling, M.-M.; Jung, Y.; Fischer, D. A.; Roberts, M. E.; Lin, E. K.; Bao, Z. N. *J. Am. Chem. Soc.* **2006**, *128*, 16579.

(60) Yuan, Q.; Mannsfeld, S. C. B.; Tang, M. L.; Toney, M. F.; Lüning, J.; Bao, Z. N. *J. Am. Chem. Soc.* **2008**, *130*, 3502.

(61) Brocorens, P.; van Vooren, A.; Chabinyc, M. L.; Toney, M. F.; Shkunov, M.; Heeney, M.; McCulloch, I.; Cornil, J.; Lazzaroni, R. *Adv. Mater.* **2009**, *21*, 1193.

(62) Hüfner, S. *Photoelectron Spectroscopy*, 2nd ed.; Springer: Berlin, 1996.

(63) Ishii, H.; Sugiyama, K.; Ito, E.; Seki, K. *Adv. Mater.* **1999**, *11*, 605.

(64) Zahn, D. R. T.; Gavrila, G. N.; Salvan, G. *Chem. Rev.* **2007**, *107*, 1161.

(65) Cahen, D.; Kahn, A. *Adv. Mater.* **2003**, *15*, 271.

(66) Duhm, S.; Heimel, G.; Salzmann, I.; Glowatzki, H.; Johnson, R. L.; Vollmer, A.; Rabe, J. P.; Koch, N. *Nat. Mater.* **2008**, *7*, 326.

(67) Facchetti, A.; Mushrush, M.; Yoon, M.-H.; Hutchison, G. R.; Ratner, M. A.; Marks, T. J. *J. Am. Chem. Soc.* **2004**, *126*, 13859.

(68) Glowatzki, S. D. H.; Rabe, J. P.; Koch, N.; Johnson, R. L. *Appl. Phys. Lett.* **2006**, *88*, 203109.

(69) Kera, S.; Yabuuchi, Y.; Yamane, H.; Setoyama, H.; Okudaira, K. K.; Kahn, A.; Ueno, N. *Phys. Rev. B* **2004**, *70*, 085304.

(70) Amy, F.; Chan, C.; Kahn, A. *Org. Electron* **2005**, *6*, 85.

(71) Necliudov, P. V.; Shur, M. S.; Gundlach, D. J.; Jackson, T. N. *Solid-State Electron.* **2003**, *47*, 259.

(72) Rhee, S.-W.; Yun, D.-J. *J. Mater. Chem.* **2008**, *18*, 5437.

(73) Cho, S. W.; Jeong, J. G.; Park, S. H.; Cho, M.-H.; Jeong, K.; Whang, C.-N.; Yi, Y. *Appl. Phys. Lett.* **2008**, *92*, 213302.

(74) Griffiths, P. R.; de Haseth, J. A. *Fourier Transform Infrared Spectrometry*, 2nd ed.; Wiley-Interscience: 2007.

(75) Zhuo, J.-M.; Zhao, L.-H.; Png, R.-Q.; Wong, L.-K.; Chia, P.-J.; Tang, J.-C.; Sivaramakrishnan, S.; Zhou, M.; Qu, E. C.-W.; Chua, S.-J.; Sim, W.-S.; Chua, L.-L.; Ho, P. K.-H. *Adv. Mater.* **2009**, *21*, 4747.

(76) Berlin, A.; Grimoldi, S.; Zotti, G.; Osuna, R. M.; Delgado, M. C. R.; Ortiz, R. P.; Casado, J.; Hernandez, V.; Navarrete, J. T. L. *J. Phys. Chem. B* **2005**, *109*, 22308.

(77) Lee, D.-H.; Jeong, H.-D. *J. Phys. Chem. C* **2008**, *112*, 16984.

(78) Furukawa, Y.; Yamamoto, J.; Cho, D.-C.; Mori, T. *Macromol. Symp.* **2004**, *205*, 9.

(79) Ito, Y.; Virkar, A. A.; Mannsfeld, S.; Oh, J. H.; Toney, M.; Locklin, J.; Bao, Z. N. *J. Am. Chem. Soc.* **2009**, *131*, 9396.

(80) Shen, Y. R. *Nature* **1989**, *337*, 519.

(81) Zhang, D.; Gracias, D. H.; Ward, R.; Gauckler, M.; Tian, Y.; Shen, Y. R.; Somorjai, G. A. *J. Phys. Chem. B* **1998**, *102*, 6225.

(82) Ye, H. K.; Gu, Z. Y.; Gracias, D. H. *Langmuir* **2006**, *22*, 1863.

(83) Ye, H. K.; Abu-Akeel, A.; Huang, J.; Katz, H. E.; Gracias, D. H. *J. Am. Chem. Soc.* **2006**, *128*, 6528.

(84) Cheng, H.-L.; Chou, W.-Y.; Kuo, C.-W.; Wang, Y.-W.; Mai, Y.-S.; Tang, F.-C.; Chu, S.-W. *Adv. Funct. Mater.* **2008**, *18*, 285.

(85) Faltermeier, D.; Gompf, B.; Dressel, M.; Tripathi, A. K.; Pflaum, J. *Phys. Rev. B* **2006**, *74*, 125416.

(86) Cheng, H. L.; Chou, W. Y.; Kuo, C. W.; Tang, F. C.; Wang, Y. W. *Appl. Phys. Lett.* **2006**, *88*, 161918.

(87) Cheng, H.-L.; Mai, Y.-S.; Chou, W.-Y.; Chang, L.-R. *Appl. Phys. Lett.* **2007**, *90*, 171926.

(88) Jakabovic, J.; Kovac, J.; Weis, M.; Hasko, D.; Srnanek, R.; Valent, P.; Resel, R. *Microelectronics* **2009**, *3*, 595.

(89) Hosoia, Y.; Deyraa, D. M.; Nakajimaa, K.; Furukawaa, Y. *Mol. Cryst. Liq. Cryst.* **2008**, *491*, 317.

(90) Tsai, J.-H.; Lee, W.-Y.; Chen, W.-C.; Yu, C.-Y.; Hwang, G.-W.; Ting, C. *Chem. Mater.* **2010**, *22*, 3290.

(91) Videlot-Ackermann, C.; Brisset, H.; Ackermann, J.; Zhang, J.; Raynal, P.; Fages, F.; Mehl, G. H.; Tnanisawa, T.; Yoshimoto, T. *Org. Electron.* **2009**, *9*, 591.

(92) Yoon, M.-H.; Facchetti, A.; Stern, C. E.; Marks, T. J. *J. Am. Chem. Soc.* **2006**, *128*, 5792.

(93) Gwinner, M. C.; Khodabakhsh, S.; Song, M. H.; Schweizer, H.; Giessen, H.; Sirringhaus, H. *Adv. Funct. Mater.* **2009**, *19*, 1360.

(94) Deng, Y. Y.; Sirringhaus, H. *Phys. Rev. B* **2005**, *72*, 045207.

(95) Guo, X. F.; Myers, M.; Xiao, S. X.; Lefenfeld, M.; Steiner, R.; Tulevski, G. S.; Tang, J. Y.; Baumert, J.; Leibfarth, F.; Yardley, J. T.; Steigerwwald, M. L.; Kim, P.; Nuckolls, C. *Proc. Natl. Acad. Sci. U.S.A.* **2006**, *103*, 11452.

(96) Tulevski, G. S.; Miao, Q.; Futuko, M.; Abram, R.; Ocko, B.; Pindak, R.; Steigerwwald, M. L.; Kagan, C. R.; Nuckolls, C. *J. Am. Chem. Soc.* **2004**, *126*, 15048.

(97) Smits, E. C. P.; Mathijssen, S. G. J.; van Hal, P. A.; Setayesh, S.; Geuns, T. C. T.; Mutsaers, K. A. H. A.; Cantatore, E.; Wondergem, H. J.; Werzer, O.; Resel, R.; Kemerink, M.; Kirchmeyer, S.; Muzafarov, A. M.;

3401

dx.doi.org/10.1021/cr1001904 |*Chem. Rev.* 2011, 111, 3358–3406

Ponomarenko, S. A.; de Boer, B.; Blom, P. W. M.; de Leeuw, D. M. *Nature* **2008**, *455*, 956.

(98) Fritz, S. E.; Martin, S. M.; Frisbie, C. D.; Ward, M. D.; Toney, M. F. *J. Am. Chem. Soc.* **2004**, *126*, 4084.

(99) Kline, R. J.; Mcgehee, M. D.; Toney, M. F. *Nat. Mater.* **2006**, *5*, 222.

(100) Sirringhaus, H.; Brown, P. J.; Friend, R. H.; Nielsen, M. M.; Bechgaard, K.; Langeeveld-Voss, B. M. W.; Spiering, A. J. H.; Janssen, R. A. J.; Meijer, E. W.; Herwig, P.; de Leeuw, D. M. *Nature* **1999**, *401*, 685.

(101) Osaka, I.; Zhang, R.; Sauvé, G.; Smilgies, D.-M.; Kowalewski, T.; McCullough, R. D. *J. Am. Chem. Soc.* **2009**, *131*, 2521.

(102) Kim, D. H.; Lee, B.-L.; Moon, H.; Kang, H. M.; Jeong, E. J.; Park, J.-I; Han, K.-M.; Lee, S.; Yoo, B. W.; Koo, B. W.; Kim, J. Y.; Lee, W. H.; Cho, H.; Becerril, H. A.; Bao, Z. N. *J. Am. Chem. Soc.* **2009**, *131*, 6124.

(103) Zhang, W.; Smith, J.; Watkins, S. E.; Gysel, R.; McGehee, M.; Salleo, A.; Kirkpatrick, J.; Ashraf, S.; Anthopoulos, T.; Heeney, M.; McCulloch, I. *J. Am. Chem. Soc.* **2010**, *132*, 11437.

(104) Rivnay, J.; Toney, M. F.; Zheng, Y.; Kauvar, I. V.; Chen, Z.; Wagner, V.; Facchetti, A.; Salleo, A. *Adv. Mater.* **2010**, *22*, 4359.

(105) Beaujuge, P. M.; Pisula, W.; Tsao, H. N.; Ellinger, S.; Müllen, K.; Reynolds, J. R. *J. Am. Chem. Soc.* **2009**, *131*, 7514.

(106) Tsao, H. N.; Cho, D.; Andreasen, W.; Rouhanipour, A.; Breiby, D. W.; Pisula, W.; Müllen, K. *Adv. Mater.* **2009**, *21*, 209.

(107) Weckhuysen, B. M.; Heidler, R.; Schoonheydt, R. A. *Electron Spin Resonance Spectroscopy*; Springer-Verlag: Berlin Heidelberg, 2004.

(108) Tanaka, H.; Watanabe, S.-i.; Ito, H.; Marumoto, K.; Kuroda, S.-i. *Appl. Phys. Lett.* **2009**, *94*, 103308.

(109) Marumoto, K.; Kuroda, S.-i.; Takenobu, T.; Iwasa, Y. *Phys. Rev. Lett.* **2006**, *97*, 256603.

(110) Matsui, H.; Hasegawa, T.; Tokura, Y.; Hiraoka, M.; Yamada, T. *Phys. Rev. Lett.* **2008**, *100*, 126601.

(111) Wang, Y.; Wang, H. M.; Liu, Y. Q.; Di, C.-a.; Sun, Y. M.; Wu, W. P.; Yu, G.; Zhang, D. Q.; Zhu, D. B. *J. Am. Chem. Soc.* **2006**, *128*, 13058.

(112) Sugiyama, K.; Kojima, T.; Fukuda, H.; Yashiro, H.; Matsuura, T.; Shimoyama, Y. *Thin Solid Films* **2008**, *516*, 2691.

(113) Fernández-Torrente, I.; Franke, K. J.; Pascual, J. I. *Phys. Rev. Lett.* **2008**, *101*, 217203.

(114) Calhoun, M. F.; Sanchez, J.; Olaya, D.; Gershenson, M. E.; Podzorov, V. *Nat. Mater.* **2008**, *7*, 84.

(115) Daillant, J.; Gibaud, A. *X-ray and Neutron Reflectivity: Principles and Applications*; Springer: Berlin Heidelberg, 2009.

(116) Kang, J.; Shin, N.; Jang, D. Y.; Prabhu, V. M.; Yoon, D. Y. *J. Am. Chem. Soc.* **2008**, *130*, 12273.

(117) Vincze, A.; Jakabovic, J.; Srnanek, R.; Satka, A.; Kovac, J.; Kovac, J. *Cent. Eur. J. Phys.* **2009**, *2*, 270.

(118) Hamilton, R.; Smith, J.; Ogier, S.; Heeney, M.; Anthony, J. E.; McCulloch, I.; Veres, J.; Bradley, D. D. C.; Anthopoulos, T. D. *Adv. Mater.* **2009**, *21*, 1166.

(119) Yamada, D.; Manaka, T.; Lim, E.; Tamura, R.; Iwamoto, M. *J. Appl. Phys.* **2008**, *103*, 084118.

(120) Weis, M.; Manaka, T.; Iwamoto, M. *J. Appl. Phys.* **2009**, *105*, 024505.

(121) Manaka, T.; Lim, E.; Tamura, R.; Iwamoto, M. *Appl. Phys. Lett.* **2005**, *87*, 222107.

(122) Nakao, M.; Manaka, T.; Weis, M.; Lim, E.; Iwamoto, M. *J. Appl. Phys.* **2009**, *106*, 014511.

(123) Manaka, T.; Liu, F.; Weis, M.; Iwamoto, M. *Phys. Rev. B* **2008**, *78*, 121302.

(124) Manaka, T.; Nakao, M.; Weis, M.; Liu, F.; Iwamoto, M. *Thin Solid Films* **2009**, *518*, 485.

(125) Lim, E.; Manaka, T.; Iwamoto, M. *J. Appl. Phys.* **2008**, *104*, 054511.

(126) Wang, L.; Park, S.-J.; Lee, S.-H.; Kim, Y.-J.; Book, Y.-J.; Kuo, S.-W.; van Horn, R. M.; Cheng, S. Z. D.; Lee, M.-H.; Jeong, K.-U. *Chem. Mater.* **2009**, *21*, 3838.

(127) Kastler, M.; Pisula, W.; Laquai, F.; Kumar, A.; Davies, R. J.; Baluschev, S.; Garcia-Gutiérrez, M.-C.; Wasserfallen, D.; Butt, H.-J.; Riekel, C.; Wegner, G.; Müllen, K. *Adv. Mater.* **2006**, *18*, 2255.

(128) An, Z. S.; Yu, J. S.; Jones, S. C.; Barlow, S.; Yoo, S.; Domercq, B.; Prins, P.; Siebbeles, L. A. D.; Kippelen, B.; Marder, S. R. *Adv. Mater.* **2005**, *17*, 2580.

(129) Bao, Q.; Li, J.; Li, C. M.; Dong, Z. L.; Lu, Z.; Qin, F.; Gong, C.; Guo, J. *J. Phys. Chem. B* **2008**, *112*, 12270.

(130) Tsung, K. K.; So, S. K. *Appl. Phys. Lett.* **2008**, *92*, 103315.

(131) Tse, S. C.; Tsang, S. W.; So, S. K. *J. Appl. Phys.* **2006**, *100*, 063708.

(132) Jaiswal, M.; Menon, R. *Appl. Phys. Lett.* **2006**, *88*, 123504.

(133) Hamedi, M.; Herlogsson, L.; Crispin, X.; Marcilla, R.; Berggren, M.; Inganas, O. *Adv. Mater.* **2009**, *21*, 573.

(134) Lin, J.; Weis, M.; Taguchi, D.; Manaka, T.; Iwamoto, M. *Thin Solid Films* **2009**, *518*, 448.

(135) Lenski, D. R.; Southard, A.; Fuhrer, M. S. *Appl. Phys. Lett.* **2009**, *94*, 232103.

(136) Bittle, E. G.; Brill, J. W.; Anthony, J. E. *Appl. Phys. Lett.* **2010**, *97*, 013302.

(137) Yang, Y. S.; Kim, S. H.; Lee, J.-I.; Chu, H. Y.; Do, L.-M.; Lee, H.; Oh, J.; Zyung, T.; Ryu, M. K.; Jang, M. S. *Appl. Phys. Lett.* **2002**, *80*, 1595.

(138) Matsushima, T.; Yahiro, M.; Adachi, C. *Appl. Phys. Lett.* **2007**, *91*, 103505.

(139) Menard, E.; Meitl, M. A.; Sun, Y. G.; Park, J.-U.; Shir, D. J.-L.; Nam, Y.-S.; Jeon, S.; Rogers, J. A. *Chem. Rev.* **2007**, *107*, 1117.

(140) Gates, B. D.; Xu, Q. B.; Stewart, M.; Ryan, D.; Willson, C. G.; Whitesides, G. M. *Chem. Rev.* **2005**, *105*, 1171.

(141) Xia, Y. N.; Rogers, J. A.; Paul, K. E.; Whitesides, G. M. *Chem. Rev.* **1999**, *99*, 1823.

(142) (a) Ling, M. M.; Bao, Z. N. *Chem. Mater.* **2004**, *16*, 4824. (b) Zhang, L.; Di, C.-a.; Yu, G.; Liu, Y. Q. *J. Mater. Chem.* **2010**, *20*, 7059.

(143) http://www.reed-electronics.com/semiconductor/article/CA6319061.

(144) DeFranco, J. A.; Schmidt, B. S.; Lipson, M.; Malliaras, G. G. *Org. Electron.* **2006**, *7*, 22.

(145) Nakajima, Y.; Takei, T.; Tsuzuki, T.; Suzuki, M.; Fukagawa, H.; Yamamoto, T.; Tokito, S. *Soc. Inf. Display* **2009**, *8*, 629.

(146) Afzali, A.; Dimitrakopoulos, C. D.; Graham, T. O. *Adv. Mater.* **2003**, *15*, 2066.

(147) Weidkamp, K. P.; Afzali, A.; Tromp, R. M.; Hamers, R. J. *J. Am. Chem. Soc.* **2004**, *126*, 12740.

(148) Balocco, C.; Majewski, L. A.; Song, A. M. *Org. Electron* **2006**, *7*, 500.

(149) Chan, J. R.; Huang, X. Q.; Song, A. M. *J. Appl. Phys.* **2006**, *99*, 023710.

(150) Park, S. K.; Mourey, D. A.; Subramanian, S.; Anthony, J. E.; Jackson, T. N. *Adv. Mater.* **2008**, *20*, 4145.

(151) Debucquoy, M.; Bode, D.; Genoe, J.; Gelinck, G. H.; Heremans, P. *Appl. Phys. Lett.* **2009**, *95*, 103311.

(152) Eder, F.; Klauk, H.; Halik, M.; Zschieschang, U.; Schmid, G.; Dehm, C. *Appl. Phys. Lett.* **2004**, *84*, 2673.

(153) Drury, C. J.; Mutsaers, C. M. J.; Hart, C. M.; Matters, M.; de leeuw, D. M. *Appl. Phys. Lett.* **1998**, *73*, 108.

(154) Lee, C.-W.; Seo, Y.-H.; Lee, S.-H. *Macromolecules* **2004**, *37*, 4070.

(155) Halik, M.; Klauk, H.; Zschieschang, U.; Kriem, T.; Schmid, G.; Radlik, W.; Wussow, K. *Appl. Phys. Lett.* **2002**, *81*, 289.

(156) Touwslager, F. J.; Willard, N. P.; de Leeuw, D. M. *Appl. Phys. Lett.* **2002**, *81*, 4556.

(157) Lee, T.-W.; Byun, Y.; Koo, B.-W.; Kang, I.-N.; Lyu, Y.-Y.; Lee, C. H.; Pu, L.; Lee, S. Y. *Adv. Mater.* **2005**, *17*, 2180.

(158) Png, R.-Q.; Chia, P.-J.; Tang, J.-C.; Liu, B.; Sivaramakrishnan, S.; Zhou, M.; Khong, S.-H.; Chan, H. S. O.; Burroughes, J. H.; Chua, L.-L.; Friend, R. H.; Ho, P. K. H. *Nat. Mater.* **2010**, *9*, 152.

(159) Rogers, J. A.; Dodabalapur, A.; Bao, Z. N.; Katz, H. E. *Appl. Phys. Lett.* **1999**, *75*, 1010.

(160) Huang, Y. Y.; Zhou, W. X.; Hsia, K. J.; Menard, E.; Park, J.-U.; Rogers, J. A.; Alleyne, A. G. *Langmuir* **2005**, *21*, 8058.

(161) Zhou, W. X.; Huang, Y. Y.; Menard, E.; Aluru, N. R.; Rogers, J. A.; Alleyne, A. G. *Appl. Phys. Lett.* **2005**, *87*, 251925.

(162) Hsia, K. J.; Huang, Y. Y.; Menard, E.; Park, J.-U.; Zhou, W. X.; Rogers, J. A.; Fulton, J. M. *Appl. Phys. Lett.* **2005**, *86*, 154106.

(163) Huang, J.; Xia, R.; Kim, Y.; Wang, X.; Dane, J.; Hofmann, O.; Mosley, A.; de Mello, A. J.; de Mello, J. C.; Bradley, D. D. C. *J. Mater. Chem.* **2007**, *17*, 1043.

(164) Henzie, J.; Barton, J. E.; Stender, C. L.; Odom, T. W. *Acc. Chem. Res.* **2006**, *39*, 249.

(165) Hua, F.; Sun, Y. G.; Gaur, A.; Meitl, M. A.; Bilhaut, L.; Rotkina, L.; Wang, J. F.; Geil, P.; Shim, M.; Rogers, J. A. *Nano Lett.* **2004**, *4*, 2467.

(166) Gates, B. D.; Whitesides, G. M. *J. Am. Chem. Soc.* **2003**, *125*, 14986.

(167) Truong, T. T.; Lin, R. S.; Jeon, S.; Lee, H. H.; Maria, J.; Gaur, A.; Hua, F.; Meinel, I.; Rogers, J. A. *Langmuir* **2007**, *23*, 2898.

(168) Rolland, J. P.; Hagberg, E. C.; Denison, G. M.; Carter, K. R.; de Simone, J. M. *Angew. Chem., Int. Ed.* **2004**, *43*, 5796.

(169) Jeon, N. L.; Choi, I. S.; Xu, B.; Whitesides, G. M. *Adv. Mater.* **1999**, *11*, 946.

(170) Pisignano, D.; Sariconi, E.; Mazzeo, M.; Gigli, G.; Cingolani, R. *Adv. Mater.* **2002**, *14*, 1565.

(171) Rogers, J. A.; Bao, Z. N.; Raju, V. R. *Appl. Phys. Lett.* **1998**, *72*, 2716.

(172) Maltezos, G.; Nortrup, R.; Jeon, S.; Zaumseil, J.; Rogers, J. A. *Appl. Phys. Lett.* **2003**, *83*, 2067.

(173) Park, J.-U.; Meitl, M. A.; Hur, S.-H.; Usrey, M. L.; Strano, M. S.; Kenis, P. J. A.; Rogers, J. A. *Angew. Chem., Int. Ed.* **2006**, *45*, 581.

(174) Cavallini, M.; Stoliar, P.; Moulin, J.-F.; Surin, M.; Leclère, P.; Lazzaroni, R.; Breiby, D. W.; Andreason, J. W.; Nielson, M. M.; Sonar, P.; Grimsdale, A. C.; Müllen, K.; Biscarini, F. *Nano Lett.* **2005**, *5*, 2422.

(175) Salleo, A.; Wong, W. S.; Chabinyc, M. L.; Paul, K. E.; Street, R. A. *Adv. Funct. Mater.* **2005**, *15*, 1105.

(176) Loo, Y.-L.; Someya, T.; Baldwin, K. W.; Bao, Z. N.; Ho, P.; Dodabalapur, A.; Katz, H. E.; Rogers, J. A. *Proc. Natl. Acad. Sci. U.S.A.* **2002**, *99*, 10252.

(177) Ofuji, M.; Lovinger, A. J.; Kloc, C.; Siegrist, T.; Maliakal, A.; Katz, H. E. *Chem. Mater.* **2005**, *17*, 5748.

(178) Zaumseil, J.; Baldwin, K. W.; Rogers, J. A. *J. Appl. Phys.* **2003**, *93*, 6117.

(179) Ling, M.-M.; Bao, Z. N.; Li, D. W. *Appl. Phys. Lett.* **2006**, *88*, 033502.

(180) Chabinyc, M. L.; Salleo, A.; Wu, Y. L.; Liu, P.; Ong, B. S.; Heeney, M.; McCulloch, I. *J. Am. Chem. Soc.* **2004**, *126*, 13928.

(181) Sun, Q. J.; Kim, J.-H.; Park, J.-H.; Seo, S. *Appl. Phys. Lett.* **2010**, *96*, 103301.

(182) Chakra, E. B.; Hannes, B.; Dilosquer, G.; Mansfield, C. D.; Cabrera, M. *Rev. Sci. Instrum.* **2008**, *79*, 064102.

(183) Kagan, C. R.; Breen, T. L.; Kosbar, L. L. *Appl. Phys. Lett.* **2001**, *79*, 3536.

(184) Chandekar, A.; Alabran, M.; Sengupta, S. K.; Lee, J. S.; Mead, J. L.; Barry, C. M. F.; Whitten, J. E.; Somu, S.; Busnaina, A. A. *Microelectron. Eng.* **2008**, *85*, 187.

(185) Perl, A.; Reinhoudt, D. N.; Huskens, J. *Adv. Mater.* **2009**, *21*, 2257.

(186) Leufgen, M.; Lebib, A.; Muck, T.; Bass, U.; Wagner, V.; Borzenko, T.; Schimdt, G.; Geurts, J.; Molenkamp, L. W. *Appl. Phys. Lett.* **2004**, *84*, 1582.

(187) Rogers, J. A.; Bao, Z. N.; Makhija, A.; Braun, P. *Adv. Mater.* **1999**, *11*, 741.

(188) Zschieschang, U.; Klauk, H.; Halik, M.; Schmid, G.; Dehm, C. *Adv. Mater.* **2003**, *15*, 1147.

(189) Parashkov, R.; Becker, E.; Riedl, T.; Johannes, H.-H.; Kowalsky, W. *Adv. Mater.* **2005**, *17*, 1523.

(190) Lee, K. S.; Blanchet, G. B.; Gao, F.; Loo, Y.-L. *Appl. Phys. Lett.* **2005**, *86*, 074102.

(191) Briseno, A. L.; Roberts, M.; Ling, M.-M.; Moon, H.; Nemanick, E. J.; Bao, Z. N. *J. Am. Chem. Soc.* **2006**, *128*, 3880.

(192) Ahn, J.-H.; Kim, H.-S.; Lee, K. J.; Jeon, S.; Kang, S. J.; Sun, Y. G.; Nuzzo, R. G.; Rogers, J. A. *Science* **2006**, *314*, 1754.

(193) Yim, K.-H.; Zheng, Z. J.; Liang, Z. Q.; Friend, R. H.; Huck, W. T. S.; Kim, J.-S. *Adv. Funct. Mater.* **2008**, *18*, 1102.

(194) Meitl, M. A.; Zhu, Z.-T.; Kumar, V.; Lee, K. J.; Feng, X.; Huang, Y. Y.; Adesida, I.; Nuzzo, R. G.; Rogers, J. A. *Nat. Mater.* **2006**, *5*, 33.

(195) Loo, Y.-L.; Willett, R. L.; Baldwin, K. W.; Rogers, J. A. *J. Am. Chem. Soc.* **2002**, *124*, 7654.

(196) Loo, Y.-L.; Hsu, J. W. P.; Willett, R. L.; Baldwin, K. W.; West, K. W.; Rogers, J. A. *J. Vac. Sci. Technol. B* **2002**, *20*, 2853.

(197) Loo, Y.-L.; Willett, R. L.; Baldwin, K. W.; Rogers, J. A. *Appl. Phys. Lett.* **2002**, *81*, 562.

(198) Hur, S.-H.; Khang, D.-Y.; Kocabas, C.; Rogers, J. A. *Appl. Phys. Lett.* **2004**, *85*, 5730.

(199) Wang, Z.; Yuan, J. F.; Zhang, J.; Xing, R. B.; Yan, D. H.; Han, Y. C. *Adv. Mater.* **2003**, *15*, 1009.

(200) Li, D. W.; Guo, L. J. *Appl. Phys. Lett.* **2006**, *88*, 063513.

(201) Hines, D. R.; Mezhenny, S.; Breban, M.; Williams, E. D.; Ballarotto, V. W.; Eson, G.; Southard, A.; Fuhrer, M. S. *Appl. Phys. Lett.* **2005**, *86*, 163101.

(202) Park, S. K.; Kim, Y. H.; Han, J. I.; Moon, D. G.; Kim, W. K. *IEEE. Trans. Electron. Devices* **2002**, *49*, 2008.

(203) Kim, H.; Yoon, B.; Sung, J.; Choi, D.-G.; Park, C. *J. Mater. Chem.* **2008**, *18*, 3489.

(204) Guo, L. J. *Adv. Mater.* **2007**, *19*, 495.

(205) Zhang, W.; Chou, S. Y. *Appl. Phys. Lett.* **2003**, *83*, 1632.

(206) Austin, M. D.; Chou, S. Y. *Appl. Phys. Lett.* **2002**, *81*, 4431.

(207) Wang, J. Z.; Gu, J.; Zenhausern, F.; Sirringhaus, H. *Appl. Phys. Lett.* **2006**, *88*, 133502.

(208) Auner, C.; Palfinger, U.; Gold, H.; Kraxner, J.; Haase, A.; Haber, T.; Sezen, M.; Grogger, W.; Jakopic, G.; Krenn, J. R.; Leising, G.; Stadlober, B. *Org. Electron* **2010**, *11*, 552.

(209) Zheng, Z. J.; Yim, K.-H.; Saifullah, M. S. M.; Welland, M. E.; Friend, R. H.; Kim, J.-S.; Huck, W. T. S. *Nano Lett.* **2007**, *7*, 987.

(210) Lin, R. S.; Rogers, J. A. *Nano Lett.* **2007**, *7*, 1613.

(211) Park, I.; Ko, S. H.; Pan, H.; Grigoropoulos, C. P.; Pisano, A. P.; Fréchet, J. M. J.; Lee, E.-S.; Jeong, J.-H. *Adv. Mater.* **2008**, *20*, 489.

(212) Jo, S. J.; Kim, C. S.; Lee, M. J.; Kim, J. B.; Ryu, S. Y.; Noh, J. H.; Ihm, K.; Baik, H. K.; Kim, Y. S. *Adv. Mater.* **2008**, *20*, 1146.

(213) Visconti, P.; Pisignano, D.; Della, T. A.; Persano, L.; Maruccio, G.; Biasco, A.; Cingolani, R.; Rinaldi, R. *Mater. Sci. Eng. C-Biomim. Supramol. Syst.* **2005**, *25*, 848.

(214) Henrichsen, H. H.; Boggild, P. *Microelectron. Eng.* **2010**, *87*, 1120.

(215) Yagi, I.; Tsukagoshi, K.; Aoyagi, Y. *Appl. Phys. Lett.* **2004**, *84*, 813.

(216) Schrödner, M.; Stohn, R.-I.; Schultheis, K.; Sensfuss, S.; Roth, H.-K. *Org. Electron* **2005**, *6*, 161.

(217) Itoh, E.; Torres, I.; Hayden, C.; Taylor, D. M. *Synth. Met.* **2006**, *156*, 129.

(218) Shin, H.-S.; Baek, K.-H.; Park, S.-S.; Song, K.-C.; Lee, G.-W.; Lee, H.-D.; Wang, J.-S.; Lee, K.; Do, L.-M. *J. Nanosci. Nanotechnol.* **2010**, *10*, 3185.

(219) Dzwilewski, A.; Wagberg, T.; Edman, L. *J. Am. Chem. Soc.* **2009**, *131*, 4006.

(220) Cavallini, M.; Biscarini, F. *Nano Lett.* **2003**, *3*, 1269.

(221) Chang, J.-F.; Sirringhaus, H. *Adv. Mater.* **2009**, *21*, 2530.

(222) Chabinyc, M. L.; Wong, W. S.; Salleo, A.; Paul, K. E. *Appl. Phys. Lett.* **2002**, *81*, 4260.

(223) Liu, S. H.; Becerril, H. A.; LeMieux, M. C.; Wang, W. M.; Oh, J. H.; Bao, Z. N. *Adv. Mater.* **2009**, *21*, 1266.

(224) Kim, C.; Shtein, M.; Forrest, S. R. *Appl. Phys. Lett.* **2002**, *80*, 4051.

(225) Scheinert, S.; Doll, T.; Scherer, A.; Paasch, G.; Hörselmann, I. *Appl. Phys. Lett.* **2004**, *84*, 4427.

(226) Fujita, K.; Tasuda, T.; Tsutsui, T. *Appl. Phys. Lett.* **2003**, *82*, 4373.

(227) Kang, H.; Park, J.; Lee, H. H. *Adv. Mater.* **2006**, *18*, 1603.

(228) Park, S. Y.; Kwon, T.; Lee, H. H. *Adv. Mater.* **2006**, *18*, 1861.

(229) Kwon, T.; Baek, C.; Lee, H. H. *Org. Electron* **2007**, *8*, 615.

(230) Wang, Z.; Zhang, J.; Xing, R. B.; Yuang, J. F.; Yan, D. H.; Han, Y. C. *J. Am. Chem. Soc.* **2003**, *125*, 15278.

(231) Stutzmann, N.; Tervoort, T. A.; Broer, D. J.; Sirringhaus, H.; Friend, R. H.; Smith, P. *Adv. Funct. Mater.* **2002**, *12*, 105.

(232) Stutzmann, N.; Friend, R. H.; Sirringhaus, H. *Science* **2003**, *299*, 1881.

(233) Arias, A. C.; Ready, S. E.; Lugan, R.; Wong, W. S.; Paul, K. E.; Salleo, A.; Chabinyc, M. L.; Wu, Y.; Liu, P.; Ong, B. *Appl. Phys. Lett.* **2004**, *85*, 3304.

(234) Street, R. A.; Wong, W. S.; Ready, S. E.; Chabinyc, M. L.; Arias, A. C.; Limb, S.; Salleo, A.; Lugan, R. *Mater. Today* **2006**, *9*, 32.

(235) Sekitani, T.; Takamiya, M.; Noguchi, Y.; Nakano, S.; Kato, Y.; Sakurai, T.; Someya, T. *Nat. Mater.* **2007**, *6*, 413.

(236) Singh, M.; Haverinen, H. M.; Dhagat, P.; Jabbour, G. E. *Adv. Mater.* **2010**, *22*, DOI: 10.1002/adma.201090011.

(237) Parashko, R.; Becker, E.; Riedl, T.; Johannes, H. H.; Kowalsky, W. *Proc. IEEE* **2005**, *93*, 1321.

(238) Park, J.-U.; Hardy, M.; Kang, S. J.; Barton, K.; Adair, K.; Mukhopadhyay, D. K.; Lee, C. Y.; Strano, M. S.; Alleyne, A. G.; Georgiadis, J. G.; Ferreira, P. M.; Rogers, J. A. *Nat. Mater.* **2007**, *6*, 782.

(239) Sekitani, T.; Noguchi, Y.; Zschieschang, U.; Klauk, H.; Someya, T. *Proc. Natl. Acad. Sci. U.S.A.* **2008**, *105*, 4976.

(240) Wang, J. Z.; Zheng, Z. H.; Li, H. W.; Huck, W. T. S.; Sirringhaus, H. *Nat. Mater.* **2004**, *3*, 171.

(241) Sele, C. W.; von Werne, T.; Friend, R. H.; Sirringhaus, H. *Adv. Mater.* **2005**, *17*, 997.

(242) Noh, Y.-Y.; Zhao, N.; Caironi, M.; Sirringhaus, H. *Nat. Nanotechnol.* **2007**, *2*, 784.

(243) Caironi, M.; Gili, E.; Sakanoue, T.; Cheng, X. Y.; Sirringhaus, H. *ACS Nano* **2010**, *4*, 1451.

(244) Paul, K. E.; Wong, W. S.; Ready, S. E.; Street, R. A. *Appl. Phys. Lett.* **2003**, *83*, 2070.

(245) Li, Y. N.; Wu, Y. L.; Ong, B. S. *J. Am. Chem. Soc.* **2005**, *127*, 3266.

(246) Wu, Y. L.; Li, Y. N.; Ong, B. S. *J. Am. Chem. Soc.* **2006**, *128*, 4202.

(247) Wu, Y. L.; Li, Y. N.; Ong, B. S.; Liu, P.; Gardner, S.; Chiang, B. *Adv. Mater.* **2005**, *17*, 184.

(248) Kim, D.; Jeong, S.; Shin, H.; Xia, Y. N.; Moon, J. *Adv. Mater.* **2008**, *20*, 3084.

(249) Kawase, T.; Sirringhaus, H.; Friend, R. H.; Shimoda, T. *Adv. Mater.* **2001**, *13*, 1601.

(250) Barret, M.; Sanaur, S.; Collot, P. *Org. Electron.* **2008**, *9*, 1093.

(251) Sirringhaus, H.; Kawase, T.; Friend, R. H.; Shimoda, T.; Inbasekaran, M.; Wu, W.; Woo, E. P. *Science* **2000**, *290*, 2123.

(252) Lee, S. H.; Choi, M. H.; Han, S. H.; Choo, D. J.; Jang, J.; Kwon, S. K. *Org. Electron.* **2008**, *9*, 721.

(253) Yan, H.; Chen, Z. H.; Zheng, Y.; Newman, C.; Quinn, J. R.; Bötz, F.; Kastler, M.; Facchetti, A. *Nature* **2009**, *457*, 679.

(254) Shtein, M.; Peumans, P.; Benziger, J. B.; Forrest, S. R. *Adv. Mater.* **2004**, *16*, 1615.

(255) Shtein, M.; Peumans, P.; Benziger, J. B.; Forrest, S. R. *J. Appl. Phys.* **2004**, *96*, 4500.

(256) Waser, R. *Nanoelectronics and Information Technology*; Wiley-VCH Verlag: Weinheim, Germany, 2003.

(257) Yun, D.-J.; Lim, S.-H.; Cho, S.-H.; Kim, B.-S.; Rhee, S.-W. *J. Electrochem. Soc.* **2009**, *156*, H634.

(258) Kelley, T. W.; Baude, P. F.; Gerlach, C.; Ender, D. E.; Muyres, D.; Haase, M. A.; Vogel, D. E.; Theiss, S. D. *Chem. Mater.* **2004**, *16*, 4413.

(259) Blanchet, G. B.; Loo, Y.-L.; Rogers, J. A.; Gao, F.; Fincher, C. R. *Appl. Phys. Lett.* **2003**, *82*, 463.

(260) Rapp, L.; Diallo, A. K.; Alloncle, A. P.; Videlot-Ackermann, C.; Fages, F.; Delaporte, P. *Appl. Phys. Lett.* **2009**, *95*, 171109.

(261) Wada, H.; Mori, T. *Appl. Phys. Lett.* **2009**, *95*, 253307.

(262) Lim, S. C.; Kim, S. H.; Yang, Y. S.; Lee, M. Y.; Nam, S. Y.; Bin, K. J. *Jpn. J. Appl. Phys.* **2009**, *48*, 081503.

(263) Zielke, D.; Hübler, A. C.; Hahn, U.; Brandt, N.; Bartzsch, M.; Fügmann, U.; Fischer, T.; Veres, J.; Ogier, S. *Appl. Phys. Lett.* **2005**, *87*, 123508.

(264) Mäkelä, T.; Jussila, S.; Kosonen, H.; Bäcklund, T. G.; Sandberg, H. G. O.; Stubb, H. *Synth. Met.* **2005**, *153*, 285.

(265) Huebler, A. C.; Doetz, F.; Kempa, H.; Katz, H. E.; Bartzsch, M.; Brandt, N.; Hennig, I.; Fuegmann, U.; Vaidyanathan, S.; Granstrom, J.; Liu, S.; Sydorenko, A.; Zillger, T.; Schmidt, G.; Preissler, K.; Prichmanis, E.; Eckerle, P.; Richter, F.; Fischer, T.; Hahn, U. *Org. Electron.* **2007**, *8*, 480.

(266) Bartzsch, M.; Kempa, H.; Otto, M.; Hubler, A.; Zielke, D. *Org. Electron.* **2007**, *8*, 431.

(267) Park, J.-e.; Lee, M.-y.; Song, C.-k. *Extended Abstracts of the 2010 International Conference on Solid State Devices and Materials*; September 22−24, 2010, Tokyo, Japan; SSDM Organizing Committee: Tokyo, 2010; p 533.

(268) De la Fuente Vornbrock, A. *Roll Printed Electronics: Development and Scaling of Gravure Printing Techniques*; Electrical Engineering and Computer Sciences University of California: Berkeley, CA, 2009.

(269) Schmidt, G. C.; Bellmann, M.; Meier, B.; Hambsch, M.; Reuter, K.; Kempa, H.; Hubler, A. C. *Org. Electron* **2010**, *11*, 1683.

(270) Voigt, M. M.; Guite, A.; Chung, D.-Y.; Khan, R. U. A.; Campbell, A. J.; Bradley, D. D. C.; Meng, F.; Steinke, J. H. G.; Tierney, S.; McCulloch, I.; Penxten, H.; Lutsen, L.; Douheret, O.; Manca, J.; Brokmann, U.; Sonnichsen, K.; Hulsenberg, D.; Bock, W.; Barron, C.; Blanckaert, S.; Springer, S.; Grupp, J.; Mosley, A. *Adv. Funct. Mater.* **2010**, *20*, 239.

(271) Hambsch, M.; Reuter, K.; Stanel, M.; Schmidt, G.; Kempa, H.; Fugmann, U.; Hahn, U.; Hubler, A. C. *Mater. Sci. Eng, B* **2010**, *170*, 93.

(272) Verilhac, J.-M.; Benwadih, M.; Seiler, A.-L.; Jacob, S.; Bory, C.; Bablet, J.; Heitzman, M.; Tallal, J.; Barbut, L.; Frere, P.; Sicard, G.; Gwoziecki, R.; Chartier, I.; Coppard, R.; Serbutoviez, C. *Org. Electron.* **2010**, *11*, 456.

(273) Knobloch, A.; Manuelli, A.; Bernds, A.; Clemens, W. *J. Appl. Phys.* **2004**, *96*, 2286.

(274) Maccioni, M.; Orgiu, E.; Cosseddu, P.; Locci, S.; Bonfiglio, A. *Appl. Phys. Lett.* **2006**, *89*, 143515.

(275) Parashkov, R.; Becker, E.; Ginev, G.; Riedl, T.; Brandes, M.; Johannes, H.-H.; Kowalsky, W. *Appl. Phys. Lett.* **2004**, *85*, 5751.

(276) Parashkov, R.; Becker, E.; Hartmann, S.; Ginev, G.; Schneider, D.; Krautwald, H.; Dobbertin, T.; Metzdorf, D.; Brunetti, F.; Schildknecht, C.; Kammoun, A.; Brandes, M.; Riedl, T.; Johannes, H.-H.; Kowalsky, W. *Appl. Phys. Lett.* **2003**, *82*, 4579.

(277) Baek, C.; Seo, S.-m. *Appl. Phys. Lett.* **2009**, *94*, 153305.

(278) Ben-Sasson, A. J.; Avnon, E.; Ploshnik, E.; Globerman, O.; Shenhar, R.; Frey, G. L.; Tessler, N. *Appl. Phys. Lett.* **2009**, *95*, 213301.

(279) Cho, S.; Lee, K.; Heeger, A. J. *Adv. Mater.* **2009**, *21*, 1941.

(280) Arias, A. C.; Endicott, F.; Street, R. A. *Adv. Mater.* **2006**, *18*, 2900.

(281) Scharnberg, M.; Zaporojtchenko, V.; Adelung, R.; Faupel, F.; Pannemann, C.; Diekmann, T.; Hilleringmann, U. *Appl. Phys. Lett.* **2007**, *90*, 013501.

(282) Wittmann, J. C.; Smith, P. *Nature* **1991**, *352*, 414.

(283) Amundson, K. R.; Sapjeta, B. J.; Lovinger, A. J.; Bao, Z. N. *Thin Solid Films* **2002**, *414*, 143.

(284) Nagamatsu, S.; Takashima, W.; Kaneto, K.; Yoshida, Y.; Tanigaki, N.; Yase, K. *Appl. Phys. Lett.* **2004**, *84*, 4608.

(285) Kihara, H.; Ueda, Y.; Unno, A.; Hirai, T. *Mol. Cryst. Liq. Cryst.* **2004**, *424*, 195.

(286) van de Craats, A. M.; Stutzmann, N.; Bunk, O.; Nielson, M. M.; Watson, M.; Müllen, K.; Chanzy, H. D.; Sirringhaus, H.; Friend, R. H. *Adv. Mater.* **2003**, *15*, 495.

(287) http://www.chemchinanet.com/wholesale-nanotechnology_companies/

(288) Sirringhaus, H.; Wilson, R. J.; Friend, R. H.; Inbasekaran, M.; Wu, W.; Woo, E. P.; Grell, M.; Bradley, D. D. C. *Appl. Phys. Lett.* **2000**, *77*, 406.

(289) Yasuda, T.; Fujita, K.; Tsutsui, T.; Geng, Y. H.; Culligan, S. W.; Chen, S. H. *Chem. Mater.* **2005**, *17*, 264.

(290) van Breemen, A. J. J. M.; Herwig, P. T.; Chlon, C. H. T.; Sweelssen, J.; Schoo, H. F. M.; Setayesh, S.; Hardman, W. M.; Martin, C. A.; de leeuw, D. M.; Valeton, J. J. P.; Bastiaansen, C. W. M.; Broer, D. J.; Popa-Merticaru, A. R.; Meskers, S. C. J. *J. Am. Chem. Soc.* **2006**, *128*, 2336.

(291) Yu, C.-J.; Bae, J.-H.; Keum, C.-M.; Lee, S.-D. *Curr. Appl. Phys.* **2010**, *10*, 64.

(292) Chen, X. L.; Lovinger, A. J.; Bao, Z. N.; Sapjeta, J. *Chem. Mater.* **2001**, *13*, 1341.

(293) Chou, W.-Y.; Cheng, H.-L. *Adv. Funct. Mater.* **2004**, *14*, 811.

(294) Fritz, S. E.; Kelley, T. W.; Frisbie, C. D. *J. Phys. Chem. B* **2005**, *109*, 10574.

(295) Nishikawa, M.; Taheri, B.; West, J. L. *Appl. Phys. Lett.* **1998**, *72*, 2403.

(296) Fujiwara, T.; Locklin, J.; Bao, Z. N. *Appl. Phys. Lett.* **2007**, *90*, 232108.

(297) Guo, D.; Sakamoto, K.; Miki, K.; Ikeda, S.; Saiki, K. *Appl. Phys. Lett.* **2007**, *90*, 102117.

(298) Jin, S.-H.; Seo, H.-U.; Nam, D.-H.; Shin, W. S.; Choi, J.-H.; Yoon, U. C.; Lee, J.-W.; Song, J.-G.; Shin, D.-M.; Gal, Y.-S. *J. Mater. Chem.* **2005**, *15*, 5029.

(299) Hu, B.; Yan, L.; Shao, M. *Adv. Mater.* **2009**, *21*, 1500.

(300) Shklyarecskiy, I. O.; Jonkheijm, P.; Christiansen, P. C. M.; Schenning, A. P. H. J.; Guerzo, A. D.; DesverGne, J.-P.; Meijer, E. W.; Maan, J. C. *Langmuir* **2005**, *21*, 2108.

(301) Boamfa, M. I.; Viertler, K.; Wewerka, A.; Stelzer, F.; Christiansen, P. C. M.; Maan, J. C. *Phys. Rev. Lett.* **2003**, *90*, 025501.

(302) Shklyarecskiy, I. O.; Jonkheijm, P.; Stutzmann, N.; Wasserberg, D.; Wondergem, H. J.; Christiansen, P. C. M.; Schenning, A. P. H. J.; de leeuw, D. M.; Tomovic, Z.; Wu, J.; Müllen, K.; Maan, J. C. *J. Am. Chem. Soc.* **2005**, *127*, 16233.

(303) Noh, Y.-Y.; Kim, J.-J.; Yase, K.; Nagamatsu, S. *Appl. Phys. Lett.* **2003**, *83*, 1243.

(304) Noh, Y.-Y.; Kim, J.-J.; Yoshida, Y.; Yase, K. *Adv. Mater.* **2003**, *15*, 699.

(305) Wang, H. B.; Zhu, F.; Yang, J. L.; Geng, Y. H.; Yan, D. H. *Adv. Mater.* **2007**, *19*, 2168.

(306) Wu, J. S.; Pisula, W.; Müllen, K. *Chem. Rev.* **2007**, *107*, 718.

(307) Xu, G. F.; Bao, Z. A.; Groves, J. T. *Langmuir* **2000**, *16*, 1834.

(308) Pisula, W.; Menon, A.; Stepputat, M.; Lieberwirth, I.; Kolb, U.; Tracz, A.; Sirringhaus, H.; Pacula, T.; Müllen, K. *Adv. Mater.* **2005**, *17*, 684.

(309) Pisula, W.; Tomovic, Z.; Stepputat, M.; Kolb, U.; Pacula, T.; Müllen, K. *Chem. Mater.* **2005**, *17*, 2641.

(310) Tracz, A.; Jeszka, J. K.; Watson, M. D.; Pisula, W.; Müllen, K.; Pacula, T. *J. Am. Chem. Soc.* **2003**, *125*, 1682.

(311) Duffy, C. M.; Andreasen, J. W.; Breiby, D. W.; Nielson, M. M.; Ando, M.; Minakata, T.; Sirringhaus, H. *Chem. Mater.* **2008**, *20*, 7252.

(312) Becerril, H. A.; Roberts, M. E.; Liu, Z. H.; Locklin, J.; Bao, Z. N. *Adv. Mater.* **2008**, *20*, 2588.

(313) Dierking, I. *Textures of Liquid Crystals*; Wiley-VCH: Germany, Weinheim, 2003.

(314) Maunoury, J. C.; Howse, J. R.; Turner, M. L. *Adv. Mater.* **2007**, *19*, 805.

(315) Wei, Q. S.; Tajima, K.; Hashimoto, K. *ACS Appl. Mater. Interfaces* **2009**, *1*, 1865.

(316) Stutzmann, N.; Smits, E.; Wondergem, H.; Tanase, C.; Blom, P.; Smith, P.; de leeuw, D. M. *Nat. Mater.* **2005**, *4*, 601.

(317) Salleo, A.; Arias, A. C. *Adv. Mater.* **2007**, *19*, 3540.

(318) Lee, W. H.; Lim, J. A.; Kwak, D.; Cho, J. H.; Lee, H.; S.; Choi, H. H.; Cho, K. *Adv. Mater.* **2009**, *21*, 4243.

(319) Madec, M.-B.; Crouch, D.; Llorente, G. R.; Whittle, T. J.; Geoghegen, M.; Yeates, S. G. *J. Mater. Chem.* **2008**, *18*, 3230.

(320) Lee, S. S.; Kim, C. S.; Gomez, E. D.; Purushothaman, B.; Toney, M. F.; Wang, C.; Hexemer, A.; Anthony, J. E.; Loo, Y.-L. *Adv. Mater.* **2009**, *21*, 3605.

(321) (a) Facchetti, A.; Yoon, M.-H.; Marks, T. J. *Adv. Mater.* **2005**, *17*, 1705. (b) Sun, X. N.; Di, C.-a.; Liu, Y. Q. *J. Mater. Chem.* **2010**, *20*, 2599.

(322) Braga, D.; Horowitz, G. *Adv. Mater.* **2009**, *21*, 1473.

(323) Ortiz, R. P.; Facchetti, A.; Marks, T. J. *Chem. Rev.* **2010**, *110*, 205.

(324) Yoon, M.-H.; Kim, C.; Facchetti, A.; Marks, T. J. *J. Am. Chem. Soc.* **2006**, *128*, 12851.

(325) Kim, C. S.; Jo, S. J.; Lee, S. W.; Kim, W. J.; Baik, H. K.; Lee, S. J. *Adv. Funct. Mater.* **2007**, *17*, 958.

(326) Kobayashi, S.; Nishikawa, T.; Takenobu, T.; Mori, S.; Shimoda, T.; Mitani, T.; Shimotani, H.; Yoshimoto, N.; Ogawa, S.; Iwasa, Y. *Nat. Mater.* **2004**, *3*, 317.

(327) Ma, H.; Acton, O.; Ting, G.; Ka, J. W.; Yip, H.-L.; Tucker, N.; Schofield, R.; Jen, A. K.-Y. *Appl. Phys. Lett.* **2008**, *92*, 113303.

(328) Kim, D. H.; Lee, H. S.; Yang, H. C.; Yang, L.; Cho, K. *Adv. Funct. Mater.* **2008**, *18*, 1363.

(329) Virkar, A.; Mannsfeld, S.; Oh, J. H.; Toney, M. F.; Tan, Y. H.; Liu, G.-y.; Scott, J. C.; Miller, R.; Bao, Z. N. *Adv. Funct. Mater.* **2009**, *19*, 1962.

(330) Liu, Z. H.; Oh, J. H.; Roberts, M. E.; Wei, P.; Paul, B. C.; Okajima, M.; Nishi, Y.; Bao, Z. N. *Appl. Phys. Lett.* **2009**, *94*, 203301.

(331) Kim, C. S.; Jo, S. J.; Kim, J. B.; Ryu, S. Y.; Noh, J. H.; Baik, H. K.; Lee, S. J.; Kim, Y. S. *Appl. Phys. Lett.* **2007**, *91*, 063503.

(332) Li, M. F.; Nathan, A.; Wu, Y. L.; Ong, B. S. *J. Appl. Phys.* **2008**, *104*, 124504.

(333) Liu, P.; Wu, Y. L.; Li, Y. N.; Ong, B. S.; Zhu, S. P. *J. Am. Chem. Soc.* **2006**, *128*, 4554.

(334) Wu, Y. L.; Liu, P.; Ong, B. S. *Appl. Phys. Lett.* **2006**, *89*, 013505.

(335) Chen, F.-C.; Liao, C.-H. *Appl. Phys. Lett.* **2008**, *93*, 103310.

(336) Ogawa, S.; Kimura, Y.; Niwano, M.; Ishii, H. *Appl. Phys. Lett.* **2007**, *90*, 033504.

(337) Katz, H. E.; Johnson, J.; Lovinger, A. J.; Li, W. J. *J. Am. Chem. Soc.* **2000**, *122*, 7787.

(338) Kymissis, I.; Dimitrakopolous, C. D.; Purushothaman, S. *IEEE. Trans. Electron. Devices* **2001**, *48*, 1060.

(339) Wen, Y. G.; Liu, Y. Q.; Di, C.-a.; Wang, Y.; Sun, X. N.; Guo, Y. L.; Zheng, J.; Wu, W. P.; Ye, S. H.; Yu, G. *Adv. Mater.* **2009**, *21*, 1631.

(340) Gundlach, D. J.; Royer, J. E.; Park, S. K.; Subramanian, S.; Jurchescu, O. D.; Hamadani, B. H.; Moad, A. J.; Kline, R. J.; Teague, L. C.; Kirillov, O.; Richter, C. A.; Kushmerick, J. G.; Richter, L. J.; Parkin, S. R.; Jackson, T. N.; Anthony, J. E. *Nat. Mater.* **2008**, *7*, 216.

(341) (a) Cho, S.; Seo, J. H.; Lee, K.; Heeger, A. J. *Adv. Funct. Mater.* **2009**, *19*, 1459. (b) Di, C.-a.; Yu, G.; Liu, Y. Q.; Xu, X. J.; Wei, D. C.; Song, Y. B.; Sun, Y. M.; Wang, Y.; Zhu, D. B.; Liu, J.; Liu, X. Y.; Wu, D. X. *J. Am. Chem. Soc.* **2006**, *128*, 16418. (c) Di, C.-a.; Yu, G.; Liu, Y. Q.; Guo, Y. L.; Wu, W. P.; Wei, D. C.; Zhu, D. B. *Phys. Chem. Chem. Phys.* **2008**, *10*, 2302. (d) Di, C.-a.; Liu, Y. Q.; Yu, G.; Zhu, D. B. *Acc. Chem. Res.* **2009**, *42*, 1573.

(342) Seol, Y. G.; Lee, N.-E.; Park, S. H.; Bae, J. Y. *Org. Electron* **2008**, *9*, 413.

(343) Stadlober, B.; Haas, U.; Gold, H.; Haase, A.; Jakopic, G.; Leising, G.; Koch, N.; Rentenberger, S.; Zojer, E. *Adv. Funct. Mater.* **2007**, *17*, 2687.

(344) Koezuka, H.; Tsumura, A.; Fuchigami, H.; Kuramoto, K. *Appl. Phys. Lett.* **1993**, *62*, 1794.

(345) Lim, J. A.; Cho, J. H.; Park, Y. D.; Kim, D. H.; Hwang, M.; Cho, K. *Appl. Phys. Lett.* **2006**, *88*, 082102.

(346) Wada, H.; Shibata, K.; Bando, Y.; Mori, T. *J. Mater. Chem.* **2008**, *18*, 4165.

(347) Hiraoka, M.; Hasegama, T.; Abe, Y.; Yamada, T.; Tokura, Y.; Yamochi, H.; Saito, G.; Akutagawa, T.; Nakamura, T. *Appl. Phys. Lett.* **2006**, *89*, 173504.

(348) Shibata, K.; Wada, H.; Ishikawa, K.; Takezoe, H.; Mori, T. *Appl. Phys. Lett.* **2007**, *90*, 193509.

(349) Hiraoka, M.; Hasegama, T.; Yamada, T.; Takahashi, Y.; Horiuchi, S.; Tokura, Y. *Adv. Mater.* **2007**, *19*, 3248.

(350) Qi, P. F.; Javey, A.; Rolandi, M.; Wang, Q.; Yenilmez, E.; Dai, H. J. *J. Am. Chem. Soc.* **2004**, *126*, 11774.

(351) Feldman, A. K.; Steigerwald, M. L.; Guo, X. F.; Nuckolls, C. *Acc. Chem. Res.* **2008**, *41*, 1731.

3405

dx.doi.org/10.1021/cr1001904 |*Chem. Rev.* 2011, 111, 3358–3406

(352) Hong, K.; Nam, S.; Yang, C.; Kim, S. H.; Chung, D. S.; Yun, W. M.; Park, C. E. *Org. Electron* **2009**, *10*, 363.

(353) Wada, H.; Mori, T. *Appl. Phys. Lett.* **2008**, *93*, 213303.

(354) Cao, Y.; Liu, S.; Shen, Q.; Yan, K.; Li, P. J.; Xu, J.; Yu, D. P.; Steigerwald, M. L.; Nuckolls, C.; Liu, Z. F.; Guo, X. F. *Adv. Funct. Mater.* **2009**, *19*, 2743.

(355) Pang, S. P.; Tsao, H. N.; Feng, X. L.; Müllen, K. *Adv. Mater.* **2009**, *21*, 3488.

(356) Di, C.-a.; Wei, D. C.; Yu, G.; Liu, Y. Q.; Guo, Y. L.; Zhu, D. B. *Adv. Mater.* **2008**, *20*, 3289.

(357) Shimada, T.; Saiki, K. *J. Electron. Spec. Rel. Phenom.* **2007**, *154*, 119.

(358) Ke, L.; Dolmanan, S. B.; Shen, L.; Vijila, C.; Chua, S. J.; Png, R.-Q.; Chia, P.-J.; Chua, L.-L.; Ho, P. K.-H. *J. Appl. Phys.* **2008**, *104*, 124502.

(359) Saeki, A.; Seki, S.; Tagawa, S. *J. Appl. Phys.* **2006**, *100*, 023703.

(360) Pal, B. N.; Dhar, B. M.; See, K. C.; Katz, H. E. *Nat. Mater.* **2009**, *8*, 898.

(361) Ahn, B. Y.; Duoss, E. B.; Motala, M. J.; Guo, X. Y.; Park, S.-I.; Xiong, Y. J.; Yoon, J.; Nuzzo, R. G.; Rogers, J. A.; Lewis, J. A. *Science* **2009**, *323*, 1590.

(362) Kanungo, M.; Lu, H. L.; Malliaras, G. G.; Blanchet, G. B. *Science* **2009**, *323*, 234.

(363) Unpublished results.